THE STUDY OF METHANIMINE IN INTERSTELLAR MEDIUM

A Thesis

Submitted in partial fulfillment of the requirements for the

award of the degree of

DOCTOR OF PHILOSOPHY

in

PHYSICS

By

Neeraj Kumar

(41400735)

Supervised By

Prof. Suresh Chandra

Co-Supervised by

Prof. Niti Kant

LOVELY PROFESSIONAL UNIVERSITY

PUNJAB

2020

CANDIDATE'S DECLARATION

I, Neeraj Kumar, hereby declare that the thesis entitled "The Study of Methanimine in Interstellar Medium", submitted to Lovely Faculty of Physical Sciences, Lovely Professional University, Phagwara, in partial fulfillment of the requirement for the award of the degree of Doctor of Philosophy in Physics is the original work carried out by me under the supervision of Prof. Suresh Chandra and Co-supervision of Prof. Niti Kant. No part of the thesis has been formed the basis for the award of any degree or diploma at any other university or institute.

Neeraj Kumar

Reg. No. 41400735

CERTIFICATE

I certify that the thesis entitled 'THE STUDY OF METHANIMINE IN INTERSTELLAR MEDIUM', submitted to the Lovely School of Sciences, Lovely Professional University, Punjab, for the award of the degree of DOCTOR OF PHILOSOPHY in PHYSICS is the result of research work carried out by Mr. NEERAJ KUMAR under my guidance and supervision.

Signature of Supervisor
Prof. Suresh Chandra
Deputy Director
Amity Centre for Astronomy and Astrophysics
Amity Institute of Applied Sciences
Amity University, Noida, U.P. 201313

Signature of Co-Supervisor
Prof. Niti Kant
Department of Physics
Lovely Professional University
Phagwara, Punjab 144411

ABSTRACT

The interstellar medium (ISM) is the region between stars in the universe. It consists of dust, gases (atoms, molecules, ions, and plasma) and high energy cosmic rays. The unfavorable conditions of the ISM were perceived to be a hindrance to the simple chemical entities found in the ISM to give rise to other complex chemical entities by the process of chemical transformation. This reasoning was based on a very low temperature and low number density of molecules in ISM. But, after the discovery of the OH molecule in the interstellar medium in 1963, the research to find the contents of the interstellar medium intensified. To date, more than 200 molecules and ions have been detected in the interstellar medium, from simple diatomic to large organic molecules. For this reason, the ISM may be viewed as a unique synthetic laboratory. The study of molecules in cosmic objects is of great importance, as it provides information about the physical conditions prevailing there and the chemical process going on there. Thus, it is of great interest to identify all the possible molecules in astronomical objects.

The cosmic objects emit radiation in all the ranges of the electromagnetic spectrum from radio waves to gamma rays depending upon its kinetic temperature. These radiations propagate in all the possible directions. The radiations coming towards earth interact with the atmosphere of the earth. The atmosphere of the earth is capable of absorbing many of these radiations. However, the atmosphere of the earth is transparent to the radiations lying in the optical and radio window. Although the radiations reaching the earth's surface lie in the optical and radio windows, our eyes can see the radiations lying in the optical window only. As the scattering of radiation is inversely proportional to the fourth power of its wavelength, thus scattering of radiation in the radio window is small. Also, the temperature in cosmic objects is low, so the transitions between only rotational energy levels are possible that lie in the radio window.

A large number of researchers around the world are working to identify interstellar prebiotic molecules that may provide a crucial understanding of our solar system and even the evidence of the origin of life in cosmic objects. The ISM consists

of a large variety of molecules ranging from very simple to complex forms, with astrobiological importance, which might have undergone evolution and recycling continuously and repeatedly, and may be able to provide valuable insight to the origin of life.

In the present investigation, we have studied the methanimine molecule in the interstellar medium. It is a planar asymmetric top type molecule having both a and b type dipole moment components of μ_a =1.340 D and μ_b =1.446 D respectively. The methanimine (CH_2NH) molecule is a potential precursor of Glycine, the simplest amino acid. The amino-acids like Glycine are building blocks of proteins that are essential for life to occur. So, the detection of methanimine in ISM would lead to the presence of amino acids in ISM that may further give information about the existence of life in ISM.

The methanimine molecule (CH_2NH) was detected for the first time in 1973 by microwave spectroscopy in the molecular cloud Sgr B2 towards the galactic center. It was further identified in a few cosmic objects and some of its spectral lines have been detected. Also, its laboratory spectrum is obtained from time to time. For methanimine molecule, both the radiative and collisional transitions may occur, so the rate coefficients of both types of transitions are required. In our research work, we have obtained the energies for the lowest 69 rotational energy levels, having energies up to 141 cm^{-1}. The Einstein A-coefficients and line strengths for all the radiative transitions between these energy levels are calculated in accordance with the selection rules. Those lines are reported which are expected to be prominent under conditions in the interstellar medium by applying two criteria, namely the upper energy level must be sufficiently populated and the radiative transition probability must be sufficiently large. Besides the observed transitions, we have found more than 100 lines of methanimine satisfying the said conditions which are not observed earlier and are expected to play an important role in the identification of methanimine in the interstellar space.

The geometrical coordinates of methanimine are optimized with the help of Gaussian software. By using the molecular symmetries in methanimine, the allowed

radiative and collisional transitions between the lowest 15 rotational energy levels are presented in tabular form. The collisional rates are important to determine the population density of a molecule while solving the set of statistical equilibrium equations coupled with the equations of radiative transfer. The brightness temperature for the transitions $1_{10} - 1_{11}$, $2_{11} - 2_{12}$, $3_{12} - 3_{13}$, $4_{13} - 4_{14}$, and $1_{11} - 2_{02}$ is plotted against the hydrogen molecular density. A weak maser action in the transition 1_{10}–1_{11} and anomalous absorption in the transition 1_{11}–2_{02} is obtained with the rest of the transitions showing emission feature. The maser action of transition $1_{10} - 1_{11}$ is also determined by an analytical method using scaled values of collisional rate coefficients which shows a little contribution of collisional transitions as compared to radiative transitions.

ACKNOWLEDGMENT

With great pleasure, I express my sincere and profound gratitude to my supervisor Prof. Suresh Chandra, for his erudite and invaluable guidance throughout my research work. It is by virtue of his patience, motivation, exuberance, and immense knowledge that led to the completion of my Ph.d. work. His guidance helped me throughout my research work and inditing of the thesis. I could not have imagined a better guide for my Ph.D.

I would relish thanking my co-supervisor Prof. Niti Kant, for guidance, encouragement, moral support, and valuable suggestions which helped me a lot in carrying out my research work. His generous behavior and motivation have always encouraged me throughout my Ph.d. I would also like to thank Dr. Mohit Kumar Sharma, who inspired and helped me a lot in carrying out the research work.

I would extend my thanks to Prof. Kailash Juglan, Head, Department of Physics, for his kind support and suggestions throughout my research work. I would also like to thank Prof. Ramesh Thakur, HOS, Physical Sciences, for his inspiration and regular support for my research work.

I would like to express my deep sense of gratitude to Mr. Ashok Mittal, Honorable Chancellor, LPU; Ms. Rashmi Mittal, Pro-Chancellor, LPU, Dr. Ramesh Kanwar, Vice-Chancellor, LPU and Dr. Lovi Raj Gupta, Executive Dean, LFTS, for providing the necessary support and environment to carry out my research work.

I want to convey a special thanks to my dearest friend Mr. Alok Jain, who has consistently encouraged and supported me in my research work. I would also thank Dr. Suman Rani, for her generous behavior and moral support. Also, I feel fortunate to have Mr. Rajan Miglani and Ms. Preeti Khurana as my good friends who always motivated me throughout my work.

Finally, I would like to thank my family for their consistent inspiration, encouragement, and moral support throughout my life. It is because of the blessings of my beloved mother, who is no longer between us, but continues to inspire through her teachings, which enabled me to complete this research work.

Last, but not the least, I appreciate the patience, support, and understanding of my wife Nidhi, without whose support, the work would never have been completed. I would also express affection for my lovely daughter Navya, who is always a source of happiness for me.

Neeraj Kumar

CONTENTS

LIST OF TABLES

LIST OF FIGURES

LIST OF ABBREVIATIONS

CMB	Cosmic Microwave Background
IR	Infrared
ISM	Interstellar Medium
LTE	Local Thermal Equilibrium
LVG	Large Velocity Gradient
MASER	Microwave Amplification by Stimulated Emission of Radiation
MOI	Moment of Inertia
NLTE	Non-Local Thermal Equilibrium
OW	Optical Window
RW	Radio Window
SETI	Search for Extraterrestrial Intelligence
UV	Ultraviolet
VLBI	Very Long Baseline Interferometry

CHAPTER 1: INTRODUCTION

The universe, as we know today, is postulated to be evolved from a Big Bang that occurred some 13.7 billion years ago. It consists of a voluminous number of galaxies including our galaxy, the Milky Way, which contains more than 10^{11} stars. These stars appear sparkling points of light when seen through naked eyes. However, not all of them are stars. These can be galaxies, star clusters, planetary nebulae (clouds of gas and dust, which may have stars embedded in them) etc. It is arduous to resolve them with the naked eye because of their astronomically immense distance from us. Besides these illuminating objects, some regions are not illuminating because their temperature is not amply high. These objects emit radiation of longer wavelengths. These cool regions, as well as illuminating ones, are commonly known as cosmic objects.

The spectrum obtained from cosmic objects led to the revelation of a number of molecules in them. The study of molecules in cosmic objects is of great importance, as it provides information about the physical environments there and the chemical process going on there. Thus, it is essential to identify all the possible molecules in astronomical objects.

1.1 Interstellar Medium and its Constituents

The interstellar medium (ISM) is the region between stars in a galaxy. The ISM consists of dust, gases (atoms, molecules, ions and plasma) and high energy cosmic rays. The major components are of H_2 and He gases that make up 99% of the ISM [1–3]. By mass, the ISM contains 70% H_2, 28% He, with other elements making up the remaining 2%. The carbon, nitrogen and oxygen represent a majority of the final 2% with heavier elements being less abundant.

The temperature and density of the ISM varies and differs between two types of clouds that are distinguished as per their physical and chemical properties. It varies from extremely hot (10000 K) diffuse clouds (1 molecule/cm^3) which are easily penetrated by starlight, to extremely cold (5K) dark cloud (>10^4 molecules/cm^3)

which are dense and impermeable to starlight [4], conditions that permit the existence of more intricate chemical species [5].

The inauspicious conditions of the ISM were perceived to be an obstruction to the simple chemical entities found in the ISM to give elevate to other complex chemical entities by the process of chemical transformation [6]. This reasoning was predicated on a very low temperature and low number density of molecules in ISM. However, in modern times, several spectral observations from the intervening space utilizing a number of techniques and instruments have revealed an abundance of information with many more revelations made each year [7–10]. For this reason, the ISM may be viewed as a unique synthetic laboratory.

1.2 Radiation from Cosmic Objects- Optical and Radio Window

The cosmic objects emit radiation in all the ranges of the electromagnetic spectrum from radio waves to gamma rays depending upon its kinetic temperature. These radiations propagate in all the possible directions. The radiations coming towards earth interact with the atmosphere of the earth. The high energy rays (X-rays and gamma rays) produce electrons and positively charged particles in the ionosphere on their absorption. The ozone layer below this absorbs UV rays making life safe on the surface of the earth.

The troposphere mainly consists of N_2, O_2, CO_2, and water vapors which are capable of absorbing IR radiations. So, most of the part of the Electromagnetic spectrum coming from the ISM is unable to transmit through the atmosphere to reach the surface of the earth. However, there are few bands of spectrum for which the atmosphere of earth is transparent, and two of them are very wide and hence consequential to discuss. These are known as Optical Window and Radio Window.

The optical-window has radiations having the wavelengths from 3000 Å to 10000 Å, whereas the radio-window has radiations having wavelengths from few millimeters to few decameters. The electromagnetic radiations which the human eyes can see lies in the optical window. The electromagnetic radiations lying in the radio-

window cannot be seen by the human eyes so they are detected with the help of some specific detectors.

1.3 Advantage of the Radio Window

The radiations reaching on the earth's surface lie in the optical and radio windows but our eyes can see the radiations lying in the optical window only. However, in the context of the distant objects, the radio window has remarkable advantages over the optical window. As we know that the scattering of radiation is inversely proportional to the fourth power of its wavelength and wavelengths of the radiations in the optical window are smaller than those in the radio window by a factor of about 10^5. So, the scattering of the radiations in the optical window is about 10^{20} times larger than that of the radiations in the radio window. Thus, from the distant objects, most of the optical radiations would be lost before reaching the earth's surface. Hence, it is the radio radiations which can bring valuable information about the cosmic objects, situated at very large distances, generally, several hundred light-years.

However, when we use a single-dish radio telescope, the resolving power of the telescope becomes very poor. For example, for optical radiation of 6000 Å, optically canvassed by an optical telescope of diameter 2 m, the limit of resolution of the telescope is

$$\text{Limit of Resolution} \approx \lambda/D = 3 \times 10^{-7} \text{ rad}$$

Now, for a radio wave of 1 m wavelength, observed by a single-dish radio telescope of diameter 100 m, the limit of resolution of the telescope is

$$\text{Limit of Resolution} \approx \lambda/D = 1 \times 10^{-2} \text{ rad}$$

As Resolving Power is inverse of the limit of resolution, it implies that the Resolving power of a single dish telescope is very small relative to an optical telescope. However, the resolving power of a radio telescope can be enhanced tremendously by making use of the Very Long Baseline Interferometry (VLBI) technique in which two radio telescopes situated at two different places, separated by a large distance, are made to behave like two outer segments of a large telescope (figure 1.1). The distance

between these two telescopes is known as the baseline. The largest baseline on the earth can be equal to the diameter of the earth, which is about 12,700 km. The limit of resolution of a radio telescope using the VLBI technique may be obtained using λ = 1 m and D = 12700 km.

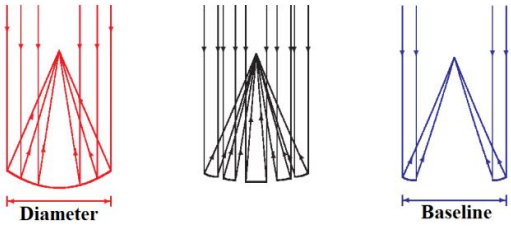

Figure 1.1: The VLBI Technique

Limit of Resolution $\approx \lambda/D = 7.87 \times 10^{-8}$ rad

The resolving power obtained is even better than that of an optical telescope. For further improvement in the resolving power of a radio telescope, one of the telescopes used in the VLBI technique is to be installed in the sky on an artificial satellite, orbiting around the earth. Now, the question arises, which radiations, lying in the radio-window, would provide information about the physical environments in the distant cosmic objects.

The universe is made up of atoms, molecules, ions, and dust. Atoms and ions generally produce radiations lying in the UV and visible regions. The radiations produced by molecules lie in the IR region and in the radio-window. The molecules, besides the electronic levels, have vibrational levels and rotational levels. The transitions between the vibrational levels produce IR radiations whereas the transitions between the rotational levels produce the radiations lying in the radio window. These radiations from the cosmic molecules can bring information about the physical conditions existing in the distant cosmic objects and the chemical reactions going on in them. Therefore, the discovery of the radio window provided a new way to the knowledge of astronomical constituents.

1.4 Cosmic Microwave Background

Today we accept the formation of the universe given by big bang theory which occurred 13.8 billion years ago. George Gamow [11] in 1948 proposed that the density and temperature of the universe at that time were infinitely large. With the passage of time, the temperature decreased and the formation of elements

commenced. He predicted that the current cosmos is filled with black body radiation at a kinetic temperature of the order of 10 Kelvin. The radio astronomical technology is now a day's advanced enough to record these radiations which were not possible earlier. These radiations are known as Cosmic Microwave Background (CMB). The accurate measurement of its kinetic temperature was done independently by two young engineers of Penzias and Wilson Bell Telephone Laboratories. The temperature of CMB was discovered to be 2.73 Kelvin precisely.

1.5 Molecules in Cosmic Objects

Earlier, the majority of the scientific community was having opinion against the existence of molecules in the interstellar medium, except a small section of scientists. This section of scientists believed that molecules do exist at low temperatures in the interstellar medium, However, the detection of molecules was a difficult task because molecules don't emit in the visible region. Even after the discovery of the radio window by Karl Jansky in 1932, no molecule was detected in ISM for three decades. In 1963, Weinrab et al. [12] discovered OH, the first molecule detected in ISM through its 18 cm radiation. This finding intensified the research to find molecules in cosmic objects. To date, over 200 molecules and ions have been identified in the cosmic objects, from simple diatomic to large organic molecules [13–31]. A list consisting of most of the molecules found in various cosmic objects is given in Table 1.1. The region in interstellar space which contains a large variety of molecules is called a cosmic molecular laboratory. Some of these cosmic laboratories are given in Table 1.2 along with their astronomical co-ordinates.

1.6 Classification of Molecules

Two or more atoms cohered by chemical bonds make a molecule. It is electrically neutral as a whole but can have a different arrangement of atoms. A diatomic molecule can be homo-nuclear or hetero-nuclear depending upon whether the two atoms forming a molecule are the same or different respectively. The homo-nuclear molecules like O_2, H_2, N_2 etc. are non-polar as the center of positive and negative charges are at the same point. However, the hetero-nuclear diatomic molecules like CO, SiO, CH, OH, etc. possess a permanent dipole moment as the centers of positive

and negative charges are separated. A polyatomic molecule may or may not be polar, depending upon the type of atoms in it and its structure.

The molecule's transition from one rotational energy state to another rotational energy state involves angular momentum changes. Let the moments of inertia (MOI) of the molecule about co-ordinate axes are I_a, I_b, and I_c where I_c is the largest one. These are associated with rotational constants A, B and C (where A > B > C) as

$$A = \frac{h}{8\pi^2 I_a c}, \qquad B = \frac{h}{8\pi^2 I_b c}, \qquad C = \frac{h}{8\pi^2 I_c c}$$

Depending on the magnitude of these three moments of inertia, the molecules are classified into the following four types:

(i) Linear Molecules: The molecules in which atoms are arranged in a linear fashion so that the dipole moment is along the line joining the atoms. e.g. H_2, CO_2, HCN, OCS, etc. The MOI of the molecule is zero about an axis along its length and equal about the other two axes. i.e. $I_a = 0$ and $I_b = I_c$.

(ii) Spherical Top Molecules: If MOI of the molecule about all the three axes of inertia are the same ($I_a = I_b = I_c$), it is known as a spherical top molecule. e.g. CH_4, CCl_4, etc.

(iii) Symmetric Top Molecules: If two of the three MOI are equal, it is known as symmetric top molecule. Depending upon which moment of inertia are equal, these are further categorized into two types, namely oblate and prolate type.

(a) Oblate Symmetric Top Molecules: If $I_a = I_b < I_c$, the molecule is called the oblate type molecule. e.g. C_2H_5Cl, C_2H_5Br, BF_3, etc. Here, the inertial axis "c" is the axis of symmetry and is used as the preferential direction. The projection of rotational quantum number J on the c-axis is denoted as k_c which has values ranging from –J to +J with a gap of 1. Also, the rotational energy levels are written as J_{kc}.

(b) Prolate Symmetric Top Molecules: If $I_a < I_b = I_c$, the molecule is named as prolate type symmetric top molecule. e.g. CH_3Cl, CH_3I, NH_3, etc. Here, the inertial axis "a" is the axis of symmetry and is used as the preferential direction. The

projection of J on a-axis is denoted as k_a which has values ranging from –J to +J with a gap of 1. Also, the rotational energy levels are written as J_{ka}.

(iv) Asymmetric Top Molecules: In this case, all three moments of inertia of a molecule are different. The MOI about the c-axis is largest as it is taken perpendicular to the plane of the molecule. A planar molecule is called a-type asymmetric top molecule if its dipole moment is along a-axis. e.g. H_2CO, SiC_2, etc. Similarly, molecules like H_2O have dipole moment oriented along the b-axis, thus known as b-type asymmetric top molecule. If dipole moment is inclined to both a and b axis, then this type of planar molecule is called a and b-type asymmetric top molecule. e.g. CH_2NH etc.

1.7 Transitions in Molecules

A molecule consists of two or more atoms bonded together, in which both electronic and nuclear motions do exist, that can be separated. A spectral line is formed due to the emission of a photon when a molecule changes from higher to lower energy state. The change in energy level can be caused due to electronic, vibrational, or rotational transition as discussed below:

(i). Electronic Transitions: The electronic transitions are rapid transitions that do not involve any change in inter-nuclear distance between the atoms of the molecule. These transitions cause the excitation of electrons of the atoms in a molecule by absorption or emission of a large amount of energy. The transitions between electronic energy levels produce spectral lines in visible or UV region.

(ii). Vibrational Transitions: Vibrational transitions involve the periodic motion of atoms in the molecule keeping the center of mass fixed. These transitions arise between different vibrational levels of an electronic state when a molecule absorbs an amount of energy equal to the gap between vibrational levels. The energy of vibrational transitions is smaller than the electronic transitions that produce spectral lines in the IR region.

(iii). Rotational Transitions: The rotational transitions involves smaller energies by which the polar molecules rotate about an axis. These transitions generally occur

between rotational states of a vibrational state although there exist many vibration-rotation combined transitions also, for lighter molecules. The transitions between rotational energy levels produce spectral lines in millimeter range which lies in radio wave region and are of particular interest in astrophysics.

The molecules are found in cosmic objects where the kinetic temperature is of the order of a few tens of Kelvin. So, the transitions between vibrational and electronic energy levels are not possible. Therefore, we take into account only the transitions between rotational energy levels in the ground state vibrational and electronic energy level.

1.8 Rotational Spectra of Molecules

The rotational transitions are possible for molecules having permanent dipole moments (polar molecules). The electric dipole moments of rotating polar molecules appear to oscillate with a frequency equal to the frequency of their rotation, so these molecules radiate at this frequency.

1.8.1 Rotational Spectra of Diatomic Molecules

(i) Rigid Diatomic Molecules: A rigid diatomic molecule may be approximated as a rigid rotator in which two atoms of masses m_1 and m_2 are separated by distance r equal to the length of bond between them. For rotation of this molecule about an axis passing through the center of mass and perpendicular to plane of the molecule, the energy eigenvalues are given by

$$E = \frac{\mathbf{J}^2}{2I} = \frac{J(J+1)\hbar^2}{2I}$$

Where **J** is rotational angular momentum, I is the moment of inertia of the molecule about the rotational axis and J is the rotational quantum number having $(2J + 1)$ degenerate values. Also, $I = \mu r^2$, where μ is the reduced mass of the system of particles.

In spectroscopy, it is often convenient to represent energy in terms of wave-number having units cm^{-1}, given by the following expression

$$F(J) = \frac{E}{hc} = \frac{J(J+1)h}{8\pi^2 cI} = BJ(J+1)$$

where $B = \frac{h}{8\pi^2 cI}$ is the rotational constant having units cm^{-1}. The wave-number (or energy in cm^{-1}) for a transition between level J and $(J + 1)$ will be

$$\bar{\nu} = F(J+1) - F(J) = 2B(J+1)$$

We find that the transitions can have values of wave-number 2B, 4B, 6B, 8B, and so on, in accordance with the selection rule $\Delta J = \pm 1$ and $J = 0,1,2,3$ and so on. Thus, the adjacent energy levels are equally spaced. Also, the frequency of emitted radiation between rotational energy levels depends upon the moment of inertia of a molecule. For heavier molecules, the emitted radiations will be of longer wavelengths as compared to lighter molecules.

(ii) Non-rigid Diatomic Molecule: According to experimental observations, the spacing between adjacent energy levels is found to decrease with an increase in J value which suggests that the assumption of a rigid molecule is not true. The bond lengths might change due to elastic behavior, which will add a correction term to the energy values. Thus, we have

$$F(J) = BJ(J+1) - DJ^2(J+1)^2$$

where D is known as centrifugal distortion constant. Also, the wave-number of transition between level J and $(J + 1)$ becomes

$$\bar{\nu} = 2B(J+1) - 4D(J+1)^3$$

The centrifugal force for a rotating molecule increases with an increase in angular momentum quantum number J. So the transitions between fast-rotating molecules will become slightly lower in frequency due to centrifugal forces.

1.8.2 Rotational Spectra of Polyatomic Molecules

(i) Linear Molecules: A linear molecule can be assumed similar to a diatomic molecule with n –1 bonds between n atoms. As $I_a = 0$, $I_b = I_c$ for linear molecules, its spectra is the same as that of a diatomic molecule as given in section 1.8.1.

(ii) Spherical Top Molecules: The spherical top molecules are non-polar so the electric field of an incident photon can't accelerate the rotation of dipole moment. Thus, a pure rotational spectrum is not observed for these molecules.

(iii) Symmetric Top Molecules: As energy values depend upon the moment of inertia, therefore, the energy levels for prolate and oblate molecules are different for symmetric top molecules, as explained below:

(a) Oblate Symmetric Top Molecules: For a rigid oblate symmetric top molecule, we have $I_a = I_b < I_c$. The energy of an energy level is given by

$$E(A, B, C) = \frac{\mathbf{J}_a^2 + \mathbf{J}_b^2}{2I_a} + \frac{\mathbf{J}_c^2}{2I_c}$$

where A, B, C are rotational constants, $\mathbf{J}_a$, $\mathbf{J}_b$, and $\mathbf{J}_c$ are components of angular momentum, related to rotational quantum number J by the following expressions

$$\mathbf{J}_a^2 + \mathbf{J}_b^2 + \mathbf{J}_c^2 = J(J + 1)\hbar^2$$

and

$$\mathbf{J}_c = K\hbar$$

where K is the projection of rotational angular momentum on the symmetry axis (c-axis), also written as k_c. The eigenvalues of wave-numbers of an energy level are given by

$$F(J, K) = BJ(J + 1) - (B - C)K^2$$

Also, the wave-number of radiative transition between level J and $(J + 1)$ will be given by

$$\bar{\nu} = F(J + 1, K) - F(J, K) = 2B(J + 1)$$

If the molecule is not rigid, the centrifugal stretching will come in to play. So, for an energy level

$$F(J, K) = BJ(J + 1) - (B - C)K^2 - D_J J^2(J + 1)^2 - D_{JK} J(J + 1)K^2 - D_K K^4$$

where D_J, D_{JK}, and D_K are known as distortion constants. By considering centrifugal distortion, the wave-number of a radiative transition between level J and $(J + 1)$ will become

$$\bar{\nu} = 2B(J + 1) - 4D_J(J + 1)^3 - 2D_{JK}J(J + 1)K^2$$

(b) Prolate Symmetric Top Molecules: For a rigid prolate symmetric top molecule, we have $I_a < I_b = I_c$. The energy of an energy level is given by

$$E(A, B, C) = \frac{\mathbf{J}_a^2}{2I_a} + \frac{\mathbf{J}_b^2 + \mathbf{J}_c^2}{2I_c}$$

where $\mathbf{J}_a$, $\mathbf{J}_b$, and $\mathbf{J}_c$ are components of angular momentum, related to rotational quantum number by the following expressions

$$\mathbf{J}_a^2 + \mathbf{J}_b^2 + \mathbf{J}_c^2 = J(J + 1)\hbar^2$$

and

$$\mathbf{J}_c = K\hbar$$

where K is the projection of rotational angular momentum on a-axis, also written as k_a. The eigenvalues of the wave-number of an energy level are given by

$$F(J, K) = BJ(J + 1) + (A - B)K^2$$

Also, the wave-number of radiative transition between level J and $(J + 1)$ becomes will be given by

$$\bar{\nu} = F(J + 1, K) - F(J, K) = 2B(J + 1)$$

If the molecule is not rigid, the centrifugal stretching will come in to play. So, for an energy level

$$F(J, K) = BJ(J + 1) + (A - B)K^2 - D_J J^2(J + 1)^2 - D_{JK}J(J + 1)K^2 - D_K K^4$$

where D_J, D_{JK}, and D_K are known as distortion constants. By considering centrifugal distortion, the wave-number of a radiative transition between level J and $(J + 1)$ will become

$$\bar{\nu} = 2B(J+1) - 4D_J(J+1)^3 - 2D_{JK}J(J+1)K^2$$

(iv) Asymmetric Top Molecules: For asymmetric top molecules, we have $I_a < I_b < I_c$. The energy of an energy level is given by

$$E(A,B,C) = \frac{\mathbf{J}_a^2}{2I_a} + \frac{\mathbf{J}_b^2}{2I_b} + \frac{\mathbf{J}_c^2}{2I_c}$$

Thus, we will get

$$F(A,B,C) = \frac{A\mathbf{J}_a^2 + B\mathbf{J}_b^2 + C\mathbf{J}_c^2}{\hbar^2}$$

For asymmetric top molecules, K is not a good quantum number. The energy levels for a given value of J are represented as $J_{ka,kc}$ or J_τ, where $\tau = k_a - k_c$, is the pseudo quantum number having values ranging from $-J$ to $+J$ in increments of one. Also, there is no preferential axis so the inertial axes a,b, and c can be identified in six possible ways w.r.t space fixed axes x, y, and z which will give the energy of transition between rotational energy levels.

1.9 Theory of Radiative Transitions

In any atomic, molecular, or ionic system, there exist a number of discrete energy levels. A system (particle) goes from a lower level to a higher level by absorbing energy exactly equal to the gap between those energy levels. The process is known as excitation. An equal amount of energy is released in the de-excitation process. The process of excitation and de-excitation may or may not involve a photon. The process will be called radiative if a photon is involved. A non-radiative process does not involve a photon. The collisional excitation and de-excitation are non-radiative processes. The number of excitations due to collisional transitions will be small if the gap between energy levels is large as compared to k_BT, where k_B is Boltzmann's constant. In this section, we will discuss the types and importance of radiative transitions.

1.9.1 Types of Radiative Transitions

The radiative transitions are categorized into three types as described below:

(i). Induced (Stimulated) Absorption: A transition from lower energy level *i* to higher energy level *j* with the application of external energy source is known as stimulated or induced absorption. The energy *hv* required for absorption is exactly equal to the gap between energy levels i.e. $hv = E_j - E_i$, provided that the transition is allowed by selection rules.

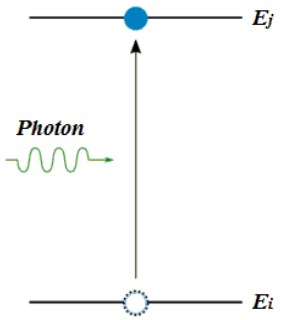

Figure 1.2: Induced absorption in two energy levels

This process tends to increase the population of the upper energy state. The rate of change of population of higher energy state is proportional to the number of atoms n_i in the lower energy state and energy density ρ(ν) of photons. Thus, we will get

$$\frac{dn_j}{dt} = B_{ij} n_i \rho(\nu)$$

The proportionality constant B_{ij} is known as Einstein B-coefficient for induced absorption. It represents the probability of induced absorption of radiation.

(ii). Spontaneous Emission: A system in excited state has a very small lifetime so it quickly de-excites to lower state by emitting a photon of energy *hv* same as the gap between higher and lower energy levels *i.e.* $hv = E_j - E_i$. The emission process is known as spontaneous as no external source is required for this transition.

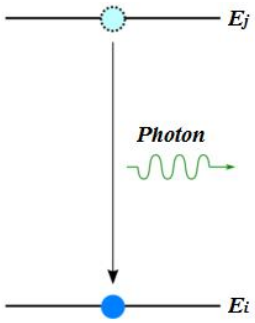

Figure 1.3: Spontaneous emission in two energy levels.

This emission occurs in an isotropic manner i.e. the probability of emission is the same in every direction. This transition tends to decrease the population of the upper energy level. The rate of change of population of higher energy state depends on the number of atoms n_j in the upper energy level only as no other agency is involved. Thus, we will get

$$-\frac{dn_j}{dt} = A_{ji}n_j$$

Here, the negative sign represents the decrease in population of level j. Also, the proportionality constant A_{ji} is known as Einstein A-coefficient for a radiative transition. It gives the probability of spontaneous emission of radiation.

(iii). Stimulated Emission: If a photon of energy $h\nu = E_j - E_i$ strikes a molecule in an excited state, it may cause its de-excitation resulting in the emission of two coherent photons i.e. two photons of same energy $h\nu$ which are in phase with each other.

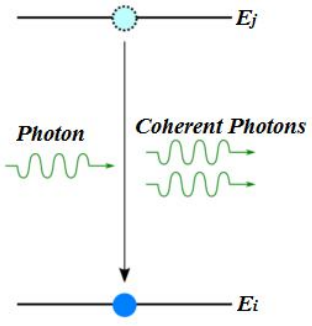

Figure 1.4: Stimulated emission in two energy levels.

The radiative lifetime of the system in the upper energy state should be large for this transition to be more probable. The rate of decrease of the population of the upper energy state is proportional to the number of atoms n_j in the higher energy state and energy density ρ(ν) of photons. Thus, we will get

$$-\frac{dn_j}{dt} = B_{ji} n_j \rho(\nu)$$

The negative sign again represents the decrease in population of level *j*. Also, the proportionality constant B_{ji} is known as Einstein B-coefficient for stimulated emission. It represents the probability of stimulated emission of radiation, which is responsible for MASER action.

1.9.2 Relation Between Einstein A and B Coefficients

To calculate the net rate of change of population in any energy level *j*, we have to consider all three transitions discussed above. At equilibrium, the net rate should become zero *i.e.* the total number of absorptions and emissions will become equal. Thus at equilibrium, we will have

$$\frac{dn_j}{dt} = B_{ij} n_i \rho(\nu) - A_{ji} n_j - B_{ji} n_j \rho(\nu) = 0$$

which implies

$$\rho(\nu) = \frac{A_{ji}}{\frac{B_{ij} n_i}{n_j} - B_{ji}}$$

The Planck's radiation law for energy density of radiation is

$$\rho(\nu) = \frac{8\pi h\nu^3}{c^3} \frac{1}{e^{\frac{h\nu}{kT}} - 1}$$

where T is the kinetic temperature. The ratio of population densities in two energy levels is given by Boltzmann relation as

$$\frac{n_j}{n_i} = \frac{g_j e^{\frac{-E_j}{kT}}}{g_i e^{\frac{-E_i}{kT}}} = \frac{g_j}{g_i} e^{\frac{-(E_j - E_i)}{kT}}$$

where g_j and g_i are statistical weights, E_j and E_i are the energies of higher and lower levels respectively. Thus, we will get

$$\frac{n_j}{n_i} = \frac{g_j}{g_i} e^{\frac{-h\nu}{kT}}$$

where $h\nu = E_j - E_i$ denotes the energy gap between two levels. From the above equations, we get

$$g_i B_{ij} = g_j B_{ji}$$

and

$$A_{ji} = \frac{8\pi h\nu^3}{c^3} B_{ji}$$

The above equations give the relation between Einstein's coefficients. Therefore, once the Einstein A-coefficient for an allowed radiative transition is known, both the Einstein B-coefficients can be determined with the help of these equations.

1.10 Theory of Collisional Transitions

A molecule may be excited or de-excited due to collision with other molecules in that region [32–37]. Let us describe a general collision of a particle X with a molecule M. Let the molecule M is in its initial state (*i*), then this state may change after the collision due to exchange of energy with the particle X. Let the final state of molecule be represented as (*f*). Thus, the transition may be written as

$$M(i) + X \rightarrow M(f) + X$$

In excitation of the molecule, the energy of the final state is more than the energy of the initial state (*i*) while it is lesser than the energy of the initial state in de-excitation. The collisional transitions dominate when the gap between energy levels is small. Unlike radiative transitions, the collisional transitions do not obey any selection rules. However, the colliding partner X must have sufficient energy for the excitation of the molecule.

The most abundant element in ISM is hydrogen (H). In the regions where molecules are found, the hydrogen is in the form of molecular hydrogen (H_2).

Therefore, we neglect the collisions of our molecule with other molecules and consider collisions with only H_2 molecules. The rates of collisional transitions may play a crucial role in the calculation of population density of molecules at a level.

1.11 Various Temperatures used in Study of Interstellar Molecules

(i). Kinetic Temperature (T): A temperature representing the thermal motion of the molecules is known as kinetic temperature. The thermal energy of molecules is equal to the kinetic energy of the molecules and the distribution of their velocities follows Maxwell-Boltzmann distribution.

(ii). Excitation Temperature (T_{ex}): When molecules absorb energy through radiative, collisional, or any other means, it reaches to an excited energy state. This excitation energy of the transition is represented by the excitation temperature of the molecule.

(iii). Background Temperature (T_{bg}): The radiations from cosmic microwave background are continuously being emitted. The temperature of CMB is T_{bg} = 2.73 K.

(iv). Brightness Temperature (T_B): A measure of the received intensity of a spectral line w.r.t. the CMB. Its value is positive if the intensity of the observed line is more than CMB, thus representing the net emission of a molecule w.r.t. CMB. It will be negative if the intensity of the observed line is less than that of CMB, known as anomalous absorption.

1.12 Anomalous Phenomena in Interstellar Molecules

In addition to normal emission and absorption, certain molecules in the interstellar medium are observed to exhibit anomalous phenomena. There are two types of anomalous phenomena the molecules can show; namely MASER action and Anomalous absorption.

1.12.1 Microwave Amplification by Stimulated Emission of Radiation (MASER)

The MASER is possible when the population of a higher energy level becomes greater than the lower energy level. The intensity of observed radiation, in this case,

will be large. The molecules exhibiting this phenomenon are known as natural Masers.

The OH molecule was the first molecule that was detected in the interstellar medium in 1963. The line profile of its 18 cm line provided a kinetic temperature around 100 K and brightness temperature around 1000 K. From the line profile, the kinetic temperature is found by half-width and brightness temperature is obtained by the height of the line profile. Such a high brightness temperature indicated maser action but the idea of natural masers was not easily accepted by the majority of the scientists, so the measurements were again done by using Very Large Baseline Interferometry (VLBI) with much-improved resolution. For the 18cm line, the kinetic temperature was again found to be near 100 K but the brightness temperature was found to be approximately 10^{12} K. The kinetic temperature can't have such a high value of temperature so the only option left was to accept the existence of natural masers. In cosmic objects, SiO, H_2O, and OH are the best examples of masing molecules.

1.12.2 Anomalous Absorption

The cosmic microwave background plays a significant role in the study of interstellar molecules. It has a temperature of 2.73 Kelvin, so all the observed transitions are expected to have brightness temperature more than background temperature. However, there are few observed transitions that are found to have a brightness temperature of less than 2.73 Kelvin, which shows the absorption against the CMB. This is known as anomalous absorption.

Table 1.1: List of molecules detected in various cosmic objects.

No. of atoms	Molecules detected in ISM
2	OH, CO, SiO, NO, H_2, N_2, C_2, O_2, HCl, NaCl, KCl, CP, CS, CN, CH, SO, SH, PN, PO, HF, NH, NS, AlF, AlCl, AlO, SiN, SiS, SiO, SiC, FeO, HD, TiO, CO^+, NO^+, CH^+, SO^+, ArH^+, MgH^+, SH^+, HeH^+, CN^+, CN^-, CF^+, OH^+.
3	HCN, KCN, H_2O, CO_2, SO_2, NaOH, C_3, C_2H, NaCN, O_3, AlNC, AlOH, CCN, HCS, C_2O, C_2S, C_2P, CaNC, FeCN, H_2C, HO_2, MgNC, OCS, H_2S, HNC, HCO, HDO, D_2O, DCN, DCO, DNC, HCP, HNO, HSC, MgCN, NH_2, N_2O, *c*-SiC2, SiCSi, SiCN, SiNC, TiO_2, H_2O^+, HN_2^+, N_2D^+, HD_2^+, H_2D^+, HCO^+, HCS^+, HOC^+, H_3^+, H_2Cl^+.
4	NH_3, CH_3, H_2CO, H_2SiO, H_2CS, H_2CN, SiC_3, *l*-C_3H, *c*-C_3H, C_3O, C_3N, HCCO, HNO_2, HMgNC, HSCN, HNCS, HOOH, HNCO, CNCN, HCNO, C_2H_2, PH_3, ND_3, NHD_2, NH_2D, DNCO, HDCO, C_2HD, D_2CO, D_2CS, $HOCO^+$, $HCNH^+$, H_3O^+, C_3N^-, *l*-C_3H^+.
5	CH_4, H_2CCN, H_2C_2O, SiH_4, SiC_4, C_5, HCOCN, HCOOH, HNCNH, CH_3O, *c*-C_3H_2, *l*-H_2C_3, C_4H, HCCNC, NH_2CN, CH_2NH, $NCCNH^+$, H_2COH^+, NH_3D^+, CH_4^-, NH_4^+.
6	CH_3OH, CH_3CN, C_5H, C_5N, C_5S, HC_2CHO, HC_4N, CH_2CNH, $HCONH_2$, *l*-H_2C_4, *c*-H_2C_3O, HNCHCN, C_2H_4, CH_3NC, CH_3SH, NH_2CDO, NHDCHO, HC_3NH^+.
7	H_3CNH_2, H_2CHCOH, C_6H, CH_3NCO, $HOCH_2CN$, *c*-C_2H_4O, CH_3C_2H, CH_2CHCN, CH_2DCCH, CH_3CCD, HC_4CN, HC_5O, CH_3CHO, C_6H^-.
8	CH_3COOH, CH_2CHCHO, H_3CC_2CN, NH_2CH_2CN, $H_2COHCHO$, $HCOOCH_3$, H_2C_6, $(NH_2)_2CN$, CH_2CCHCN, CH_3CHNH, C_7H.
9	CH_3OCH_3, CH_3CH_2OH, CH_3CHCH_2, CH_3C_4H, CH_3CH_2CN, CH_3CONH_2, HC_7N, CH_3CH_2SH, C_8H.
10	NH_2CH_2COOH, $(CH_3)_2CO$, CH_3C_5N, $(CH_2OH)_2$, CH_3CHCH_2O. CH_3CH_2CHO, CH_3OCH_2OH.
>10 atoms	CH_3COOCH_3, HC_8CN, C_2H_5OCHO, CH_3C_6H, C_6H_6, $(CH_3)_2CHCN$, C_3H_7CN, $HC_{10}CN$, C_6H_5CN, C_{60}, C_{70}, C_{60}^+.

Table 1.2: List of cosmic molecular laboratories

Object	**Right ascension (α)**	**Declination (δ)**
16 Cygni B	$19^h\ 41^m\ 48.95^s$	$50^o\ 31'\ 30.2''$
55 Cygni	$20^h\ 48^m\ 56.29^s$	$46^o\ 06'\ 50.88''$
B1-b Cloud	$3^h\ 33^m\ 20.8^s$	$31^o\ 07'\ 34''$
Benard 1	$3^h\ 33^m\ 20.8^s$	$31^o\ 7'\ 34''$
Cassiopeia A	$23^h\ 23^m\ 26^s$	$58^o\ 48'\ 00''$
Cernis 52	$3^h\ 43^m\ 0.3^s$	$31^o\ 58'\ 26''$
CLD 2	$4^h\ 38^m\ 21^s$	$25^o\ 41'\ 00''$
CRL 618	$4^h\ 42^m\ 53.64^s$	$36^o\ 00'\ 53.5''$
Cygni OB2-12	$20^h\ 32^m\ 40.95^s$	$41^o\ 14'\ 29.28''$
DR21(OH)	$20^h\ 39^m\ 02^s$	$42^o\ 19'\ 38''$
Epsilon Persei	$03^h\ 57^m\ 51.232^s$	$40^o\ 00'\ 36.7752''$
GL 2591	$20^h\ 27^m\ 35.8^s$	$40^o\ 01'\ 14''$
HD 124314	$14^h\ 15^m\ 1.606^s$	$-16^o\ 42'\ 24.38''$
HD 27778	$4^h\ 23^m\ 59.76^s$	$24^o\ 18'\ 3.563''$
Horsehead Nebula	$5^h\ 40^m\ 59^s$	$-02^o\ 27'\ 30''$
IC 443G Nebula	$06^h\ 13^m\ 42^s$	$22^o\ 33'\ 30''$
IRAS 04368+2557	$4^h\ 39^m\ 53.59^s$	$26^o\ 03'\ 5.5''$
IRAS 16293-2422	$16^h\ 32^m\ 22.6^s$	$-24^o\ 28'\ 33.0''$
IRC+10216	$09^h\ 47^m\ 57.406^s$	$13^o\ 16'\ 43.56''$
L134 (Dark Cloud)	$15^h\ 51^m\ 26^s$	$-2^o\ 43'\ 31''$
NGC 1333	$3^h\ 29^m\ 02^s$	$31^o\ 20'\ 5''$
NGC 1333 IRAS 2	$3^h\ 28^m\ 49.7^s$	$31^o\ 14'\ 47''$
NGC 1333 IRAS 4A	$3^h\ 29^m\ 10.49^s$	$31^o\ 13'\ 31''$
NGC 1952	$5^h\ 34^m\ 30^s$	$22^o\ 01'\ 00''$
NGC 2024	$5^h\ 41^m\ 54^s$	$-01^o\ 51'\ 00''$
NGC 2264	$06^h\ 41^m\ 06^s$	$09^o\ 53'\ 00''$
NGC 4945	$13^h\ 05^m\ 27.5^s$	$-49^o\ 28'\ 06''$
NGC 6210	$16^h\ 44^m\ 29.5^s$	$23^o\ 47'\ 59.7''$
NGC 6334	$17^h\ 19^m\ 58^s$	$-35^o\ 57'\ 47''$

Object	**Right ascension (α)**	**Declination (δ)**
NGC 7023	$21^h\ 00^m\ 05^s$	$68^o\ 10'\ 00''$
NGC 7027	$21^h\ 07^m\ 1.7^s$	$42^o\ 14'\ 11''$
NGC 7538	$23^h\ 13^m\ 45.7^s$	$61^o\ 28'\ 21''$
NGC 7822	$0^h\ 3^m\ 00^s$	$68^o\ 37'\ 00''$
Orion Nebula	$05^h\ 35^m\ 17.3^s$	$-05^o\ 23'\ 28''$
Red rectangle nebula	$6^h\ 19^m\ 58.21^s$	$-10^o\ 38'\ 14.69''$
Rho Ophiuchi	$16^h\ 28^m\ 06^s$	$-24^o\ 32'\ 30''$
Rosette Nebula	$06^h\ 33^m\ 45^s$	$04^o\ 59'\ 54''$
Sgr B2	$17^h\ 44^m\ 9.5^s$	$-28^o\ 21'\ 20''$
SK 66-169	$05^h\ 36^m\ 54.50^s$	$-66^o\ 38'\ 25''$
TMC 1	$4^h\ 38^m\ 38.6^s$	$25^o\ 36'\ 18''$
V Y Canis Majoris	$7^h\ 22^m\ 58.32^s$	$-25^o\ 46'\ 3.23''$
W3 (OH)	$2^h\ 27^m\ 4.1^s$	$61^o\ 52'\ 22''$
W33A	$18^h\ 14^m\ 14.4^s$	$-17^o\ 55'\ 50''$
W49	$19^h\ 10^m\ 17^s$	$9^o\ 06'\ 00''$
W51	$19^h\ 21^m\ 27^s$	$14^o\ 24'\ 30''$
Zeta Ophichuhi	$16^h\ 37^m\ 9.539^s$	$-10^o\ 34'\ 1.52''$
Zeta Persei	$03^h\ 54^m\ 7.922^s$	$31^o\ 53'\ 1.0812''$

CHAPTER 2: LITERATURE REVIEW

2.1 Prebiotic Molecules and Origin of Life

The molecules which are related to or are responsible for the origin of life are known as prebiotic molecules. It is believed that prebiotic evolution from minuscule to astronomically immense and intricate molecules may have resulted in the inception of life [38–47]. Alexandre Oparin (1924) and J.B.S. Haldane (1929) proposed that the primitive earth contained a reducing atmosphere in which organic molecules were produced from abiogenic (inorganic) materials. This was verified experimentally in 1953 by Harold Urey and his student Stanley Miller, which is famously known as Miller-Urey experiment. They demonstrated the synthesis of organic materials from inorganic materials which contravened prevalent sense at that time. The details of the Miller-Urey Experiment are given below:

In 1952, Harold Urey endeavored to ascertain the atmospheric content of the primitive Earth. From his calculations, he concluded that the early atmosphere consisted of methane, ammonia, hydrogen, and water. He asked his student Stanley Miller to experimentally synthesize the organic compounds in that kind of atmosphere. Miller followed the advice and attempted an experiment [48]. He took all the above-said gases, along with water in a flask, and passed an electric discharge of 60 kV voltage. The experimental arrangement of the Urey Miller experiment is shown in figure 2.1.

It was observed that ammonia and methane were consumed in a week, and the carbon monoxide and nitrogen were the main gaseous products. But, to his surprise, there was a dark material accumulated on water. Their analysis of this material confirmed the presence of amino acids in it. The amino acids are basic units of proteins which are essential building blocks of biological systems. This research was immediately recognized as a major breakthrough in the theory of the origin of life. It was concluded that the primitive earth consisted of these kinds of molecules that could have been formed in the conditions as described by Oparin and Haldane. These prebiotic molecules then underwent various chemical processes, leading to the inception of life.

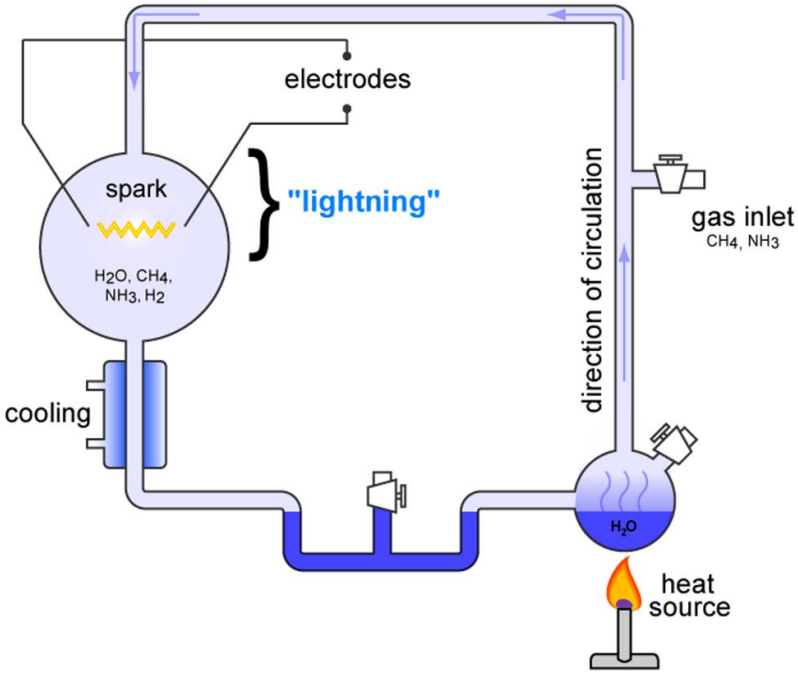

Figure 2.1 Experimental setup of the Miller-Urey experiment

2.2 Attempts for the Search of Life in the Interstellar Medium

Since the beginning of civilization, people have a curiosity about whether we are alone in the universe or any other intelligent life form exists elsewhere. The scientific investigation about the search for life began at the start of the twentieth century. Some of the major efforts made are described below:

(i) Search for Extraterrestrial Intelligence (SETI) Program

After some preliminary ideas in the early twentieth century, scientists formulated a new approach to answering this question in 1959 by using radio astronomy to listen for extraterrestrial intelligent life. SETI is a collective term for the search for intelligent extraterrestrial life which primarily includes tracking the electromagnetic radiations for signs of transmissions from civilizations on other planets.

The National Aeronautics and Space Administration (NASA) joined the program in 1975 and left in 1993. The Berkeley SETI Research center (BSRC) has

several searches operating at different wavelengths from radio to visible light. These include SERENDIP, SEVENDIP, NIROSETI, SETI@home, Breakthrough Listen, etc. The latest project "Breakthrough Listen" (2016) seeks to discover evidence of extraterrestrial life by looking for radio waves across stars and galaxies. The quest is carried out on the Green Bank Telescope in the Northern Hemisphere and the Parkes Telescope in the Southern Hemisphere. It is the most extensive attempt for alien communications to date and is expected to be completed in the year 2026.

As many SETI initiatives have progressed, some scientists have questioned early claims as being too euphoric where the results are unlikely to be positive. Some critics also call it a form of pseudoscience as it is alleged that no phenomenon is observed which can prove the existence of extraterrestrial intelligence. However, SETI remains a part of mainstream astronomy as it can't avoid affiliation with believers in UFOs and other crackpots of this kind. SETI is also potentially not a falsifiable study because of how extensively the cosmos is scanned, the null finding of radio silence will not rule out the presence of alien cultures. It may be attributed to the reason that those civilizations might not be using radio waves to communicate.

(ii) Mars Exploration

(a) NASA's Follow the Water Strategy: The liquid water (H_2O) is a necessary but not sufficient condition for the existence of life, as habitability is a function of a multitude of environmental parameters. The scientists are eagerly searching for liquid water in regions other than Earth. If discovered, such locations will be the most convincing sites to search for an answer to the issue of whether life exists outside our home planet. The strategy of NASA is to find the locations on Mars with signs of past or present water activity and the materials suitable for the survival of any bio-signatures or life-habitable environments.

(b) ISRO: Mars Orbiter Mission: Mars Orbiter Mission (MOM) of Indian Space Research Organisation (ISRO) is India's first bid into the interplanetary space. In this mission, along with studying and examining the Mars surface features, mineralogy and atmosphere, an advanced search for Methane (CH_4) and Carbon Dioxide (CO_2)

in the Martian atmosphere is carried out that will provide information of future or past presence of life on the planet.

From the above discussion and present-day knowledge about all forms of life, we have found that existence of some or all of the four key elements namely, Carbon (C), Nitrogen (N), Hydrogen (H) and Oxygen (O) have greater significance in the existence of life. Thus, the search of methanimine molecule (CH_2NH) is also of particular importance.

2.3 Prebiotic Molecules in the Interstellar Medium

A great deal of attention has been focused by many researchers around the world to identify interstellar prebiotic molecules that may provide a crucial understanding of our solar system and even the evidence of the origin of life outside, i.e. in the interstellar medium [49–52]. This is because the interstellar medium is enriched with astronomically immense varieties of molecules ranging from very simple to complex forms, with astrobiological importance, which might have undergone evolution and recycling continuously and repeatedly, and may be able to provide valuable insight to the origin of life.

The amino acids on earth are building blocks of proteins which are vital components of all living organisms. A number of attempts to search the simplest amino acid glycine (NH_2CH_2COOH) in cosmic objects were reported to be unsuccessful [53,54] before its detection was given by Kuan et al. [55]. However, the presence of glycine in the interstellar medium is not confirmed in subsequent studies [56]. It is still one of the most challenging tasks to modern astronomers and astrologists with quite a number of interesting perceived views on the formation of amino acids in the ISM [57–62]. The precursors of amino acids are considered as prebiotic molecules and their identification in cosmic objects is of particular importance for scientists and researchers across the world. Some of the prebiotic molecules identified in the interstellar medium are given in Table 2.1.

2.4 Methanimine (CH_2NH) Molecule

Methanimine is the simplest molecule containing a C=N double bond. It is also known as methyleneimine or formaldimine. It is an a and b type asymmetric top molecule with the magnitude of electric dipole moment components along a & b molecular axes as 1.3396 Debye and 1.4461 Debye [63], respectively. The methanimine is considered a prebiotic molecule as it is a potential precursor of aminoacetonitrile (NH_2CH_2CN) [58,64] which is a key molecule in the formation of glycine (NH_2CH_2COOH), the simplest amino acid [65,66]. The amino-acids like glycine on earth are elementary constituents of proteins, which are necessary for life to occur. The search for the mechanism of the formation of amino acids and their prebiotic precursor molecules is crucial to help reveal the processes that may have led to the origin of life [60]. Their origin in the prebiotic environment of early Earth is a fascinating subject for researchers around the world [67–69]. The focus of our research work is on their precursor molecule methanimine in the interstellar medium that will enhance our understanding of the universe and of life existing anywhere in the universe.

2.5 Formation of Methanimine in Interstellar Medium

The formation of CH_2NH in the ISM is a matter of debate among the researchers. A number of possible paths are described which lead to the formation of Methanimine in ISM. The ion-molecule reactions are one of them which are taken as the dominant gas-phase reactions at low temperatures as given below:

$$CH_3^+ + NH_2 \rightarrow CH_2NH_2^+ + H$$

Further, the dissociative recombination of $CH_2NH_2^+$ with an electron produces CH_2NH [70]. The gas grain chemical simulations done by Suzuki et al. [71] predicted that in gas phase, the methanimine is mostly formed by neutral-neutral reactions instead of the thermal evaporation from dust surfaces. The reaction NH + CH_3 was found to be the dominating process of the formation of Methanimine. Another mechanism of formation of CH_2NH is taken as a series of hydrogenation reactions [72–74] that may occur on the grain surface as given below:

$$HCN \xrightarrow{H} CH_2N \xrightarrow{H} CH_2NH \xrightarrow{H} CH_2NH_2 \xrightarrow{H} CH_3NH_2$$

The CH_2N and CH_2NH_2 are radical species which are expected to be short-lived. The methanimine is an intermediate molecule that is a stable molecule that may yield methylamine upon saturation. The CH_2NH molecule can also be formed by ammonia (NH_3) and formaldehyde (HCHO) [75], which are well-known species in ISM, by the following reaction

$$NH_3 + HCHO \rightarrow CH_2NH + H_2O$$

The possibility of formation of Methanimine in IRC+10216 cloud by gas-phase neutral–neutral reactions is reported by Tenenbaum [76], which considers the creation of CH_2NH molecule by the reaction of CH and NH_3, with subsequent decomposition to CH_2NH and H.

2.6 Detection of Methanimine in Interstellar Medium

The methanimine molecule is of particular interest among researchers across the globe. It was first detected in 1973 by Godfrey [77] et al. and since then, it is found in many cosmic objects as given in Table 2.2. The detailed explanation is given below:

Godfrey et al. (1973) [77] detected the methanimine molecule (CH_2NH) for the first time by microwave spectroscopy in the molecular cloud Sgr B2 towards the galactic center. Its presence was estimated in the interstellar medium because similar species like formaldehyde [75] and thioformaldehyde [78] were already found there. Also, nitrogen itself was found to be present in a number of molecules like CN, HCN, NH_3, HC_3N, CH_3CN, HCNO and $HCONH_2$ etc. Sufficiently large concentrations of ammonia and formaldehyde were found in the galactic center and this appeared to be the best place to search for methanimine. This identification of Methanimine was done using a 64 m telescope at Parkes that was equipped with a 6 cm cryogenic parametric receiver with 90 Kelvin as system noise temperature. The beamwidth of the telescope was 3.8 arc min at 5.3 GHz, the aperture efficiency, and beam efficiency of about 45% and 70% respectively. The receiver output was analyzed with a 64 channel spectrometer with a filter bandwidth of 33 kHz. The data was analyzed by a PDP-9 computer. The performance of the receiver was checked by observation of the

H107 alpha recombination line at 5.293733 GHz in Sgr B2 and Orion A. The $1_{10} \rightarrow 1_{11}$ transition of CH_2NH was detected in the emission of Sgr B2 at 5.29 GHz at a radial velocity of about 63000 m/sec, at which the frequency was in accordance with the transitions detected in the laboratory.

Turner et al. (1989) [79] performed the survey observations of giant molecular cloud Sgr B2 in 70 to 115 GHz range using NRAO 11m telescope. They reported the $4_{04} \rightarrow 3_{13}$ transition of CH_2NH in Sgr B2 and Orion KL at 105.795 GHz frequency.

Sutton et al. (1991) [80] surveyed submillimeter molecular line emission in dense cores in Sgr B2 and found sharp variation in chemical composition at small spatial scales. They reported three transitions of methanimine in Sgr B2(M) namely, $5_{14} \rightarrow 4_{13}$ transition at 332.5728 GHz, $3_{13} \rightarrow 2_{02}$ at 340.3538 GHz, and $10_{1,9} \rightarrow 10_{0,10}$ at 351.9543 GHz.

Dickens et al. (1997) [81] conducted a survey for methanimine in molecular clouds Orion-KL, W51, W49, G34.3 + 0.15, Ori 3N, TMC 1 and L134N and determined the abundance of methanimine there. They detected 15 transitions of methanimine as given in Table 2.2.

Nummelin et al. (1998) [82] conducted a spectral line survey of Sgr B2 in the range of 218 GHz to 263 GHz using the Swedish-ESO submillimeter telescope and reported the transitions $1_{11} \rightarrow 0_{00}$ and $6_{15} \rightarrow 6_{06}$ of methanimine at 225.555 GHz and 226.5490 GHz respectively.

Turner et al. (1999) [70] reported the weaker $2_{11} \rightarrow 1_{10}$ and $1_{11} \rightarrow 0_{00}$ transitions of CH_2NH at 133.272047 GHz and 225.554690 GHz respectively in L183 using NRAO 12 m telescope. However, it was not detected in the large column density translucent objects CB 17, CB24, and CB288.

White et al. (2003) [83] made a submillimeter wavelength spectral line survey of Orion-KL hot cloud core in the range 455.1 GHz to 507.4 GHz using James Clerk Maxwell Telescope in Hawaii. He reported three transitions of methanimine $7_{16} \rightarrow 6_{15}$, $2_{21} \rightarrow 2_{12,}$ and $8_{08} \rightarrow 7_{07}$ at frequency 464.570359 GHz, 500.475691 GHz, and 501.679997 GHz respectively.

Jones et al. (2008, 2011) [84][85] mapped the distribution of Methanimine in Sgr B2 at 3 mm and 7 mm using the MOPRA telescope and noticed it spreading from Sgr B2(N) to Sgr B2 (S), with an emission peak close to Sgr B2 (N). They have reported the transitions $4_{04} \rightarrow 3_{13}$ and $3_{03} \rightarrow 2_{12}$ of methanimine at 105.79 GHz and 35.07 GHz respectively.

Salter et al. (2008) [86] reported the detection of methanimine in Arp 220 galaxy in its spectral line survey in the range 1.1 GHz to 10 GHz. They have reported the transition $1_{10} \rightarrow 1_{11}$ at 5.289813 GHz and predicted a considerably high abundance of CH_2NH.

Qin et al. (2010) [87] presented the submillimeter array observations of spectral lines in the molecular cloud G19.61-0.23 in the range 330 GHz to 340 GHz. They have reported the transition $3_{13} \rightarrow 2_{02}$ at 340.354315 GHz for methanimine molecule.

Tenenbaum et al. (2010) [76] performed a spectral line survey of IRC+10216 using 1 mm SMT of Arizona Radio Observatory. They have detected 9 transitions of methanimine in the circumstellar envelope of IRC+10216 in the range 215-285 GHz as given in Table 2.2.

Halfen et al. (2013) [88] performed a molecular line survey of Sgr B2(N)at 1,2 and 3mm using SMT at Arizona Radio Observatory from frequency 68 GHz to 280 GHz. The 23 reported transitions of methanimine are given in Table 2.2. The methanimine is found to be present in cold gas near Sgr B2(N) and not only confined to the hot cores.

Suzuki et al. (2016) [71] conducted survey observations of CH_2NH towards eight high mass forming regions G10.47 + 0.03, NGC6334F, Orion KL, G34.3 + 0.2, G 31.41 + 0.31, DR21 (OH), W51 e1/e2, G 19.61 – 0.23 using NRO 45m telescope. Out of these, there are four new sources G10.47 + 0.03, NGC6334F, G 31.41 + 0.31, and DR21 (OH) in which CH_2NH was detected. They detected four transitions $4_{04} \rightarrow 3_{13}$, $1_{11} \rightarrow 0_{00}$, $4_{14} \rightarrow 3_{13,}$ and $4_{23} \rightarrow 3_{22}$ of methanimine at 105.794062 GHz, 225.554609 GHz, 245.125806 GHz, and 255.840311 GHz respectively.

2.7 Laboratory Spectrum of Methanimine

A number of transitions between rotational energy levels of methanimine are observed in terrestrial laboratories shown in Table 2.3. The detailed explanation is given below:

Johnson and Lovas (1972) [89] were first to record the laboratory microwave rotational spectrum of methanimine in the gas phase in the frequency range of 60 GHz to 123 GHz. Several high J rotational transitions were observed from which rotational constants were derived. The study was extended to many isotopologues of Methanimine by Pearson and Lovas(1977) [90].

Halonen and Duxbury (1985) [91] recorded the infrared spectrum of CH_2NH in 10 μm region with a resolution of 0.0048 cm^{-1} using the National Solar Observatory Fourier Transform spectrometer. The spectrum of methanimine was found to be more complex than HCOOH and H_2N_2 due to large values of coriolis coupling constants.

Dore et al. (2010) [92] recorded the transitions having frequency between 64 GHz to 172 GHz in CH_2NH. In the rotational spectrum of methanimine, they examined the magnetic hyperfine structure using lamb dip technique. Again, Dore et al. (2012) [93] extended the measurements into submillimetre- wave region (329 – 629 GHz) to provide the accurate rest frequencies of Methanimine.

Y. Motoki et al. (2014) [94] studied the terahertz spectroscopy of Methanimine in the frequency range 120 – 1600 GHz. The detail of all the reported transitions in the laboratory spectrum of CH_2NH is shown in Table 2.3. The rotational and centrifugal distortion constants were measured with great accuracy and are given in Table 2.4.

Table 2.1: Some of the prebiotic molecules detected in the interstellar medium

Molecule	Reference
Carbon Monoxide (CO)	[95–103]
Cyanide Radical (CN)	[104–106]
Hydroxyl Radical (OH)	[12,107–109]
Hydrogen Cyanide (HCN)	[110,111]
Carbon Dioxide (CO_2)	[112–116]
Methylene (CH_2)	[117–120]
Protonated Carbon Dioxide ($HOCO^+$)	[121,122]
Water (H_2O)	[123–128]
Ammonia (NH_3)	[129–133]
Methyl Radical (CH_3)	[134,135]
Methane (CH_4)	[136–138]
Formaldehyde (HCHO)	[139–148]
Methanol (CH_3OH)	[149–152]
Formic acid (HCOOH)	[153–155]
Formamide (NH_2CHO)	[156–158]
Ketenimine (CH_2CNH)	[159]
Ethanimine (CH_3CHNH)	[160–162]
E-cyanomethanimine (HNCHCN)	[163–165]
Methylamine (CH_3NH_2)	[166–169]
2-Aminopyridine ($H_2NC_5H_4N$)	[170]
Polycyclic Aromatic Hydrocarbons (PAH)	[171,172]
Aminoacetonitrile (NH_2CH_2CN)	[66]

Table 2.2: The transitions of CH_2NH detected in various cosmic objects.

Transition	**Frequency (GHz)**	**Source**	**Reference**
$1_{10} \rightarrow 1_{11}$	5.29	Sgr B2	[77]
$4_{04} \rightarrow 3_{13}$	105.795	Sgr B2, Ori-KL	[79]
$5_{14} \rightarrow 4_{13}$	332.5728	Sgr B2 (M)	[80]
$3_{13} \rightarrow 2_{02}$	340.3538		
$10_{1,9} \rightarrow 10_{0,10}$	351.9543		
$2_{11} \rightarrow 2_{02}$	172.267113	Orion-KL	[81]
$1_{11} \rightarrow 0_{00}$	225.554692		
$4_{14} \rightarrow 3_{13}$	245.125974		
$7_{16} \rightarrow 7_{07}$	250.161865		
$6_{06} \rightarrow 5_{15}$	251.421379		
$1_{11} \rightarrow 0_{00}$	225.554692	W-51	
$4_{14} \rightarrow 3_{13}$	245.125974		
$6_{06} \rightarrow 5_{15}$	251.421379		
$4_{23} \rightarrow 3_{22}$	255.840431		
$4_{14} \rightarrow 3_{13}$	245.125974	G34.3 + 0.15	
$1_{11} \rightarrow 0_{00}$	225.555	W49	
$2_{11} \rightarrow 2_{02}$	172.267113	Ori 3N	
$1_{11} \rightarrow 0_{00}$	225.555		
$1_{11} \rightarrow 0_{00}$	225.555	TMC-1	
$1_{11} \rightarrow 0_{00}$	225.555	L134N	
$1_{11} \rightarrow 0_{00}$	225.555	Sgr B2	[82]
$6_{15} \rightarrow 6_{06}$	226.5490		
$2_{11} \rightarrow 1_{10}$	133.272047	L183	[70]
$1_{11} \rightarrow 0_{00}$	225.554690		
$7_{16} \rightarrow 6_{15}$	464.570359	Orion-KL	[83]
$2_{21} \rightarrow 2_{12}$	500.475691		
$8_{08} \rightarrow 7_{07}$	501.679997		
$4_{04} \rightarrow 3_{13}$	105.79	Sgr B2	[84]
$1_{10} \rightarrow 1_{11}$	5.289813	Arp220	[86]

Transition	Frequency (GHz)	Source	Reference
$3_{13} \rightarrow 2_{02}$	340.354315	G19.61 – 0.23	[87]
$1_{11} \rightarrow 0_{00}$	225.5547		
$6_{15} \rightarrow 6_{06}$	226.5488		
$4_{14} \rightarrow 3_{13}$	245.1260		
$6_{06} \rightarrow 5_{15}$	251.4214		
$4_{04} \rightarrow 3_{03}$	254.6852	IRC + 10216	[76]
$4_{23} \rightarrow 3_{22}$	255.8404		
$4_{22} \rightarrow 3_{21}$	257.1128		
$4_{13} \rightarrow 3_{12}$	266.2701		
$2_{12} \rightarrow 1_{01}$	284.2541		
$3_{03} \rightarrow 2_{12}$	35.07	Sgr B2	[85]
$5_{14} \rightarrow 5_{15}$	79.28124		
$7_{25} \rightarrow 8_{18}$	95.30684		
$4_{04} \rightarrow 3_{13}$	105.79406		
$6_{15} \rightarrow 6_{16}$	110.89774		
$2_{11} \rightarrow 1_{10}$	133.27209		
$4_{23} \rightarrow 5_{14}$	133.73490		
$7_{16} \rightarrow 7_{17}$	147.66059		
$1_{10} \rightarrow 1_{01}$	166.85176		
$5_{23} \rightarrow 6_{16}$	170.01592		
$4_{22} \rightarrow 5_{15}$	214.92647	Sgr B2	[88]
$1_{11} \rightarrow 0_{00}$	225.55461		
$6_{15} \rightarrow 6_{06}$	226.54873		
$4_{14} \rightarrow 3_{13}$	245.12587		
$7_{16} \rightarrow 7_{07}$	250.16178		
$6_{06} \rightarrow 5_{15}$	251.42127		
$4_{04} \rightarrow 3_{03}$	254.68514		
$4_{23} \rightarrow 3_{22}$	255.84031		
$4_{32} \rightarrow 3_{31}$	256.16529		
$4_{31} \rightarrow 3_{30}$	256.17684		

Transition	Frequency (GHz)	Source	Reference
$4_{22} \rightarrow 3_{21}$	257.11263		
$3_{21} \rightarrow 4_{14}$	263.98609		
$4_{13} \rightarrow 3_{12}$	266.27002		
$8_{17} \rightarrow 8_{08}$	278.64261		
$4_{04} \rightarrow 3_{13}$	105.794062	G10.47 + 0.03,	
$1_{11} \rightarrow 0_{00}$	225.554609	NGC6334F, Orion KL,	
$4_{14} \rightarrow 3_{13}$	245.125806	G34.3 + 0.2, G 31.41 +	[71]
$4_{23} \rightarrow 3_{22}$	255.840311	0.31, DR21 (OH), W51 e1/e2, G 19.61 – 0.23	

Table 2.3: The transitions of CH_2NH identified in a terrestrial laboratory.

Transition	**Frequency (GHz)**	**Reference**
$19_{3,17} \leftarrow 18_{4,14}$	60.49112	[89]
$1_{01} \leftarrow 0_{00}$	63.993033	
$17_{3,14} \leftarrow 17_{3,15}$	65.200468	
$8_{26} \leftarrow 9_{19}$	66.955096	
$15_{4,12} \leftarrow 16_{3,13}$	70.160895	
$12_{2,10} \leftarrow 12_{2,11}$	110.83658	
$6_{15} \leftarrow 6_{16}$	110.89772	
$2_{12} \leftarrow 1_{11}$	122.69232	
$1_{10} \leftarrow 1_{11}$	5.288980	[92]
$3_{12} \leftarrow 3_{13}$	31.735172	
$1_{11} \leftarrow 2_{02}$	33.705893	
$3_{03} \leftarrow 2_{12}$	35.065090	
$26_{3,23} \leftarrow 27_{2,26}$	45.006800	
$15_{2,14} \leftarrow 14_{3,11}$	49.549511	
$4_{13} \leftarrow 4_{14}$	52.879454	
$5_{24} \leftarrow 6_{15}$	54.677350	
$25_{2,24} \leftarrow 24_{3,21}$	55.153992	
$10_{38} \leftarrow 11_{29}$	55.581300	
$14_{2,12} \leftarrow 15_{1,15}$	58.042544	
$10_{28} \leftarrow 10_{29}$	58.450784	
$17_{3,14} \leftarrow 17_{3,15}$	65.200315	
$15_{4,12} \leftarrow 16_{3,13}$	70.160654	
$5_{14} \leftarrow 5_{15}$	79.280130	
$11_{29} \leftarrow 11_{2,10}$	81.979805	
$1_{01} \leftarrow 0_{00}$	63.9927411	
$8_{26} \leftarrow 9_{19}$	66.9542701	
$11_{38} \leftarrow 12_{2,11}$	87.5272077	
$7_{25} \leftarrow 8_{18}$	95.3060646	
$4_{04} \leftarrow 3_{13}$	105.7933855	

Transition	Frequency (GHz)	Reference
$8_{17} \leftarrow 7_{26}$	109.8919759	
$12_{2,10} \leftarrow 12_{2,11}$	110.8361114	
$6_{15} \leftarrow 6_{16}$	110.8967091	
$2_{12} \leftarrow 1_{11}$	122.6912559	
$2_{02} \leftarrow 1_{01}$	127.8564858	
$2_{11} \leftarrow 1_{10}$	133.2705126	
$4_{03} \leftarrow 5_{14}$	133.7342535	
$1_{10} \leftarrow 1_{01}$	166.8501355	
$2_{11} \leftarrow 2_{02}$	172.2661067	
$12_{2,12} \leftarrow 11_{0,11}$	781.5255867	
$10_{37} \leftarrow 10_{28}$	781.6098559	
$5_{24} \leftarrow 4_{13}$	785.9380195	
$13_{1,13} \leftarrow 12_{1,12}$	788.2756000	
$12_{1,11} \leftarrow 11_{1,10}$	788.3338715	
$12_{2,10} \leftarrow 11_{29}$	790.6655597	
$9_{36} \leftarrow 9_{27}$	793.3649838	
$13_{0,13} \leftarrow 12_{0,12}$	796.7400951	
$8_{35} \leftarrow 8_{268}$	802.5890836	
$7_{34} \leftarrow 7_{25}$	809.4396281	
$6_{33} \leftarrow 6_{24}$	814.2180145	[93]
$5_{32} \leftarrow 5_{23}$	817.3099877	
$4_{31} \leftarrow 4_{22}$	819.1278552	
$3_{30} \leftarrow 3_{21}$	820.0635048	
$3_{31} \leftarrow 3_{22}$	820.6995325	
$4_{32} \leftarrow 4_{23}$	821.0246294	
$5_{33} \leftarrow 5_{24}$	821.6971333	
$6_{34} \leftarrow 6_{25}$	822.8840631	
$7_{35} \leftarrow 7_{26}$	824.7755387	
$8_{36} \leftarrow 8_{27}$	827.5795682	
$13_{1,13} \leftarrow 12_{0,12}$	831.3061854	

Transition	Frequency (GHz)	Reference
$9_{37} \leftarrow 9_{28}$	831.5163210	
$6_{25} \leftarrow 5_{14}$	836.6738796	
$10_{38} \leftarrow 10_{29}$	836.8121056	
$5_{23} \leftarrow 4_{14}$	843.2596525	
$13_{1,12} \leftarrow 12_{1,11}$	851.4619892	
$7_{26} \leftarrow 6_{15}$	884.8369203	
$6_{24} \leftarrow 5_{15}$	924.7825074	
$8_{27} \leftarrow 7_{16}$	930.5057424	
$9_{28} \leftarrow 8_{17}$	973.7917452	
$4_{40} \leftarrow 3_{31}$	1404.238028	
$5_{42} \leftarrow 4_{31}$	1468.185402	
$5_{41} \leftarrow 4_{32}$	1468.199075	
$12_{57} \leftarrow 12_{48}$	1471.199202	
$12_{58} \leftarrow 12_{49}$	1471.499403	
$9_{54} \leftarrow 9_{45}$	1473.861534	
$9_{55} \leftarrow 9_{46}$	1473.892068	[94]
$8_{53} \leftarrow 8_{44}$	1474.356250	
$8_{54} \leftarrow 8_{45}$	1474.367926	
$11_{39} \leftarrow 10_{28}$	1484.492817	
$12_{3,10} \leftarrow 11_{29}$	1532.209417	
$11_{38} \leftarrow 10_{29}$	1548.586974	
$13_{3,11} \leftarrow 12_{2,10}$	1576.363188	

Table 2.4: The experimentally observed values [94] of rotational and centrifugal distortional constants of CH_2NH in MHz.

Parameter	**Value**
$A \times 10^{-5}$	1.9621087629
$B \times 10^{-4}$	3.4641699423
$C \times 10^{-4}$	2.9351496787
$D_J \times 10^{3}$	56.00411
$D_{JK} \times 10^{3}$	598.6775
D_K	6.383483
$d_1 \times 10^{3}$	– 9.973179
$d_2 \times 10^{3}$	– 2.007905
$H_J \times 10^{6}$	0.01736
$H_{JK} \times 10^{6}$	2.6068
$H_{KJ} \times 10^{6}$	6.125
$H_K \times 10^{6}$	877.75
$h_1 \times 10^{9}$	33.067
$h_2 \times 10^{9}$	32.462
$h_3 \times 10^{9}$	9.091

CHAPTER 3: OBJECTIVES AND METHODOLOGY

3.1 Objectives

The aim of studying methanimine in the interstellar medium was started by framing the following objectives:

(i). Using the spectroscopic information about the molecule, the energies of the rotational levels and the radiative transition probabilities (Einstein A-coefficients) for radiative transitions between the levels will be calculated.

(ii). The interaction potential between the methanimine molecule and He atom will be calculated with the help of the software MOLPRO. There we shall use spherical polar coordinates whose center coincides with the center-of-mass of the molecule. The values of spherical polar coordinates would be changed so that the interaction potential with good accuracy could be obtained.

(iii). The interaction potential would be used as input to the computer code MOLSCAT whose output would be the scattering cross-sections. These scattering cross-sections would be calculated as a function of total energy (sum of the energy of colliding partner and the energy of the upper level of transition).

(iv). For a given kinetic temperature in a cosmic object, the energies of colliding partner (H_2 molecule which is replaced by He atom here for convenience of calculations) follow the Maxwellian distribution. Thus, the cross-sections would be averaged over the Maxwellian distribution to obtain the collisional rate coefficients for transitions between the levels.

(v). The collision rate coefficients along with the Einstein A-coefficients would be used for solving the statistical equilibrium equations coupled with the equations of radiative transfer. The output will be the relative population densities of energy levels. These values would be used for drawing conclusions about the observations from the cosmic objects.

3.2 Computational Techniques

A number of computer packages and programs are necessary to perform the quantum mechanical calculations to obtain the required results. The various computer software packages used in the research of interstellar molecules are described below:

(i). Gaussian: The Gaussian (2003) [173] is a general-purpose computer code that can predict many properties of molecules and reactions like structures, energies, orbitals, vibrational frequencies, electrostatic potentials, multi-pole moments, reaction energies and NMR properties.

We have used Gaussian (2003) software to determine the optimized geometrical co-ordinates of the CH_2NH molecule. The Becke 3-parameter hybrid functional in conjunction with the LYP non-local correlation functional (B3LYP) is used along with the augmented correlation consistent basis sets [174], aug-cc-pVDZ, and aug-cc-pVTZ. These include polarization functions and are augmented with diffuse functions.

(ii). ASROT: The Asymmetric rotor predictive program (ASROT) is a computer code used to calculate the energy levels and the Einstein A-coefficients for transitions between energy levels for an asymmetric rotor using Watson's Reduced Hamiltonian. The rotational and centrifugal constants are input to the ASROT program which provides Einstein A-coefficients, line strengths, frequencies of transitions, and energies of the upper levels as output.

(iii). MOLPRO: The MOLPRO is a software package used for accurate ab-initio quantum calculations for advanced molecular electronic structures. It comprises well efficient programs for computational applications, such as density functional theory (DFT) with a large choice of functionals, coupled-cluster (CC), and multi-reference wave function methods. The coupled-cluster methods generally used are CCSD [175] and CCSD (T). The CCSD refers to Coupled Cluster for Single and Double excitation and CCSD(T) refers to Coupled Cluster for complete treatment to Single and Double excitation with an estimate to connected Triples contribution is calculated using many-body perturbation theory. The output of MOLPRO is the interaction potential

between methanimine and He atom. The spherical polar coordinates are used whose origin coincides with the center of mass of the molecule and the interaction potential with good accuracy can be obtained.

(iv). MOLSCAT: The MOLSCAT (Molecular Scattering) is a free software package for quantum calculations involving the scattering of molecules. It is developed by Hutson and Green [176]. In this computer code, the collisions between molecules of interest are described by S-matrix and the time-independent Schrodinger equation is solved by extending the cumulative wave function in the basis sets of the colliding particles coupled by the intermolecular potential. This builds the combined equations ideal for the collision problem of concern which provides S matrices on solving, which are accumulated to obtain the cross-sections for collisional transitions.

For using MOLSCAT, we have to provide information about the type of collision partners i.e. Linear, rotor, symmetric, asymmetric top, etc. Also, the rotational energy levels are to be specified and collision energies of interest are to be given. The main input is the interaction potential between the collision partners which are calculated with the help of MolPro.

There are three main approaches to do calculations using MOLSCAT, namely Infinite Order Sudden (IOS), Coupled States (CS), and Close Coupling (CC) approach. The IOS approximation is useful only for very high energies of the collisional partner where the energies of rotational levels in the molecule are neglected as compared to the energy of the incident particle. Therefore, the accuracy of this approach is low. The results obtained under CS and CC approximations are accurate but the computational calculations time required is very large and extremely large respectively. The obtained cross-sections are averaged over Maxwellian distribution to get the collisional rate coefficients between energy levels.

(v). Programming in FORTRAN Language: A number of programs are made to perform various functions such as selection rules for transitions, solutions of statistical equilibrium equations, and radiative transfer calculations, etc. to determine the relative population densities of energy levels.

3.3 Einstein A-coefficients and Line Strengths of Radiative Transitions

The Einstein A-coefficient for a transition $J'_{\tau'} \rightarrow J_{\tau}$ is related to line strength by the following expression [177–181]

$$A(J'_{\tau'} \rightarrow J_{\tau}) = \frac{64\pi^4\nu^3}{3hc^3(2J'+1)} S(J'_{\tau'} \rightarrow J_{\tau})$$

Here, the line strength for a-type transition is expressed as

$$S(J'_{\tau'} \rightarrow J_{\tau}) = \mu_a^2(2J+1)[\sum_{K=-J}^{J} g_{\tau K}^{J} g_{\tau' K}^{J'} C_{JK10}^{J'K}]^2$$

where μ_a is the component of electric dipole moment along the a-axis of inertia and $C_{JK10}^{J'K}$ is the Clebsch-Gordon coefficient.

Also, the line strength for b-type transition $J'_{\tau'} \rightarrow J_{\tau}$ is given by the following expression.

$$S(J'_{\tau'} \rightarrow J_{\tau}) = \frac{\mu_b^2(2J+1)}{2}[\sum_{K=-J}^{J} g_{\tau K}^{J}(g_{\tau' K+1}^{J'} C_{JK11}^{J'K+1} + g_{\tau' K-1}^{J'} C_{JK1,-1}^{J'K-1})]^2$$

where μ_b is the component of electric dipole moment along the b-axis of inertia and $C_{JK11}^{J'K+1}$ and $C_{JK1,-1}^{J'K-1}$ are Clebsch-Gordon coefficients.

3.4 Interaction Potential and Collisional Rate Coefficients

In the interstellar medium, H_2 molecules are more abundant than any other molecule. So, the majority of collisions occur with H_2 only. It is always better to consider collisions with He atoms instead of H_2, as potential depends on the charges of the colliding partners that are the same for H_2 and He. The collisional rate coefficient for $CH_2NH + H_2$ may be obtained from the collisional rate coefficient of CH_2NH + He by multiplying with the factor given by

$$\left(\frac{\mu_{CH_2NH+He}}{\mu_{CH_2NH+H_2}}\right)^{\frac{1}{2}} = 1.371$$

The software MOLPRO is used to find the interaction potential between CH_2NH and He. The optimized coordinates obtained from Gaussian are taken as input parameters and the interaction potentials are obtained as output. The procedure contains three steps of calculations:

(i) The energy E_1 for CH_2NH + He.

(ii) The energy E_2 of CH_2NH when He is taken as a ghost atom.

(iii) The energy E_3 of He atom when the CH_2NH molecules are taken as ghost molecules.

The interaction potential is $V(R,\theta,\phi)$ is given by

$$V(R,\theta,\phi) = E_2(R,\theta,\phi) + E_3(R,\theta,\phi) - E_1(R,\theta,\phi)$$

Using the interaction potentials $V(R,\theta,\phi)$, $q(L,M,M'|E)$ coefficients are calculated using the software MOLSCAT [176]. The output given by MOLSCAT is independent of positions of energy levels in these species. The $q(L,M,M'|E)$ coefficients are further used to calculate the cross-sections and $Q(L,M,M'|T)$ coefficients. At a specific kinetic temperature, these coefficients are averaged over Maxwellian distribution to obtain the collisional de-excitation rates, as given below for a transition $J_\tau \rightarrow J'_{\tau'}$ [182] as

$$C\left(J_\tau \rightarrow J'_{\tau'}|T\right) = \left(\frac{8}{\pi\mu k^3 T^3}\right)^{\frac{1}{2}} \int_0^\infty \sigma\left(J_\tau \rightarrow J'_{\tau'}|E\right) E e^{-\frac{E}{kT}} dE$$

where μ represents the reduced mass of two molecules. Also, the cross-section for a collisional transition is given as

$$\sigma\left(J_\tau \rightarrow J'_{\tau'}|E\right) = \sum_{LMM'} S(J,\tau,J',\tau'|L,M,M') q(L,M,M'|E)$$

where L varies from $|J - J'|$ to $J + J'$ and both M and M' can have $2L+1$ values ranging from $-L$ to $+L$. Also, the spectroscopic coefficients S depends on the g-coefficients (wave-functions) of the molecule and on the angular momentum coupling factors as

$$S(J,\tau,J',\tau'|L,M,M') = \sum_{p,p',q,q'} g^{p}_{J\tau} g^{q}_{J\tau} g^{p'}_{J'\tau'} g^{q'}_{J'\tau'} \langle J,p,L,-M|J',p'\rangle \langle J,q,L,-M'|J',q'\rangle$$

where $<j_1m_1j_2m_2|jm>$ represents the C-G coefficient. The collisional rate coefficients are written as

$$C(J_\tau \rightarrow J'_{\tau'}|T) = \sum_{LMM'} S(J,\tau,J',\tau'|L,M,M') Q(L,M,M'|T)$$

where the Q parameters are given by

$$Q(L,M,M'|T) = \left(\frac{8}{\pi\mu k^3 T^3}\right)^{\frac{1}{2}} \int_0^\infty q(L,M,M'|E) E e^{-\frac{E}{kT}} dE$$

The symmetry of g-coefficients will provide us S(L,M,M′) = S(L,M′,M). Thus, the only real part of Q-parameters is required and cross-sections will be real which will further provide us the collisional rate coefficients.

3.5 Detailed Balance

Consider a pair of energy levels *i* (lower) and *j* (higher), having population densities n_i and n_j, and statistical weights g_i and g_j. The difference in energies of these levels is $\Delta E = E_j - E_i$. According to the principle of detailed balance, the collisional rate coefficients C_{ij} for excitation and C_{ji} for de-excitation are related as

$$n_i C_{ij} = n_j C_{ji}$$

or

$$C_{ij} = \frac{n_j}{n_i} C_{ji}$$

In thermal equilibrium, the population densities of levels at temperature T are related by Maxwell distribution as

$$\frac{n_j}{n_i} = \frac{g_j}{g_i} e^{\frac{-\Delta E}{kT}}$$

Thus, the collisional excitation rates can be calculated from de-excitation rates by the following expression

$$C_{ij} = \frac{g_j}{g_i} e^{\frac{-\Delta E}{kT}} C_{ji}$$

3.6 Statistical Equilibrium Equations

For rotational energy levels of Methanimine, both radiative as well as collisional transitions are possible. For these transitions occurring between rotational energy levels of CH_2NH, we can write a set of statistical equilibrium equations coupled with the equations of radiative transfer [183] as:

$$n_i \sum_{\substack{j=1 \\ j \neq i}}^{N} P_{ij} = \sum_{\substack{j=1 \\ j \neq i}}^{N} n_j P_{ij}$$

where i = 1,2,3,……., N, and n gives the population density of an energy level. Also, P_{ij} is defined as

(i) For radiatively allowed transitions

$$P_{ij} = \begin{cases} \left(A_{ij} + B_{ij} I_{\nu,bg}\right)\beta_{ij} + n_{H_2} C_{ij} & i > j \\ B_{ij} I_{\nu,bg}\beta_{ij} + n_{H_2} C_{ij} & i < j \end{cases} \quad \text{...(3.1)}$$

(ii) For radiatively forbidden transitions

$$P_{ij} = n_{H_2} C_{ij} \quad \text{…(3.2)}$$

In the above equations, A and B are Einstein coefficients for radiative transitions, C_{ij} is the collisional rate coefficient for transitions due to collision, and n_{H_2} is the density of molecular hydrogen. Also, β is known as escape probability which is related to optical thickness τ_ν as

$$\beta_{ij} = \beta_{ji} = \frac{1 - e^{-\tau_\nu}}{\tau_\nu}$$

Also, the optical thickness is expressed as

$$\tau_\nu = \frac{h\nu}{4\pi\left({}^{dv_r}/_{dr}\right)}\left(B_{ij} n_i - B_{ji} n_j\right)$$

Here, (dv_r/dr) represents the velocity gradient in the molecular cloud. For the molecular cloud under consideration, we have taken the cosmic microwave background (CMB) behind it at a temperature (T_{bg}) of 2.73 K. These statistical equilibrium equations are solved using the radiative and collisional transition rates as input parameters and by taking the thermal populations as initial populations.

CHAPTER 4: RESULTS AND DISCUSSION

SECTION - I

4.1 Rotational Energy Levels of Methanimine

The energies for the lowest 69 rotational energy levels of Methanimine are calculated with the help of the computer code ASROT [184] for which we have used the values of rotational and centrifugal distortional constants given in Table 2.4. The calculated energies for rotational energy levels having energy values up to 141 cm^{-1} as given in Table 4.1. Also, the corresponding energy level diagram is shown in figure 4.1.

4.2 Selection Rules for Radiative Transitions

The rotational level for an asymmetric top molecule is expressed as $J_{ka,kc}$ or J_{τ}, where J is rotational angular momentum quantum number and the pseudo quantum number τ is expressed as $\tau = k_a - k_c$, the k_a and k_c being the projections of rotational angular momentum on the axis of symmetry for prolate and oblate symmetric top molecules, respectively.

For the molecules with electric dipole moment along a-axis of inertia, the radiative transitions between the rotational energy levels are governed by the selection rules [180,181]:

J :	$\Delta J = 0, \pm 1$	
k_a, k_c :	odd, even ↔ odd, odd	(Group I)
	even, even ↔ even, odd	(Group II)

For the molecules with electric dipole moment along b-axis of inertia, the radiative transitions between the rotational energy levels are governed by the selection rules:

J:	$\Delta J = 0, \pm 1$	
k_a, k_c:	odd, even ↔ even, odd	(Group III)
	even, even ↔ odd, odd	(Group IV)

The methanimine has components of dipole moment along both a-axis and b-axis of inertia, so it will have both a-type and b-type radiative transitions. Thus, we will get four groups of transitions as described above.

4.3 Einstein A-coefficients for Radiative Transitions in Methanimine

Besides the calculation of the energies of rotational levels, the frequencies, line strengths, and Einstein A-coefficients for radiative transitions between the rotational levels are also calculated using the software ASROT [184] where rotational and centrifugal distortion constants given in Table 2.4 have been used. The energies of rotational levels of methanimine up to 141 cm^{-1} are calculated and 346 lines are found to be satisfying the selection rules in this energy range. These lines are categorized into 4 groups according to selection rules given in section 4.2. In Tables 4.2 to 4.5, those dominant transitions are reported for which the Einstein A-coefficient is more than 10^{-5} s^{-1} and the line strength is greater than 0.1, corresponding to each group. Also, the rest of the transitions having small transition probabilities are given in Tables 4.6 to 4.9 corresponding to all the four groups.

4.4 Radiative Lifetime of Rotational Energy Levels

Based on the selection rules, an energy level may be radiatively connected to a number of energy levels. The radiative lifetime of the level j denoted by T_j is defined by the following

$$T_j = \frac{1}{\sum_i A_{ji}}$$

where the summation is taken over all the lower levels i to which the levels j decay spontaneously. By using the values of Einstein A-coefficients, the radiative lifetimes of the energy levels of CH_2NH are computed and are given in Table 4.10.

4.5 Potential Rotational Transitions

In the interstellar medium, the excitation of a molecule from lower to the higher level generally occurs by a collisional process. For a system in a higher level, the formation of a spectral line takes place when the rate of radiative de-excitation is larger than the rate of collisional de-excitation. For a spectral line to be a strong radio emission line

under interstellar conditions, besides a sufficient abundance of the molecule under consideration, two other conditions need to be satisfied:

(i). The higher level in a transition must be sufficiently populated. As most of the excitation of molecules is due to collisions, it imposes a limit on the energy of a higher level. We have calculated the transition rates for the energy of a higher level up to 141 cm^{-1} which is sufficient for kinetic temperature up to 140 K.

(ii). For the transition, the Einstein A-coefficient must be sufficiently large. As the majority of interstellar lines are formed under non-local thermal equilibrium (NLTE) conditions, so the numbers for the individual levels can be determined only by solving the statistical equilibrium equations coupled with the equations of radiative transfer [11]. As the calculation of collisional rate coefficients is a cumbersome task, so we have made a crude approximation as explained below:

As Einstein A-coefficients represent the probability of radiative transitions so their large values imply that almost every excitation is followed by emission of at least one photon. (If a higher-lying level is populated, the molecule may cascade down to lower states by emitting a sequence of photons.) In general, the collisional rate constant for a transition from higher-level *j* to lower-level *i* is expressed as

$$C_{ji} = < v\sigma_{ji} >$$

where *v* is the relative velocity of collision partner and σ_{ji} the collision cross-section for the transition which depends on both, on the transition as well as on the collision partner. In order to obtain at least a crude estimate, we assume $\sigma_{ji} = 10^{-16}$ cm^2 and v = 10^5 cm/s, so we will get $C_{ji} = 10^{-11} cm^3 s^{-1}$ as a reasonable estimate [185]. For dense cloud conditions, $n_{H2} \approx 10^4$ cm^{-3}, so we can write an approximate order of magnitude for the collisional rate coefficient as $n_{H2}\, C_{ji} = 10^{-7}$ s^{-1}.

The probability of a photon is large if Einstein A-coefficients are larger than the collisional de-excitation rate. From all the obtained lines, the transitions which have Einstein A-coefficients greater than 10^{-5} s^{-1} and line strength greater than 0.1 are separately written in Tables 4.2 to 4.5. Along with Einstein A-coefficients, the calculated values of frequencies, line strengths of transitions, and the energy of the higher level in each case are given. Also, the line strengths of transitions having a magnitude greater than 0.1 and A-coefficients greater than 10^{-5} s^{-1} are shown in figures 4.2 and 4.3, separately for each group of radiative transitions. Thus, we find

that there are more than 100 lines having a quite large value of Einstein A coefficient and whose higher level does not have very high energy. These levels are quite promising for the identification of methanimine in the interstellar medium.

4.6 Conclusion

Based on the electric dipole moment as well as rotational and centrifugal distortion constants, the rotational energy levels, the line strengths, and Einstein A-coefficients for all the radiative transitions within the rotational energy levels up to 141 cm^{-1} have been calculated. Those lines are reported which are expected to be prominent under conditions in the interstellar medium by applying two criteria, namely the upper energy level must be sufficiently populated and the radiative transition probability must be sufficiently large. Besides the observed transitions, we have found more than 100 lines of methanimine satisfying the said conditions which are not observed earlier. These lines are expected to play an important role in the identification of methanimine in the interstellar space.

The Einstein A-coefficients and line intensities for Methanimine are published as "Methanimine in interstellar medium: Line intensities" in "Indian Journal of Physics" (SPRINGER) (2016) ***90****:733-739*. [186]

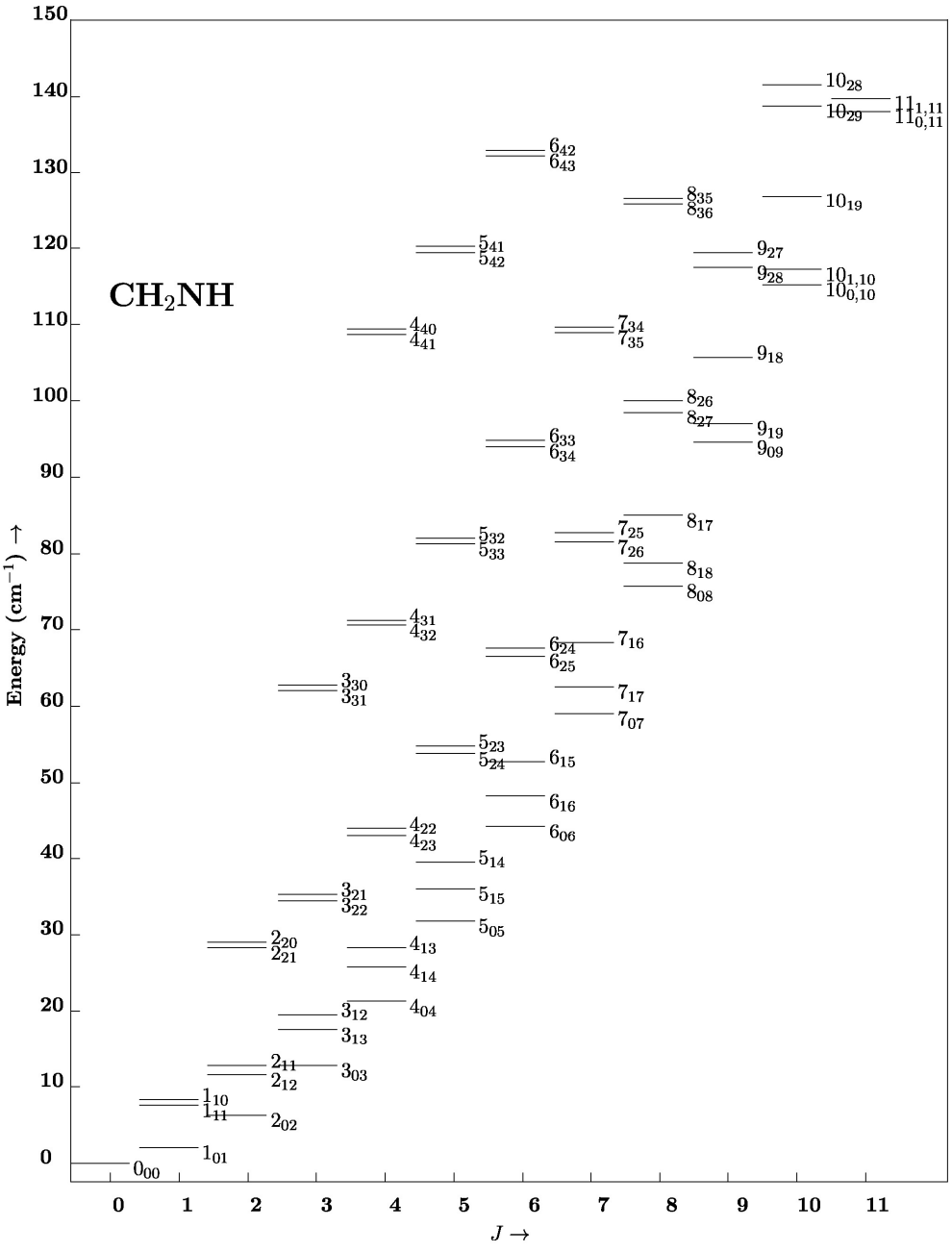

Figure 4.1: The rotational energy level diagram of CH_2NH up to energy 141 cm^{-1}.

Table 4.1: The energy values for the lowest 69 rotational energy levels of CH_2NH.

Sr. No.	Energy Level	Energy (cm^{-1})	Energy (GHz)
1	0_{00}	0.000000	0
2	1_{01}	2.133099	63.99297
3	2_{02}	6.394992	191.84976
4	1_{11}	7.518487	225.55461
5	1_{10}	7.694824	230.84472
6	2_{12}	11.608231	348.24693
7	2_{11}	12.137227	364.11681
8	3_{03}	12.777088	383.31264
9	3_{13}	17.740123	532.20369
10	3_{12}	18.798004	563.94012
11	4_{04}	21.266592	637.99776
12	4_{14}	25.910986	777.32958
13	4_{13}	27.673671	830.21013
14	2_{21}	28.290610	848.7183
15	2_{20}	28.294867	848.84601
16	5_{05}	31.846761	955.40283
17	3_{22}	34.689255	1040.67765
18	3_{21}	34.710522	1041.31566
19	5_{15}	36.116728	1083.50184
20	5_{14}	38.759436	1162.78308
21	4_{23}	43.217265	1296.51795
22	4_{22}	43.280943	1298.42829
23	6_{06}	44.497436	1334.92308
24	6_{16}	48.352469	1450.57407
25	6_{15}	52.049061	1561.47183
26	5_{24}	53.871629	1616.14887
27	5_{23}	54.019666	1620.58998
28	7_{07}	59.195979	1775.87937
29	3_{31}	62.045917	1861.37751

Sr. No.	Energy Level	Energy (cm^{-1})	Energy (GHz)
30	3_{30}	62.045981	1861.37943
31	7_{17}	62.612685	1878.38055
32	6_{25}	66.648589	1999.45767
33	6_{24}	66.942836	2008.28508
34	7_{16}	67.534705	2026.04115
35	4_{32}	70.584760	2117.5428
36	4_{31}	70.585209	2117.55627
37	8_{08}	75.918642	2277.55926
38	8_{18}	78.891368	2366.74104
39	5_{33}	81.261539	2437.84617
40	5_{32}	81.263334	2437.90002
41	7_{26}	81.543649	2446.30947
42	7_{25}	82.068262	2462.04786
43	8_{17}	85.206728	2556.20184
44	6_{34}	94.078062	2822.34186
45	6_{33}	94.083440	2822.5032
46	9_{09}	94.642251	2839.26753
47	9_{19}	97.182198	2915.46594
48	8_{27}	98.551587	2956.54761
49	8_{26}	99.414034	2982.42102
50	9_{18}	105.053479	3151.60437
51	4_{41}	108.853845	3265.61535
52	4_{40}	108.853846	3265.61538
53	7_{35}	109.036171	3271.08513
54	7_{34}	109.049589	3271.48767
55	$10_{0,10}$	115.345925	3460.37775
56	$10_{1,10}$	117.478720	3524.3616
57	9_{28}	117.666477	3529.99431
58	9_{27}	118.996814	3569.90442
59	5_{42}	119.524722	3585.74166

Sr. No.	Energy Level	Energy (cm^{-1})	Energy (GHz)
60	5_{41}	119.524730	3585.7419
61	8_{36}	126.137577	3784.12731
62	8_{35}	126.167011	3785.01033
63	10_{19}	127.061072	3811.83216
64	6_{43}	132.332390	3969.9717
65	6_{42}	132.332426	3969.97278
66	$11_{0,11}$	138.012436	4140.37308
67	10_{29}	138.881717	4166.45151
68	$11_{1,11}$	139.774504	4193.23512
69	10_{28}	140.830086	4224.90258

Table 4.2: Einstein A-coefficients, frequency (ν), line strength (S_{ji}) and energy of upper rotational energy levels (E_j) for potential radiative transitions belonging to group I, having A $>10^{-5}$ s^{-1} and S > 0.1.

Transition	**A-coefficient (s^{-1})**	**ν (GHz)**	**S_{ji}**	**E_j (cm^{-1})**
$2_{12} \rightarrow 1_{11}$	1.16 X 10^{-5}	122.692322	1.50	11.608231
$2_{11} \rightarrow 1_{10}$	1.48 X 10^{-5}	133.272089	1.50	12.137227
$3_{13} \rightarrow 2_{12}$	4.95 X 10^{-5}	183.956771	2.67	17.740123
$3_{12} \rightarrow 2_{11}$	6.35 X 10^{-5}	199.823299	2.67	18.798004
$4_{14} \rightarrow 3_{13}$	1.28 X 10^{-4}	245.125866	3.75	25.910986
$4_{32} \rightarrow 3_{31}$	6.83 X 10^{-5}	256.165294	1.75	70.584760
$4_{13} \rightarrow 3_{12}$	1.64 X 10^{-4}	266.270024	3.75	27.673671
$4_{31} \rightarrow 3_{30}$	6.83 X 10^{-5}	256.176841	1.75	70.585209
$5_{15} \rightarrow 4_{14}$	2.62 X 10^{-4}	306.172258	4.79	36.116728
$5_{33} \rightarrow 4_{32}$	2.00 X 10^{-4}	320.303375	3.19	81.261539
$5_{14} \rightarrow 4_{13}$	3.35 X 10^{-4}	332.572926	4.79	38.759436
$5_{32} \rightarrow 4_{31}$	2.00 X 10^{-4}	320.343749	3.19	81.263334
$6_{16} \rightarrow 5_{15}$	4.63 X 10^{-4}	367.072249	5.83	48.352469
$6_{34} \rightarrow 5_{33}$	4.11 X 10^{-4}	384.495705	4.50	94.078062
$6_{15} \rightarrow 5_{14}$	5.94 X 10^{-4}	398.688748	5.83	52.049061
$6_{33} \rightarrow 5_{32}$	4.11 X 10^{-4}	384.603189	4.50	94.083440
$7_{17} \rightarrow 6_{16}$	7.47 X 10^{-4}	427.806484	6.85	62.612685
$7_{35} \rightarrow 6_{34}$	7.19 X 10^{-4}	448.74326	5.72	109.036171
$7_{16} \rightarrow 6_{15}$	9.57 X 10^{-4}	464.569327	6.85	67.534705
$7_{34} \rightarrow 6_{33}$	7.20 X 10^{-4}	448.984463	5.72	109.049589
$8_{18} \rightarrow 7_{17}$	1.13 X 10^{-3}	488.360479	7.88	78.891368
$8_{36} \rightarrow 7_{35}$	1.14 X 10^{-3}	513.042178	6.87	126.137577
$8_{17} \rightarrow 7_{16}$	1.44 X 10^{-3}	530.16071	7.88	85.206728
$8_{35} \rightarrow 7_{34}$	1.14 X 10^{-3}	513.522674	6.87	126.167011
$9_{19} \rightarrow 8_{18}$	1.61 X 10^{-3}	548.724908	8.88	97.182198
$9_{18} \rightarrow 8_{17}$	2.06 X 10^{-3}	595.402514	8.88	105.053479
$10_{1,10} \rightarrow 9_{19}$	2.22 X 10^{-3}	608.895648	9.90	117.478720
$10_{19} \rightarrow 9_{18}$	2.83 X 10^{-3}	660.22779	9.88	127.061072
$11_{1,11} \rightarrow 10_{1,10}$	2.96 X 10^{-3}	668.87353	10.90	139.774504

Table 4.3: Einstein A-coefficients, frequency (ν), line strength (S_{ji}) and energy of upper rotational energy levels (E_j) for radiative transitions belonging to group II, having A $>10^{-5}$ s^{-1} and S > 0.1.

Transition	**A-coefficient (s^{-1})**	**ν (GHz)**	**S_{ji}**	**E_j (cm^{-1})**
$2_{02} \rightarrow 1_{01}$	1.75 X 10^{-5}	127.856795	2.01	6.394992
$3_{03} \rightarrow 2_{02}$	6.28 X 10^{-5}	191.46286	3.01	12.777088
$3_{21} \rightarrow 2_{20}$	3.55 X 10^{-5}	192.469661	1.67	34.710522
$3_{22} \rightarrow 2_{21}$	3.52 X 10^{-5}	191.959366	1.67	34.689255
$4_{04} \rightarrow 3_{03}$	1.53 X 10^{-4}	254.685137	4.01	21.266592
$4_{22} \rightarrow 3_{21}$	1.18 X 10^{-4}	257.112635	3.01	43.280943
$4_{23} \rightarrow 3_{22}$	1.17 X 10^{-4}	255.840311	3.01	43.217265
$5_{05} \rightarrow 4_{04}$	3.03 X 10^{-4}	317.40508	5.02	32.846761
$5_{23} \rightarrow 4_{22}$	2.67 X 10^{-4}	322.161698	4.18	54.019666
$5_{41} \rightarrow 4_{40}$	1.12 X 10^{-4}	320.126504	1.78	119.524730
$5_{24} \rightarrow 4_{23}$	2.60 X 10^{-4}	319.630917	4.18	53.871629
$5_{42} \rightarrow 4_{41}$	1.12 X 10^{-4}	320.126312	1.78	119.524722
$6_{06} \rightarrow 5_{05}$	5.26 X 10^{-4}	379.520246	5.96	44.497436
$6_{24} \rightarrow 5_{23}$	4.99 X 10^{-4}	387.695104	5.35	66.942836
$6_{42} \rightarrow 5_{41}$	3.04 X 10^{-4}	384.230893	3.34	132.332426
$6_{25} \rightarrow 5_{24}$	4.83 X 10^{-4}	383.308795	5.35	66.648589
$6_{43} \rightarrow 5_{42}$	3.04 X 10^{-4}	384.230028	3.34	132.332390
$7_{07} \rightarrow 6_{06}$	8.33 X 10^{-4}	440.956279	6.97	59.195979
$7_{25} \rightarrow 6_{24}$	8.36 X 10^{-4}	453.76278	6.41	82.068262
$7_{26} \rightarrow 6_{25}$	7.99 X 10^{-4}	446.851791	6.41	81.543649
$8_{08} \rightarrow 7_{07}$	1.24 X 10^{-3}	501.679879	7.97	75.918642
$8_{26} \rightarrow 7_{25}$	1.30 X 10^{-3}	520.373155	7.52	99.414034
$8_{27} \rightarrow 7_{26}$	1.22 X 10^{-3}	510.238147	7.52	98.551587
$9_{09} \rightarrow 8_{08}$	1.75 X 10^{-3}	561.708292	8.97	94.642251
$9_{27} \rightarrow 8_{26}$	1.91 X 10^{-3}	587.4834	8.58	118.996814
$9_{28} \rightarrow 8_{27}$	1.77 X 10^{-3}	573.446706	8.53	117.666477
$10_{0,10} \rightarrow 9_{09}$	2.37 X 10^{-3}	621.1102	9.97	115.345925

Transition	**A-coefficient (s^{-1})**	**ν (GHz)**	**S_{ji}**	**E_j (cm^{-1})**
$10_{28} \rightarrow 9_{27}$	2.68 X 10^{-3}	654.998154	9.58	140.830086
$10_{29} \rightarrow 9_{28}$	2.46 X 10^{-3}	636.457181	9.58	138.881717
$11_{0,11} \rightarrow 10_{0,10}$	3.13 X 10^{-3}	679.995352	10.92	138.012436

Table 4.4: Einstein A-coefficients, frequency (ν), line strength (S_{ji}), and energy of upper rotational energy levels (E_j) for radiative transitions belonging to group III, having A $>10^{-5}$ s^{-1} and S > 0.1.

Transition	**A-coefficient (s^{-1})**	**ν (GHz)**	**S_{ji}**	**E_j (cm^{-1})**
$1_{10} \rightarrow 1_{01}$	5.65 X 10^{-5}	166.85176	1.50	7.694824
$2_{12} \rightarrow 1_{01}$	1.68 X 10^{-4}	284.25396	1.50	11.608231
$2_{21} \rightarrow 1_{10}$	1.72 X 10^{-3}	617.87355	1.50	28.290610
$2_{21} \rightarrow 2_{12}$	5.09 X 10^{-4}	500.47136	0.83	28.290610
$2_{21} \rightarrow 3_{12}$	1.99 X 10^{-5}	284.77817	0.18	28.290610
$3_{30} \rightarrow 2_{21}$	8.99 X 10^{-3}	1012.66114	2.49	62.045981
$3_{21} \rightarrow 2_{12}$	1.84 X 10^{-3}	693.06873	1.58	34.710522
$3_{12} \rightarrow 3_{03}$	6.88 X 10^{-5}	180.62749	3.36	18.798004
$3_{21} \rightarrow 3_{12}$	5.99 X 10^{-4}	477.37554	1.58	34.710522
$3_{30} \rightarrow 3_{21}$	1.71 X 10^{-3}	820.06377	0.89	62.045981
$4_{14} \rightarrow 3_{03}$	4.24 X 10^{-4}	394.01694	2.57	25.910986
$3_{21} \rightarrow 4_{14}$	2.21 X 10^{-5}	263.98609	0.35	34.710522
$4_{32} \rightarrow 3_{21}$	8.74 X 10^{-3}	1076.22713	2.60	70.584760
$4_{23} \rightarrow 3_{12}$	2.00 X 10^{-3}	732.57784	1.88	43.217265
$3_{30} \rightarrow 4_{23}$	7.94 X 10^{-5}	564.86146	0.13	62.045981
$4_{41} \rightarrow 3_{30}$	2.61 X 10^{-2}	1404.23594	3.49	108.853845
$4_{23} \rightarrow 4_{14}$	7.45 X 10^{-4}	519.1884	1.98	43.217265
$4_{32} \rightarrow 4_{23}$	2.42 X 10^{-3}	821.02483	1.61	70.584760
$4_{41} \rightarrow 4_{32}$	3.75 X 10^{-3}	1148.07257	0.92	108.853845
$5_{32} \rightarrow 4_{23}$	9.00 X 10^{-3}	1141.38205	2.74	81.263334
$4_{41} \rightarrow 5_{32}$	1.56 X 10^{-4}	827.71535	0.10	108.853845
$5_{05} \rightarrow 4_{14}$	2.92 X 10^{-5}	178.07328	2.34	31.846761
$5_{23} \rightarrow 4_{14}$	2.37 X 10^{-3}	843.26042	1.79	54.019666
$4_{32} \rightarrow 5_{23}$	1.01 X 10^{-4}	496.9528	0.30	70.584760
$5_{41} \rightarrow 4_{32}$	2.50 X 10^{-2}	1468.1991	3.57	119.524730
$5_{14} \rightarrow 5_{05}$	9.63 X 10^{-5}	207.38023	4.88	38.759436
$5_{23} \rightarrow 5_{14}$	6.49 X 10^{-4}	457.80692	3.06	54.019666

Transition	A-coefficient (s^{-1})	ν (GHz)	S_{ji}	E_j (cm^{-1})
$5_{32} \rightarrow 5_{23}$	2.75 X 10^{-3}	817.31002	2.28	81.263334
$5_{41} \rightarrow 5_{32}$	5.65 X 10^{-3}	1147.84188	1.69	119.524730
$6_{16} \rightarrow 5_{05}$	8.58 X 10^{-4}	495.17123	3.78	48.352469
$6_{34} \rightarrow 5_{23}$	9.44 X 10^{-3}	1201.75188	2.90	94.078062
$5_{41} \rightarrow 6_{34}$	2.50 X 10^{-4}	763.40002	0.26	119.524730
$6_{25} \rightarrow 5_{14}$	2.62 X 10^{-3}	836.67461	2.39	66.648589
$5_{32} \rightarrow 6_{25}$	9.36 X 10^{-5}	438.44233	0.49	81.263334
$6_{43} \rightarrow 5_{32}$	2.49 X 10^{-2}	1532.07169	3.70	132.332390
$6_{25} \rightarrow 6_{16}$	8.93 X 10^{-4}	548.8836	2.89	66.648589
$6_{34} \rightarrow 6_{25}$	3.01 X 10^{-3}	822.88419	2.89	94.078062
$6_{43} \rightarrow 6_{34}$	6.74 X 10^{-3}	1147.62983	2.38	132.332390
$7_{34} \rightarrow 6_{25}$	1.02 X 10^{-2}	1272.02999	3.06	109.049589
$6_{43} \rightarrow 7_{34}$	2.77 X 10^{-4}	698.48404	0.43	132.332390
$7_{07} \rightarrow 6_{16}$	2.14 X 10^{-4}	325.30530	3.84	59.195979
$7_{25} \rightarrow 6_{16}$	3.08 X 10^{-3}	1011.4738	1.83	82.068262
$6_{34} \rightarrow 7_{25}$	6.30 X 10^{-5}	360.29400	0.72	94.078062
$7_{16} \rightarrow 7_{07}$	1.50 X 10^{-4}	250.16177	5.91	67.534705
$7_{25} \rightarrow 7_{16}$	6.47 X 10^{-4}	436.00673	4.81	82.068262
$7_{34} \rightarrow 7_{25}$	3.04 X 10^{-3}	809.43979	3.52	109.049589
$8_{18} \rightarrow 7_{07}$	1.54 X 10^{-3}	590.86167	5.21	78.891368
$8_{36} \rightarrow 7_{25}$	1.08 X 10^{-2}	1322.07944	3.25	126.137577
$8_{27} \rightarrow 7_{16}$	3.46 X 10^{-3}	930.50647	3.00	98.551587
$7_{34} \rightarrow 8_{27}$	4.66 X 10^{-5}	314.94005	0.92	109.049589
$8_{27} \rightarrow 8_{18}$	1.07 X 10^{-3}	589.80658	3.63	98.551587
$8_{36} \rightarrow 8_{27}$	3.31 X 10^{-3}	827.57969	4.08	126.137577
$9_{18} \rightarrow 8_{27}$	1.93 X 10^{-5}	195.05675	2.02	105.053479
$9_{09} \rightarrow 8_{18}$	7.56 X 10^{-4}	472.52650	5.59	94.642251
$9_{27} \rightarrow 8_{18}$	3.77 X 10^{-3}	1203.16339	1.69	118.996814
$8_{36} \rightarrow 9_{27}$	1.64 X 10^{-5}	214.22288	1.16	126.137577
$9_{18} \rightarrow 9_{09}$	2.49 X 10^{-4}	312.33683	6.39	105.053479

Transition	**A-coefficient (s^{-1})**	**ν (GHz)**	**S_{ji}**	**E_j (cm^{-1})**
$9_{27} \rightarrow 9_{18}$	6.43 X 10^{-4}	418.30006	6.85	118.996814
$10_{1,10} \rightarrow 9_{09}$	2.57 X 10^{-3}	685.09405	6.90	117.478720
$10_{29} \rightarrow 9_{18}$	4.51 X 10^{-3}	1014.84713	3.71	138.881717
$10_{29} \rightarrow 10_{1,10}$	1.30 X 10^{-3}	642.08991	4.24	138.881717
$11_{0,11} \rightarrow 10_{1,10}$	1.87 X 10^{-3}	616.01150	7.56	138.012436

Table 4.5: Einstein A-coefficients, frequency (ν), line strength (S_{ji}) and energy of upper rotational energy levels (E_j) for radiative transitions belonging to group IV, having A $>10^{-5}$ s^{-1} and S > 0.1.

Transition	**A-coefficient (s^{-1})**	**ν (GHz)**	**S_{ji}**	**E_j (cm^{-1})**
$1_{11} \rightarrow 0_{00}$	9.31 X 10^{-5}	225.55461	1.00	7.518487
$2_{20} \rightarrow 1_{11}$	1.74 X 10^{-3}	623.29139	1.48	28.294867
$2_{11} \rightarrow 2_{02}$	6.12 X 10^{-5}	172.26705	2.44	12.137227
$2_{20} \rightarrow 2_{11}$	4.85 X 10^{-4}	484.72917	0.86	28.294867
$3_{13} \rightarrow 2_{02}$	2.76 X 10^{-4}	340.35393	2.01	17.740123
$2_{20} \rightarrow 3_{13}$	2.48 X 10^{-5}	316.64229	0.14	28.294867
$3_{31} \rightarrow 2_{20}$	8.99 X 10^{-3}	1012.5315	2.49	62.045917
$3_{22} \rightarrow 2_{11}$	1.80 X 10^{-3}	676.56083	1.67	34.689255
$3_{22} \rightarrow 3_{13}$	6.59 X 10^{-4}	508.47395	1.43	34.689255
$3_{31} \rightarrow 3_{22}$	1.72 X 10^{-3}	820.69984	0.91	62.045917
$3_{22} \rightarrow 4_{13}$	1.32 X 10^{-5}	210.46751	0.43	34.689255
$4_{31} \rightarrow 3_{22}$	8.76 X 10^{-3}	1076.87861	2.58	70.585209
$4_{22} \rightarrow 3_{13}$	2.07 X 10^{-3}	766.22459	1.72	43.280943
$3_{31} \rightarrow 4_{22}$	7.88 X 10^{-5}	562.9492	0.14	62.045917
$4_{40} \rightarrow 3_{31}$	2.61 X 10^{-2}	1404.23789	3.49	108.853846
$4_{13} \rightarrow 4_{04}$	8.01 X 10^{-5}	192.21238	4.16	27.673671
$4_{22} \rightarrow 4_{13}$	6.37 X 10^{-4}	468.21815	2.30	43.280943
$4_{31} \rightarrow 4_{22}$	2.40 X 10^{-3}	819.12797	1.63	70.585209
$4_{40} \rightarrow 4_{31}$	3.75 X 10^{-3}	1148.05912	0.91	108.853846
$5_{15} \rightarrow 4_{04}$	6.15 X 10^{-4}	445.50406	3.16	36.116728
$4_{22} \rightarrow 5_{15}$	1.40 X 10^{-5}	214.92647	0.53	43.280943
$5_{33} \rightarrow 4_{22}$	8.97 X 10^{-3}	1139.41787	2.73	81.261539
$4_{40} \rightarrow 5_{33}$	1.56 X 10^{-4}	827.76922	0.10	108.853846
$5_{24} \rightarrow 4_{13}$	2.28 X 10^{-3}	785.93874	2.10	53.871629
$4_{31} \rightarrow 5_{24}$	1.03 X 10^{-4}	501.40738	0.29	70.585209
$5_{42} \rightarrow 4_{31}$	2.50 X 10^{-2}	1468.18541	3.59	119.524722
$5_{24} \rightarrow 5_{15}$	8.18 X 10^{-4}	532.64706	2.44	53.871629

Transition	A-coefficient (s^{-1})	ν (GHz)	S_{ji}	E_j (cm^{-1})
$5_{33} \rightarrow 5_{24}$	2.78 X 10^{-3}	821.69728	2.25	81.261539
$5_{42} \rightarrow 5_{33}$	5.65 X 10^{-3}	1147.89551	1.67	119.524722
$6_{33} \rightarrow 5_{24}$	9.52 X 10^{-3}	1206.35432	2.92	94.083440
$5_{42} \rightarrow 6_{33}$	2.50 X 10^{-4}	763.23847	0.24	119.524722
$6_{06} \rightarrow 5_{15}$	9.09 X 10^{-5}	251.42126	3.06	44.497436
$6_{24} \rightarrow 5_{15}$	2.72 X 10^{-3}	924.78327	1.82	66.942836
$5_{33} \rightarrow 6_{24}$	8.86 X 10^{-5}	429.56107	0.53	81.261539
$6_{42} \rightarrow 5_{33}$	2.49 X 10^{-2}	1532.12662	3.68	132.332426
$6_{15} \rightarrow 6_{06}$	1.19 X 10^{-4}	226.54873	5.45	52.049061
$6_{24} \rightarrow 6_{15}$	6.50 X 10^{-4}	446.81328	3.87	66.942836
$6_{33} \rightarrow 6_{24}$	2.94 X 10^{-3}	814.21811	2.92	94.083440
$6_{42} \rightarrow 6_{33}$	6.74 X 10^{-3}	1147.46958	2.39	132.332426
$7_{17} \rightarrow 6_{06}$	1.16 X 10^{-3}	543.45747	4.45	62.612685
$7_{35} \rightarrow 6_{24}$	1.01 X 10^{-2}	1262.80004	3.06	109.036171
$6_{42} \rightarrow 7_{35}$	2.77 X 10^{-4}	698.88765	0.43	132.332426
$7_{26} \rightarrow 6_{15}$	3.02 X 10^{-3}	884.83765	2.68	81.543649
$6_{33} \rightarrow 7_{26}$	7.08 X 10^{-5}	376.19373	0.72	94.083440
$7_{26} \rightarrow 7_{17}$	9.75 X 10^{-4}	567.92891	3.30	81.543649
$7_{35} \rightarrow 7_{26}$	3.17 X 10^{-3}	824.77566	3.49	109.036171
$8_{35} \rightarrow 7_{26}$	1.10 X 10^{-2}	1338.70087	3.20	126.167011
$8_{08} \rightarrow 7_{17}$	4.27 X 10^{-4}	399.17869	4.69	75.918642
$8_{26} \rightarrow 7_{17}$	3.44 X 10^{-3}	1104.04047	1.77	99.414034
$7_{35} \rightarrow 8_{26}$	3.67 X 10^{-5}	288.6641	0.96	109.036171
$8_{17} \rightarrow 8_{08}$	1.92 X 10^{-4}	278.64261	6.22	85.206728
$8_{26} \rightarrow 8_{17}$	6.43 X 10^{-4}	426.21917	5.79	99.414034
$8_{35} \rightarrow 8_{26}$	3.08 X 10^{-3}	802.58931	4.16	126.167011
$9_{19} \rightarrow 8_{08}$	2.01 X 10^{-3}	637.9067	6.03	97.182158
$9_{28} \rightarrow 8_{17}$	3.95 X 10^{-3}	973.79247	3.35	117.666477
$8_{35} \rightarrow 9_{28}$	2.67 X 10^{-5}	255.01602	1.15	126.167011
$9_{28} \rightarrow 9_{19}$	1.18 X 10^{-3}	614.52837	3.97	117.666477

Transition	**A-coefficient (s^{-1})**	**ν (GHz)**	**S_{ji}**	**E_j (cm^{-1})**
$10_{19} \rightarrow 9_{28}$	6.39 X 10^{-5}	281.83784	2.49	127.061072
$10_{0,10} \rightarrow 9_{19}$	1.23 X 10^{-3}	544.91179	6.55	115.345925
$10_{28} \rightarrow 9_{19}$	4.08 X 10^{-3}	1309.43664	1.58	140.830086
$10_{19} \rightarrow 10_{0,10}$	3.24 X 10^{-4}	351.45442	6.46	127.061072
$10_{28} \rightarrow 10_{19}$	6.48 X 10^{-4}	413.07042	7.94	140.830086
$11_{1,11} \rightarrow 10_{0,10}$	3.26 X 10^{-3}	732.85738	7.84	139.774504

Table 4.6: The transitions belonging to group I having a very small value of Einstein A-coefficients and line strength.

Transition	A-coefficient (s^{-1})	ν (GHz)	S_{ji}	E_j (cm^{-1})
$1_{10} \rightarrow 1_{11}$	1.55 X 10^{-9}	5.290123	1.50	2.133099
$2_{11} \rightarrow 2_{12}$	1.39 X 10^{-8}	15.86989	0.84	12.137227
$3_{31} \rightarrow 2_{12}$	1.63 X 10^{-6}	1513.130565	0.00	62.045917
$3_{30} \rightarrow 2_{11}$	1.66 X 10^{-6}	1497.2626	0.00	62.045981
$3_{12} \rightarrow 3_{13}$	5.57 X 10^{-8}	31.736418	0.58	18.798004
$3_{31} \rightarrow 3_{12}$	9.71 X 10^{-7}	1297.437376	0.00	62.045917
$3_{30} \rightarrow 3_{13}$	9.46 X 10^{-7}	1329.17572	0.00	62.045981
$3_{30} \rightarrow 3_{31}$	1.12 X 10^{-19}	0.001925	5.26	62.045981
$3_{31} \rightarrow 4_{14}$	1.29 X 10^{-7}	1084.047928	0.00	62.045917
$4_{32} \rightarrow 3_{13}$	3.75 X 10^{-6}	1585.339088	0.00	70.584760
$3_{30} \rightarrow 4_{13}$	1.31 X 10^{-7}	1031.169278	0.00	62.045981
$4_{31} \rightarrow 3_{12}$	3.89 X 10^{-6}	1553.616142	0.00	70.585209
$4_{13} \rightarrow 4_{14}$	1.55 X 10^{-7}	52.880576	0.45	27.673671
$4_{32} \rightarrow 4_{13}$	2.47 X 10^{-6}	1287.332646	0.00	70.584760
$4_{31} \rightarrow 4_{14}$	2.37 X 10^{-6}	1340.226695	0.00	70.585209
$4_{31} \rightarrow 4_{32}$	2.30 X 10^{-17}	0.013472	4.05	70.585209
$4_{32} \rightarrow 5_{15}$	3.08 X 10^{-7}	1034.040964	0.00	70.584760
$5_{33} \rightarrow 4_{14}$	6.55 X 10^{-6}	1660.516598	0.00	81.261539
$4_{31} \rightarrow 5_{14}$	3.09 X 10^{-7}	954.773192	0.00	70.585209
$5_{32} \rightarrow 4_{13}$	6.98 X 10^{-6}	1607.689867	0.00	81.263334
$5_{14} \rightarrow 5_{15}$	3.48 X 10^{-7}	79.281244	0.37	38.759436
$5_{33} \rightarrow 5_{14}$	4.42 X 10^{-6}	1275.063096	0.00	81.261539
$5_{32} \rightarrow 5_{15}$	4.16 X 10^{-6}	1354.398185	0.00	81.263334
$5_{32} \rightarrow 5_{33}$	9.78 X 10^{-16}	0.053846	3.31	81.263334
$5_{33} \rightarrow 6_{16}$	4.97 X 10^{-7}	987.272091	0.00	81.261539
$5_{32} \rightarrow 6_{15}$	4.87 X 10^{-7}	876.428194	0.00	81.263334
$6_{15} \rightarrow 6_{16}$	6.82 X 10^{-7}	110.897743	0.32	52.049061
$6_{34} \rightarrow 5_{15}$	1.02 X 10^{-5}	1738.840044	0.00	94.078062

Transition	A-coefficient (s^{-1})	ν (GHz)	S_{ji}	E_j (cm^{-1})
$6_{34} \rightarrow 6_{15}$	6.83 X 10^{-6}	1260.870053	0.00	94.078062
$6_{33} \rightarrow 5_{14}$	1.13 X 10^{-5}	1659.720131	0.00	94.083440
$6_{33} \rightarrow 6_{16}$	6.28 X 10^{-6}	1371.929126	0.00	94.083440
$6_{33} \rightarrow 6_{34}$	1.88 X 10^{-14}	0.16133	2.79	94.083440
$6_{34} \rightarrow 7_{17}$	6.68 X 10^{-7}	943.961312	0.00	94.078062
$6_{33} \rightarrow 7_{16}$	6.28 X 10^{-7}	796.462056	0.00	94.083440
$7_{16} \rightarrow 7_{17}$	1.21 X 10^{-6}	147.660586	0.28	67.534705
$7_{35} \rightarrow 6_{16}$	1.47 X 10^{-5}	1820.511056	0.00	109.036171
$7_{35} \rightarrow 7_{16}$	9.72 X 10^{-6}	1245.043986	0.00	109.036171
$7_{34} \rightarrow 6_{15}$	1.71 X 10^{-5}	1710.015846	0.00	109.049589
$7_{34} \rightarrow 7_{17}$	8.68 X 10^{-6}	1393.107105	0.00	109.049589
$7_{34} \rightarrow 7_{35}$	2.18 X 10^{-13}	0.402533	2.40	109.049589
$7_{35} \rightarrow 8_{18}$	8.08 X 10^{-7}	904.344093	0.00	109.036171
$7_{34} \rightarrow 8_{17}$	7.08 X 10^{-7}	715.285808	0.00	109.049589
$8_{17} \rightarrow 8_{18}$	2.01 X 10^{-6}	189.460817	0.24	85.206728
$8_{35} \rightarrow 7_{16}$	2.48 X 10^{-5}	1758.969193	0.00	126.167011
$8_{35} \rightarrow 8_{36}$	1.79 X 10^{-12}	0.883029	2.12	126.167011
$8_{36} \rightarrow 7_{17}$	2.02 X 10^{-5}	1905.74675	0.00	126.137577
$8_{36} \rightarrow 8_{17}$	1.31 X 10^{-5}	1227.925454	0.00	126.137577
$8_{35} \rightarrow 8_{18}$	1.13 X 10^{-5}	1418.2693	0.00	126.167011
$8_{36} \rightarrow 9_{19}$	9.13 X 10^{-7}	868.661363	0.00	126.137577
$8_{35} \rightarrow 9_{18}$	7.19 X 10^{-7}	633.405969	0.00	126.167011
$9_{18} \rightarrow 9_{19}$	3.15 X 10^{-6}	236.138423	0.22	105.053479
$10_{19} \rightarrow 10_{1,10}$	4.71 X 10^{-6}	287.470565	0.20	127.061072

Table 4.7: The transitions belonging to group II having a very small value of Einstein A-coefficients and line strength.

Transition	**A-coefficient (s^{-1})**	**ν (GHz)**	**S_{ji}**	**E_j (cm^{-1})**
$1_{01} \rightarrow 0_{00}$	1.83×10^{-6}	63.992972	1.00	2.133099
$2_{20} \rightarrow 1_{01}$	7.86×10^{-7}	784.853023	0.00	28.294867
$2_{21} \rightarrow 2_{02}$	7.67×10^{-7}	656.868519	0.00	28.290610
$2_{20} \rightarrow 2_{21}$	2.90×10^{-14}	0.127709	3.34	28.294867
$2_{20} \rightarrow 3_{03}$	1.09×10^{-7}	465.533368	0.00	28.294867
$3_{21} \rightarrow 2_{02}$	2.36×10^{-6}	849.465889	0.00	34.710522
$3_{22} \rightarrow 3_{03}$	1.92×10^{-6}	657.365026	0.00	34.689255
$3_{21} \rightarrow 3_{22}$	1.81×10^{-12}	0.638004	2.34	34.710522
$3_{21} \rightarrow 4_{04}$	1.87×10^{-7}	403.317892	0.00	34.710522
$4_{22} \rightarrow 3_{03}$	5.12×10^{-6}	915.115664	0.00	43.280943
$4_{40} \rightarrow 3_{21}$	3.88×10^{-6}	2224.299727	0.00	108.853846
$4_{41} \rightarrow 3_{22}$	3.89×10^{-6}	2224.937707	0.00	108.85845
$4_{23} \rightarrow 4_{04}$	3.45×10^{-6}	658.5202	0.00	43.217265
$4_{22} \rightarrow 4_{23}$	2.90×10^{-11}	1.910327	1.78	43.280943
$4_{40} \rightarrow 4_{23}$	1.61×10^{-6}	1969.09742	0.00	108.853846
$4_{41} \rightarrow 4_{22}$	1.61×10^{-6}	1967.187069	0.00	108.853845
$4_{40} \rightarrow 4_{41}$	2.32×10^{-25}	0.000024	7.19	108.853846
$4_{22} \rightarrow 5_{05}$	2.10×10^{-7}	343.025447	0.00	43.280943
$5_{23} \rightarrow 4_{04}$	9.50×10^{-6}	982.592225	0.00	54.019666
$4_{40} \rightarrow 5_{23}$	1.76×10^{-7}	1645.025395	0.00	108.853846
$5_{41} \rightarrow 4_{22}$	8.27×10^{-6}	2287.313597	0.00	119.524730
$4_{41} \rightarrow 5_{24}$	1.77×10^{-7}	1649.466478	0.00	108.853845
$5_{42} \rightarrow 4_{23}$	8.27×10^{-6}	2289.223707	0.00	119.524722
$5_{24} \rightarrow 5_{05}$	5.37×10^{-6}	660.746037	0.00	53.871629
$5_{23} \rightarrow 5_{24}$	2.42×10^{-10}	4.441108	1.45	54.019666
$5_{41} \rightarrow 5_{24}$	4.14×10^{-6}	1969.593006	0.00	119.524730
$5_{42} \rightarrow 5_{23}$	4.12×10^{-6}	1965.151682	0.00	119.524722

Transition	A-coefficient (s^{-1})	ν (GHz)	S_{ji}	E_j (cm^{-1})
$5_{41} \rightarrow 5_{42}$	1.13 X 10^{-22}	0.000216	5.85	119.524730
$5_{23} \rightarrow 6_{06}$	1.85 X 10^{-7}	285.666898	0.00	54.019666
$6_{24} \rightarrow 5_{05}$	1.59 X 10^{-5}	1052.882249	0.00	66.942836
$5_{41} \rightarrow 6_{24}$	4.85 X 10^{-7}	1577.456795	0.00	119.524730
$6_{42} \rightarrow 5_{05}$	4.40 X 10^{-8}	3014.569936	0.00	132.332426
$6_{42} \rightarrow 5_{23}$	1.35 X 10^{-5}	2349.382792	0.00	132.332426
$5_{42} \rightarrow 6_{25}$	4.93 X 10^{-7}	1586.283995	0.00	119.524722
$6_{43} \rightarrow 5_{24}$	1.36 X 10^{-5}	2353.822818	0.00	132.332390
$6_{25} \rightarrow 6_{06}$	7.67 X 10^{-6}	664.534586	0.00	66.648589
$6_{24} \rightarrow 6_{25}$	1.35 X 10^{-9}	8.827417	1.23	66.942836
$6_{42} \rightarrow 6_{25}$	7.39 X 10^{-6}	1970.515105	0.00	132.332426
$6_{43} \rightarrow 6_{06}$	5.88 X 10^{-8}	2635.048609	0.00	132.332390
$6_{43} \rightarrow 6_{24}$	7.34 X 10^{-6}	1961.686607	0.00	132.332390
$6_{42} \rightarrow 6_{43}$	1.00 X 10^{-20}	0.001081	4.96	132.332426
$6_{24} \rightarrow 7_{07}$	1.36 X 10^{-7}	232.405724	0.00	66.942836
$6_{42} \rightarrow 7_{07}$	1.70 X 10^{-8}	2194.093411	0.00	132.332426
$7_{25} \rightarrow 6_{06}$	2.47 X 10^{-5}	1127.124782	0.00	82.068262
$6_{42} \rightarrow 7_{25}$	8.54 X 10^{-7}	1507.924908	0.00	132.332426
$6_{43} \rightarrow 7_{26}$	8.75 X 10^{-7}	1523.662233	0.00	132.332390
$7_{26} \rightarrow 7_{07}$	1.03 X 10^{-5}	670.430097	0.00	81.543649
$7_{25} \rightarrow 7_{26}$	5.69 X 10^{-9}	15.738406	1.06	82.068262
$7_{25} \rightarrow 8_{08}$	8.44 X 10^{-8}	184.488624	0.00	82.068262
$8_{26} \rightarrow 7_{07}$	3.58 X 10^{-5}	1206.541658	0.00	99.414034
$8_{27} \rightarrow 8_{08}$	1.34 X 10^{-5}	678.988365	0.06	98.551587
$8_{26} \rightarrow 8_{27}$	1.94 X 10^{-8}	25.873414	0.89	99.414034
$8_{26} \rightarrow 9_{09}$	4.53 X 10^{-8}	143.153487	0.00	99.414034
$9_{27} \rightarrow 8_{08}$	4.89 X 10^{-5}	1292.345178	0.00	118.996814
$9_{28} \rightarrow 9_{09}$	1.68 X 10^{-5}	690.72678	0.06	117.666477
$9_{27} \rightarrow 9_{28}$	5.61 X 10^{-8}	39.910107	0.78	118.996814
$9_{27} \rightarrow 10_{0,10}$	2.18 X 10^{-8}	109.526687	0.00	118.996814

Transition	**A-coefficient (s^{-1})**	**ν (GHz)**	**S_{ji}**	**E_j (cm^{-1})**
$10_{28} \rightarrow 9_{09}$	6.33 X 10^{-5}	1385.63504	0.00	140.830086
$10_{29} \rightarrow 10_{0,10}$	2.06 X 10^{-5}	706.07376	0.06	138.881717
$10_{28} \rightarrow 10_{29}$	1.41 X 10^{-7}	58.45108	0.72	140.830086
$10_{28} \rightarrow 11_{0,11}$	1.01 X 10^{-8}	84.529488	0.00	140.830086

Table 4.8: The transitions belonging to group III having a very small value of Einstein A-coefficients and line strength.

Transition	**A-coefficient (s^{-1})**	**ν (GHz)**	**S_{ji}**	**E_j (cm^{-1})**
$3_{03} \rightarrow 2_{12}$	1.62 X 10^{-7}	35.0657	1.08	12.777088
$3_{30} \rightarrow 3_{03}$	2.41 X 10^{-6}	1478.06679	0.00	62.045981
$4_{32} \rightarrow 3_{03}$	9.11 X 10^{-6}	1734.23016	0.00	70.584760
$4_{41} \rightarrow 3_{12}$	1.33 X 10^{-6}	2701.67524	0.00	108.853845
$4_{41} \rightarrow 4_{14}$	1.00 X 10^{-6}	2488.28579	0.00	108.853845
$4_{23} \rightarrow 5_{14}$	4.34 X 10^{-6}	133.73489	0.67	43.217265
$4_{41} \rightarrow 5_{14}$	2.26 X 10^{-7}	2102.83229	0.00	108.853845
$4_{32} \rightarrow 5_{05}$	2.14 X 10^{-6}	1162.13995	0.00	70.584760
$5_{41} \rightarrow 4_{14}$	4.71 X 10^{-6}	2808.41232	0.00	119.524730
$5_{41} \rightarrow 5_{14}$	4.50 X 10^{-6}	2422.95882	0.00	119.524730
$5_{32} \rightarrow 5_{05}$	2.66 X 10^{-5}	1482.49717	0.00	81.263334
$5_{23} \rightarrow 6_{16}$	7.31 X 10^{-6}	170.01591	0.67	54.019666
$5_{41} \rightarrow 6_{16}$	7.54 X 10^{-7}	2135.16781	0.00	119.524730
$6_{34} \rightarrow 5_{05}$	6.13 X 10^{-5}	1866.93903	0.00	94.078062
$6_{43} \rightarrow 5_{14}$	1.34 X 10^{-5}	2807.18863	0.00	132.332390
$6_{43} \rightarrow 6_{16}$	9.61 X 10^{-6}	2519.39763	0.00	132.332390
$7_{16} \rightarrow 6_{25}$	3.91 X 10^{-8}	26.58347	1.29	67.534705
$6_{43} \rightarrow 7_{16}$	2.26 X 10^{-6}	1943.93056	0.00	132.332390
$6_{34} \rightarrow 7_{07}$	8.64 X 10^{-6}	1046.46250	0.00	94.078062
$7_{34} \rightarrow 7_{07}$	1.02 X 10^{-4}	1495.60829	0.02	109.049589
$7_{25} \rightarrow 8_{18}$	1.21 X 10^{-6}	95.30684	0.86	82.068262
$8_{36} \rightarrow 7_{07}$	2.24 X 10^{-4}	2008.24794	0.02	126.137577
$8_{36} \rightarrow 9_{09}$	1.80 X 10^{-5}	944.85977	0.02	126.137577
$9_{27} \rightarrow 10_{1,10}$	1.07 X 10^{-7}	45.54283	0.88	118.996814

Table 4.9: The transitions belonging to group IV having a very small value of Einstein A-coefficients and line strength.

Transition	**A-coefficient (s^{-1})**	**ν (GHz)**	**S_{ji}**	**E_j (cm^{-1})**
$1_{11} \rightarrow 2_{02}$	1.63 X 10^{-7}	33.70484	0.53	7.518487
$3_{31} \rightarrow 2_{02}$	1.99 X 10^{-6}	1669.52773	0.00	62.045917
$4_{04} \rightarrow 3_{13}$	5.39 X 10^{-6}	105.79406	1.67	21.266592
$3_{31} \rightarrow 4_{04}$	5.79 X 10^{-7}	1223.37973	0.00	62.045917
$4_{40} \rightarrow 3_{13}$	1.27 X 10^{-6}	2733.41168	0.00	108.853846
$4_{40} \rightarrow 4_{13}$	1.09 X 10^{-6}	2435.40524	0.00	108.853846
$4_{31} \rightarrow 4_{04}$	1.01 X 10^{-5}	1479.5585	0.00	70.585209
$4_{40} \rightarrow 5_{15}$	1.97 X 10^{-7}	2182.11356	0.00	108.853846
$5_{33} \rightarrow 4_{04}$	2.64 X 10^{-5}	1799.8484	0.00	81.261539
$5_{42} \rightarrow 4_{13}$	5.19 X 10^{-6}	2755.53153	0.00	119.524722
$5_{42} \rightarrow 5_{15}$	3.88 X 10^{-6}	2502.23985	0.00	119.524722
$5_{24} \rightarrow 6_{15}$	3.48 X 10^{-7}	54.67706	0.96	53.871629
$5_{42} \rightarrow 6_{15}$	8.81 X 10^{-7}	2024.26985	0.00	119.524722
$5_{33} \rightarrow 6_{06}$	4.85 X 10^{-6}	1102.92307	0.00	81.261539
$6_{42} \rightarrow 5_{15}$	1.14 X 10^{-5}	2886.47095	0.00	132.332426
$6_{42} \rightarrow 6_{15}$	1.18 X 10^{-5}	2408.50096	0.00	132.332426
$6_{33} \rightarrow 6_{06}$	5.60 X 10^{-5}	1487.58011	0.00	94.083440
$6_{24} \rightarrow 7_{17}$	3.23 X 10^{-6}	129.90453	0.77	66.942836
$6_{42} \rightarrow 7_{17}$	1.80 X 10^{-6}	2091.59222	0.00	132.332426
$7_{35} \rightarrow 6_{06}$	1.24 X 10^{-4}	1936.16204	0.00	109.036171
$8_{17} \rightarrow 7_{26}$	3.11 X 10^{-6}	109.89239	1.63	85.206728
$7_{35} \rightarrow 8_{08}$	1.32 X 10^{-5}	993.52588	0.00	109.036171
$8_{35} \rightarrow 8_{08}$	1.68 X 10^{-4}	1507.45109	0.05	126.167011
$8_{26} \rightarrow 9_{19}$	3.82 X 10^{-7}	66.95508	0.91	99.414034
$10_{28} \rightarrow 11_{1,11}$	3.09 X 10^{-8}	31.66746	0.86	140.830086

Table 4.10: Radiative lifetime (T_j) of CH_2NH in rotational energy levels.

Sr. No.	Energy Level	T_j (s)	Sr. No.	Energy Level	T_j (s)
1	0_{00}	INFINITY	31	7_{17}	5.23×10^2
2	1_{01}	5.48×10^5	32	6_{25}	3.21×10^2
3	2_{02}	5.73×10^4	33	6_{24}	3.09×10^2
4	1_{11}	1.07×10^4	34	7_{16}	9.02×10^2
5	1_{10}	1.77×10^4	35	4_{32}	8.90×10^1
6	2_{12}	5.58×10^3	36	4_{31}	8.90×10^1
7	2_{11}	1.31×10^4	37	8_{08}	6.01×10^2
8	3_{03}	1.59×10^4	38	8_{18}	3.75×10^2
9	3_{13}	3.07×10^3	39	5_{33}	8.34×10^1
10	3_{12}	7.56×10^3	40	5_{32}	8.34×10^1
11	4_{04}	6.31×10^3	41	7_{26}	2.62×10^2
12	4_{14}	1.81×10^3	42	7_{25}	2.54×10^2
13	4_{13}	4.09×10^3	43	8_{17}	6.10×10^2
14	2_{21}	5.80×10^2	44	6_{34}	7.73×10^1
15	2_{20}	5.75×10^2	45	6_{33}	7.73×10^1
16	5_{05}	3.01×10^3	46	9_{09}	4.00×10^2
17	3_{22}	5.46×10^2	47	9_{19}	2.76×10^2
18	3_{21}	5.34×10^2	48	8_{27}	2.13×10^2
19	5_{15}	1.14×10^3	49	8_{26}	2.10×10^2
20	5_{14}	2.32×10^3	50	9_{18}	4.29×10^2
21	4_{23}	4.71×10^2	51	4_{41}	3.82×10^1
22	4_{22}	4.56×10^2	52	4_{40}	3.82×10^1
23	6_{06}	1.62×10^3	53	7_{35}	7.10×10^1
24	6_{16}	7.57×10^2	54	7_{34}	7.10×10^1
25	6_{15}	1.40×10^3	55	$10_{0,10}$	2.78×10^2
26	5_{24}	3.92×10^2	56	$10_{1,10}$	2.09×10^2
27	5_{23}	3.77×10^2	57	9_{28}	1.74×10^2
28	7_{07}	9.54×10^2	58	9_{27}	1.75×10^2
29	3_{31}	9.34×10^1	59	5_{42}	3.98×10^1
30	3_{30}	9.34×10^1	60	5_{41}	3.98×10^1

Sr. No.	Energy Level	T_j (s)
61	8_{36}	6.47×10^{1}
62	8_{35}	6.48×10^{1}
63	10_{19}	3.10×10^{2}
64	6_{43}	3.96×10^{1}
65	6_{42}	3.97×10^{1}

Sr. No.	Energy Level	T_j (s)
66	$11_{0,11}$	2.00×10^{2}
67	10_{29}	1.43×10^{2}
68	$11_{1,11}$	1.61×10^{2}
69	10_{28}	1.47×10^{2}

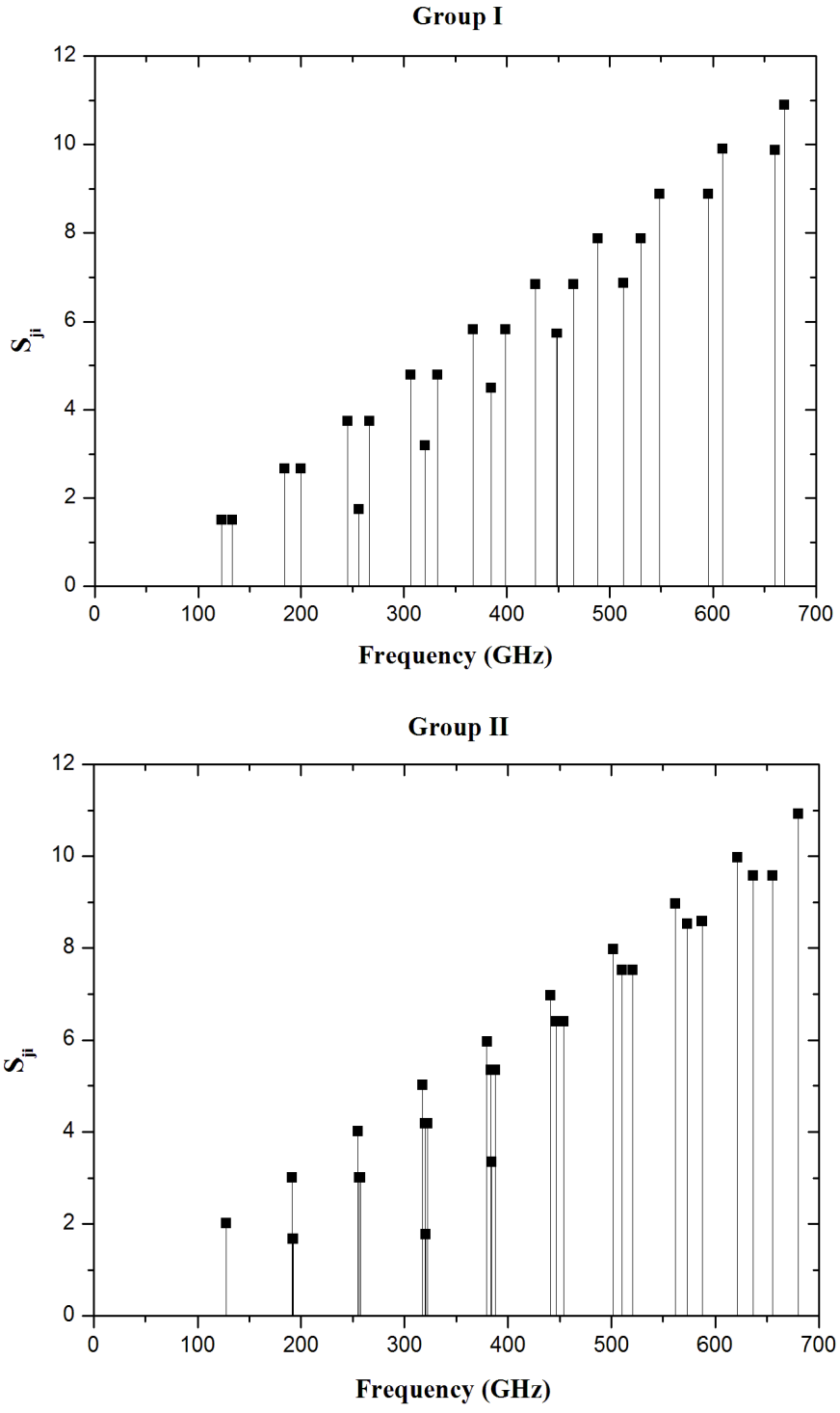

Figure 4.2: Line strengths S_{ji} for a-type transitions in CH_2NH

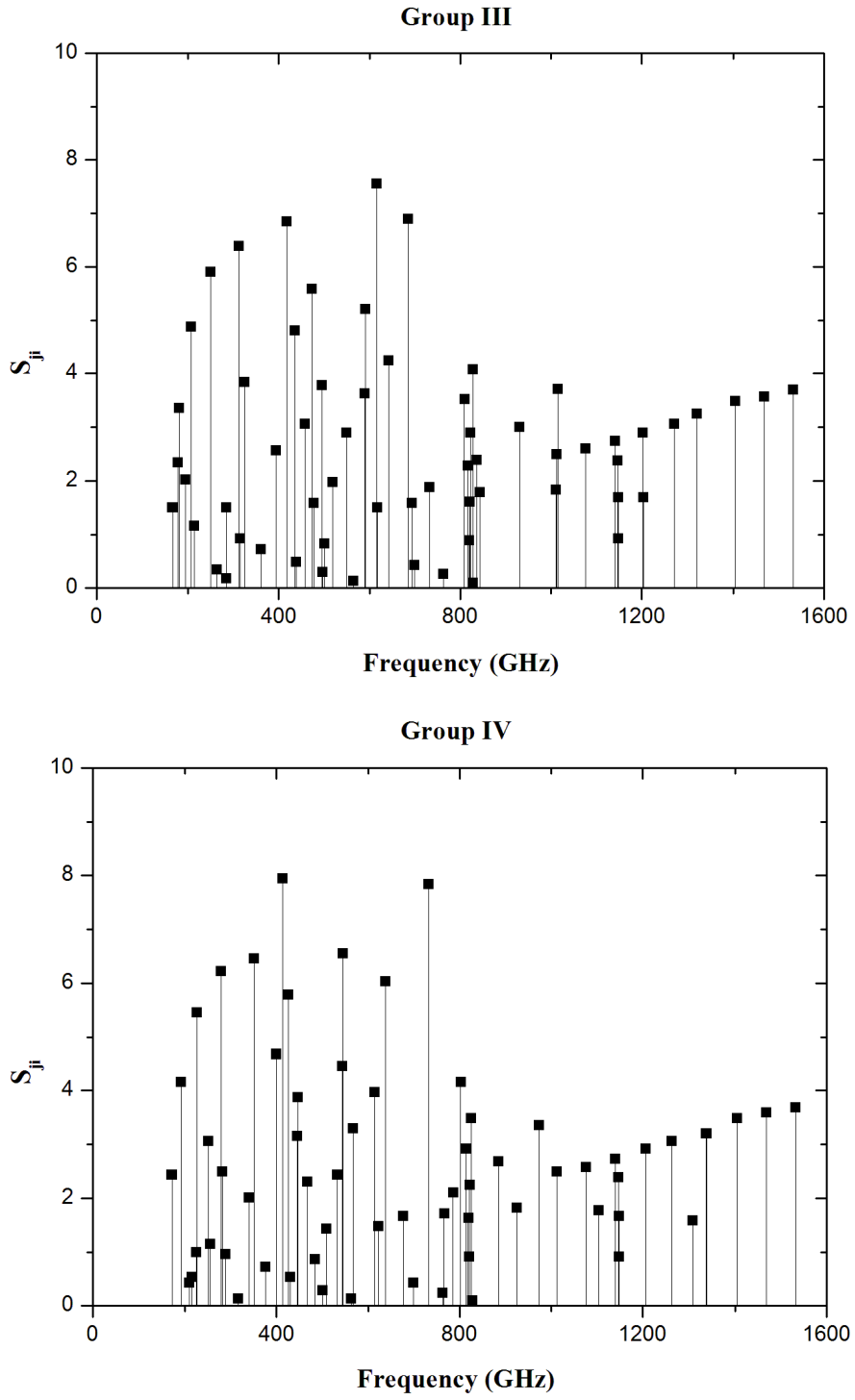

Figure 4.3: Line strengths S_{ji} for b-type transitions in CH_2NH.

SECTION - II

4.7 Molecular Symmetries in Methanimine: Classification of 15 Lowest Rotational Energy Levels

As already given in section 4.2, that in addition to the selection rule $\Delta J = 0, \pm 1$, the transitions between rotational energy levels are classified into 4 groups which are exclusive from each other. For a-type transitions, we have

k_a, k_c: odd, even ↔ odd, odd (Group I)

even, even ↔ even, odd (Group II)

For example, in the case of H_2CO (a-type asymmetric top molecule), Groups I and II are called the ortho and para species and they behave as if they are two independent molecules. That is, there are no (optical as well as collisional) transitions between these two species (Groups I and II, here).

For the electric dipole moment along a-axis, the lowest 15 rotational energy levels are classified into two groups i.e. group I and II having the levels with the serial numbers as given below:

Group I: (4, 5, 6, 7, 9, 10, 12, 13)

Group II: (1, 2, 3, 8, 11, 14, 15)

The serial number of energy levels is according to Table 4.1. Also, for the b-type transitions, the levels of Group I are connected to those of Group II as given below.

k_a, k_c: odd, even ↔ even, odd (Group III)

even, even ↔ odd, odd (Group IV)

Thus, for b-type transitions, the rotational levels are classified into two distinct groups, named as Group III and Group IV. For example, the H_2O is b-type asymmetric top molecule and its rotational levels are classified into two distinct groups III and IV called the ortho and para species. Here, also there are no transitions (radiative as well as collisional) between the levels of III and IV groups. As we have

considered both a and b type transitions together, and therefore, we have to consider transitions between all levels in each group, individually.

For the electric dipole moment along the b-axis, these 15 levels are classified into two groups III and IV having the levels with the serial numbers given below:

Group III: (2, 5, 6, 8, 10, 12, 14)

Group IV: (1, 3, 4, 7, 9, 11, 13, 15)

The radiative, as well as collisional transitions, are individually confined within each group. The transitions due to collisions do not obey selection rules unlike radiative transitions, but they are still confined within a group, individually. The allowed radiative transitions between the lowest 15 levels following selection rules are given in Table 4.11. Also, based on the propensity rules discussed above, the possible collisional transitions between 15 levels are given in Table 4.12. Here, the cross-mark indicates the allowed transition and vacant spaces represent forbidden transitions.

Also, in Table 4.12, besides 15 diagonal positions, there are 56 vacant positions. These are transitions following the selection rules:

k_a, k_c : even,odd $\leftrightarrow$ odd, odd (Group V)

even, even $\leftrightarrow$ odd, even (Group VI)

Out of 15 levels, the levels belonging to groups V and VI are as follows:

Group V: (2, 4, 7, 8, 9, 13. 14)

Group VI : (1, 3, 5, 6, 10, 11, 12, 15)

Such transitions are known as c-type transitions. Besides the diagonal positions, the 56 vacant positions in Table 4.12 are c-type transitions. As the methanimine has no component of electric dipole moment along the c-axis, so the transitions corresponding to the vacant positions in Table 4.12 cannot be included for methanimine in any circumstances. As the software MOLSCAT is used to calculate

the collisional rate coefficients which provide output values for all the transitions (allowed and forbidden) including the transition from a level to itself which is absurd. So, it is necessary to reject those numbers which are not allowed theoretically.

4.8 Collision of CH_2NH with He

For the study of the collision of methanimine molecule with He atom, we have optimized the co-ordinates of methanimine molecule with the help of software Gaussian (2003) [173]. The optimized coordinates are given in Table 4.13 and the structure of methanimine is shown in figure 4.4. Also, the collision of He with CH_2NH is represented in figure 4.5. To optimize the geometry of CH_2NH, the non-local correlation functional B3LYP [187,188] is used along with the basis sets, aug-cc-pVDZ, and aug-cc-pVTZ. The calculated values of rotational and centrifugal distortion constants are given in columns 2 and 3 in Table 4.14. These values are compared with the experimentally observed values by Motoki et al. [94] in Watson's S- reduced Hamiltonian given in column 1 of Table 4.14 and are used for the calculation of energies of rotational levels in the ground vibrational state and ground electronic state.

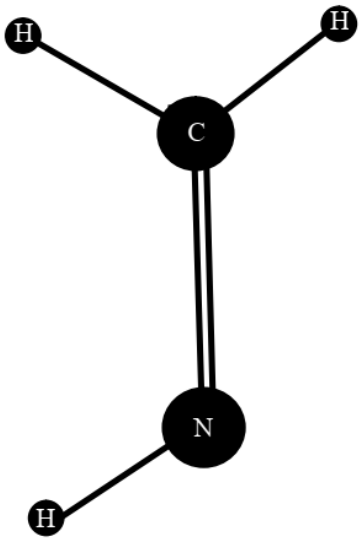

Figure 4.4: The structure of CH_2NH

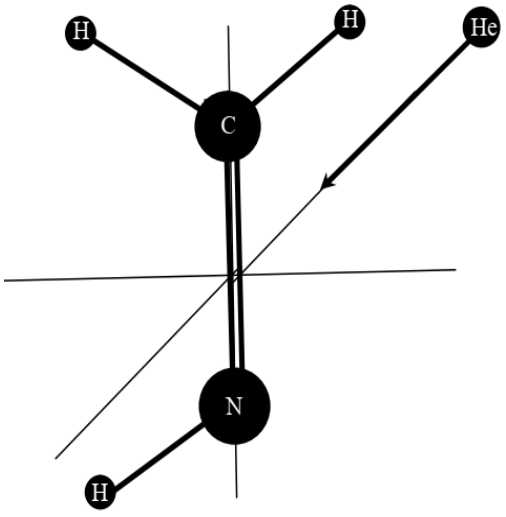

Figure 4.5: Interaction of He with CH_2NH

4.9 Collisional Transition Rates

The de-excitation collisional rate coefficients for transitions between the first 15 levels of CH_2NH are very recently (2018) determined by Faure et al.[189]. These collisional rate coefficients are used in solving the statistical equilibrium equations. However, the data provided by Faure et al. included all the possible transitions, out of which we have selected collisional rates for only 101 transitions that are in accordance with Table 4.12. These collisional rate coefficients are given in Table 4.15. Also, the excitation collision rate coefficients are calculated according to detailed balance as described in section 3.5.

The collisional rate coefficients for transitions between rotational energy levels are a function of kinetic temperature in the interstellar medium [190,191]. Figure 4.6 shows a decrease in de-excitation collisional rate coefficients with an increase in kinetic temperature. It indicates an increase in population density in the upper energy level with an increase in temperature.

4.10 Radiative Transfer Equations

The ratio of population densities in higher (j) and lower level (i) are related as

$$\frac{n_j}{n_i} = \frac{g_j}{g_i} e^{-\frac{\Delta E}{kT}} \quad \ldots (4.1)$$

where $\Delta E = h\nu$ for radiative transitions. Here, T denotes the kinetic temperature in the region where the transition occurs. The Planck's function at this temperature is given by

$$B_\nu(T) = \frac{8\pi h\nu^3}{c^3\left(\exp\left(\frac{\Delta E}{kT}\right) - 1\right)} \quad \ldots (4.2)$$

The population densities at this kinetic temperature T are known as thermal populations and the object is said to be in Local Thermal Equilibrium (LTE). In this state, the collisional transitions are very dominating as compared to radiative transitions.

In the case of Non-Local Thermal Equilibrium (NLTE), the rate of radiative transitions is comparable to the rate of collisional transitions. The population densities

of upper and lower levels are calculated under NLTE conditions. Using these values, the excitation temperature is calculated as

$$T_{ex} = \frac{\Delta E}{kln(\frac{n_i g_j}{n_j g_i})} \quad \ldots (4.3)$$

For population densities under NLTE condition, the source function is given by

$$S_\nu = \frac{8\pi h\nu^3}{c^3(\exp\left(\frac{\Delta E}{kT_{ex}}\right) - 1)} \quad \ldots (4.4)$$

which is the same as Planck's function for excitation temperature. It is different from equation (4.1) where the kinetic temperature is used that involves thermal population densities under LTE. Thus, we can write

$$S_\nu = B_\nu(T_{ex})$$

In interstellar medium, the intensity of a line produced with homogeneous excitation condition is given by

$$I_\nu - I_{\nu,bg} = \left(S_\nu - I_{\nu,bg}\right)(1 - e^{-\tau_\nu}) \quad \ldots (4.5)$$

where $I_{\nu,bg}$ is the intensity of the CMB, and τ_ν denotes the optical depth of the line. The brightness temperature T_B is related to the intensity of a line, by the expression

$$I_\nu = \frac{8\pi h\nu^3}{c^3(\exp\left(\frac{\Delta E}{kT_B}\right) - 1)} \quad \ldots (4.6)$$

which is same as Planck's function corresponding to the brightness temperature T_B, so we have

$$I_\nu = B_\nu(T_B)$$

Thus, equation (4.5) can also be written as

$$B_\nu(T_B) - B_\nu\left(T_{bg}\right) = \left[B_\nu(T_{ex}) - B_\nu\left(T_{bg}\right)\right](1 - e^{-\tau_\nu}) \quad \ldots (4.7)$$

where T_{bg} = 2.73 K represents the background temperature. In the Rayleigh-Jeans limit [ν(GHz) << 21 T(Kelvin)], we have

$$B_\nu(T_B) = \frac{8\pi h\nu^3 kT_B}{c^3\Delta E},$$

$$B_\nu(T_{ex}) = \frac{8\pi h\nu^3 kT_{ex}}{c^3\Delta E},$$

$$B_\nu(T_{bg}) = \frac{8\pi h\nu^3 kT_{bg}}{c^3\Delta E},$$

Thus, equation (4.7) becomes

$$T_B = T_{ex} + (T_{bg} - T_{ex})e^{-\tau_\nu} \quad \text{... (4.8)}$$

For optically thin case, $\tau_\nu \approx 0$, so we will get $T_B = T_{bg} = 2.73$ K.

The physical conditions prevalent in the cosmic objects decide whether the line will be observed in absorption or emission. The conditions for obtaining the anomalous phenomenon in interstellar molecules are explained below:

(i). Condition for MASER Action: In case of population inversion between two energy levels of the molecule, the excitation temperature shows a negative value. The equation (4.8) after rearrangement will become

$$T_B = T_{bg}e^{-\tau_\nu} - T_{ex}(e^{-\tau_\nu} - 1)$$

As $T_{ex} < 0$ and $\tau_\nu < 0$ for population inversion required for MASER action, the above equation shows that $T_B > T_{bg}$. For fairly large negative values of τ_ν, we will have $e^{-\tau\nu} >> 1$. Thus for MASER action,

$$T_B = (T_{bg} - T_{ex})e^{-\tau_\nu}$$

(ii). Condition for Anomalous Absorption: For anomalous absorption ($I_\nu < I_{\nu,bg}$; $T_B < T_{bg}$) with $\tau_\nu > 0$, we have positive value of T_{ex} but still less than T_{bg}, i.e. ($0 < T_{ex} < T_{bg}$) and thus $T_B > T_{ex}$ [140,192]. Hence, for anomalous absorption

$$0 < T_{ex} < T_B < T_{bg}.$$

4.11 Potential Rotational Transitions for Detection of Methanimine

By using the Einstein A-coefficients and collisional rate coefficients for transitions between rotational energy levels of methanimine, the statistical equilibrium equations coupled with the equations of radiative transfer are solved using computer

programming in FORTRAN language. These non-linear equations are solved for a given value of γ and hydrogen molecular density n_{H2}. The parameter γ is expressed as $\gamma = n_{mol} / (dv_r/dr)$, where, n_{mol} represents the number density of CH_2NH and (dv_r/dr) is the velocity gradient in the object.

The output of statistical equilibrium equations is the population densities of rotational energy levels under Non-Local Thermal Equilibrium (NLTE) conditions which are used to calculate the brightness temperature T_B for the transitions 1_{10}–1_{11}, 2_{11}–2_{12}, 3_{12}–3_{13}, 4_{13}–4_{14}, and 1_{11}–2_{02}. A plot of brightness temperature versus hydrogen molecular density is obtained for these transitions between rotational energy levels in CH_2NH molecule as shown in figures 4.7 to 4.11. The calculations are carried out for a variety of physical parameters so that a large number of cosmic objects are included that may contain CH_2NH. The variation is studied at kinetic temperatures 10K, 15K, 20K, 25K, and 30K, which is the expected temperature in cold objects. Also, the molecular hydrogen density is varied in the range 10^2 cm^{-3} to 10^6 cm^{-3} so that $\log(n_{H2})$ varies from 2 to 6. In these plots, the blue line is drawn for $\gamma = 10^{-5}$ $cm^{-3}(km/s)^{-1}$ pc and the orange line for $\gamma = 10^{-6}$ $cm^{-3}(km/s)^{-1}$ pc. Also, the collisional rates for transition with $\Delta k_a = 0$ are enhanced by a factor of 10 to test our vulnerability towards them. A detailed explanation of the obtained results is given in the following sections.

4.11.1 Transition 1_{10}–1_{11}

The brightness temperature versus hydrogen molecular density curve for the transition 1_{10}–1_{11} is shown in figure 4.7 which indicates the emission feature as T_B is greater than T_{bg}. A peak in T_B is obtained around the density $n_{H2} = 10^{4.5}$ cm^{-3} and it decreases on both sides of this density. Also, the peak is found to shift towards a low-density region when γ is increased by an order of magnitude. Thus, weak maser action is indicated in the transition. An analytical calculation of the maser action in 1_{10}–1_{11} transition is given in section 4.12 also, which proves the significance of this transition in the detection of methanimine in the interstellar medium.

4.11.2 Transition 2_{11}–2_{12}

As shown in figure 4.8, T_B is found to be slightly more than T_{bg} for the transition 2_{11}–2_{12}. There is a little variation in T_B with molecular hydrogen density for $\gamma = 10^{-6}$ $cm^{-3}(km/s)^{-1}$ pc. However, a significant increase in T_B occurs for $\gamma = 10^{-5}$ $cm^{-3}(km/s)^{-1}$ pc, showing a weak emission feature for this transition.

4.11.3 Transition 3_{12}–3_{13}

For the transition 3_{12}–3_{13}, T_B becomes greater than T_{bg} for kinetic temperature equal to or greater than 20 Kelvin and $\gamma = 10^{-5}$ $cm^{-3}(km/s)^{-1}$ pc as shown in figure 4.9, which indicates a very weak emission feature in this case.

4.11.4 Transition 4_{13}–4_{14}

For the transition 4_{13}–4_{14}, the variation in T_B becomes significantly more than T_{bg} for molecular hydrogen density greater than 10^5 cm^{-3}, which shows the emission feature for this transition as well. The brightness temperature is slightly above background temperature T_{bg} as shown in figure 4.10.

4.11.5 Transition 1_{11}–2_{02}

For transition 1_{11}–2_{02}, T_B is found to be less than T_{bg} indicating anomalous absorption as shown in figure 4.11. The brightness temperature is minimum around the density $n_{H2} = 10^{4.5}$ cm^{-3} and it rises on both sides of this density. Also, the minima shift towards low-density region when γ is increased by an order of magnitude. The anomalous absorption is an unusual phenomenon that makes the transition 1_{11}–2_{02} important in the detection of methanimine in interstellar medium.

4.12 Analytical Treatment of 1_{10}–1_{11} Transition

For the transition 1_{10}–1_{11}, let us consider only those energy levels which connect the levels 1_{10} and 1_{11} with other levels satisfying $\Delta J = 0, \pm 1$, as per division into groups given in section 4.7. The transition 1_{10}–1_{11} is an a-type transition lying in group I. We can find that no transition can occur between levels 1 and 5, between the levels 3 and 5, and between levels 2 and 4 for a-type transitions. Figure 4.12 shows all the possible

transitions to and from level 4 (1_{11}) and level 5(1_{10}). For optically thin atmosphere, the statistical equilibrium equation in the steady-state, for level 5 will be

$$n_7(A_{75} + C_{75}) + n_6C_{65} + n_4C_{45} + n_2C_{25} = n_5(A_{52} + C_{52} + C_{57} + C_{56} + A_{54} + C_{54}) \quad ...(4.9)$$

In the steady-state, the statistical equilibrium equation for level 4 is as the following.

$$n_7C_{74} + n_6(A_{64} + C_{64}) + n_5(A_{54} + C_{54}) + n_3C_{34} + n_1C_{14} - n_4(C_{47} + C_{46} + C_{45} + C_{43} + A_{43} + A_{41} + C_{41}) = 0 \quad \ldots(4.10)$$

Subtracting equation (4.10) from (4.9), we get

$$n_7(A_{75} + C_{75} - C_{74}) - n_6(A_{64} - C_{65} + C_{64}) - n_5(A_{52} + C_{52} + C_{57} + C_{56} + 2A_{54} + 2C_{54}) + n_4(2C_{45} + C_{47} + C_{46} + C_{43} + A_{43} + A_{41} + C_{41}) - n_3C_{34} + n_2C_{25} - n_1C_{14} = 0 \quad \ldots(4.11)$$

The Einstein A-coefficients from the calculated values in Tables 4.2 to 4.5 are used. Also, as a crude estimate, the collisional rate coefficients C′ for all the concerned transitions lie in the range from 10^{-10} to 10^{-12} as explained below.

In general, the collisional rate coefficients form a higher level j to a lower level i is expressed as $C'_{ji} = < v\sigma_{ji} >$ where v is the relative velocity of colliding particles and σ_{ji} is the collision cross-section for the transition [26]. A crude estimate gives us $\sigma_{ji} \approx \pi a_0^2 \approx 10^{-16}$ cm^2 and velocity $v \approx 1$ km/sec so that $C' \approx 10^{-11}$ cm^{3}s^{-1}, where a_0 is Bohr's radius. Here, the collisional rate coefficients for all the transitions starting from one level, in the downward direction, are taken to be the same. However, the actual collisional rate coefficients show a variation as given in section 4.9.

Also, for dense cloud conditions, the molecular hydrogen density $n_{H2} \approx 10^4$ cm^{-3}, the collisional rate will become $C_{ji} = C'n_{H2}$. Thus the range of collisional rates C_{ji} will become 10^{-6} to 10^{-8} s^{-1}. By substituting the values of Einstein A-coefficients and considering the largest value of the collisional rate of the order of 10^{-6} s^{-1}, the equation (4.11) becomes

$$n_5(6.15 \times 10^{-5}) = n_4(9.93 \times 10^{-5}) + n_3(10^{-6}) - n_2(10^{-6}) + n_1(10^{-6})$$

Thus,

$$\frac{n_5}{n_4} = 1.61 + 0.02\left(\frac{n_3 - n_2 + n_1}{n_4}\right)$$

The population of level 1 is much larger than those of other levels. It shows that the ratio n_5/n_4 is always larger than 1. Hence, the population inversion between levels 1_{10} and 1_{11} does exist. The same result can be found just by considering the radiative lifetimes of the levels as explained below.

As the radiative lifetime of an energy level is inversely proportional to Einstein A-coefficients, we will have

$$\frac{T_5}{T_4} = \frac{A_{41} + A_{43}}{A_{52} + A_{54}} = 1.65$$

Thus, a weak MASER action is found to occur for 1_{10}–1_{11} transition of methanimine by an analytical technique using scaled values of collisional rate coefficients. Also, it shows the little contribution of collisional transitions as compared to radiative transitions.

4.13 Conclusion

The contribution of collisional rate coefficients is found to be less significant than Einstein A-coefficients for large velocity gradient calculations for the lowest 15 rotational levels of methanimine. The Weak MASER action of 1_{10}–1_{11} and the anomalous absorption of 1_{11}–2_{02} transitions are maximum around a density of $10^{4.5}$ cm^{-3} and it decreases on both sides of this density. These transitions will play an important role in the identification of methanimine in the interstellar medium.

Table 4.11: Radiative transitions between the lowest 15 rotational energy levels of CH_2NH. The X mark shows an allowed transition.

Energy Level No.	**1**	**2**	**3**	**4**	**5**	**6**	**7**	**8**	**9**	**10**	**11**	**12**	**13**	**14**	**15**
1		X		X											
2	X		X		X	X									X
3		X		X			X	X	X					X	
4	X		X		X	X									X
5		X		X			X							X	
6		X		X			X	X	X					X	
7			X		X	X				X					X
8			X			X				X	X	X			X
9			X			X				X	X	X			X
10							X	X	X				X	X	
11								X	X				X		
12								X	X				X		
13										X	X	X			
14			X		X	X				X					X
15		X		X			X	X	X					X	

Table 4.12: Collisional transitions between the lowest 15 rotational energy levels of CH_2NH. The X mark shows an allowed transition.

Energy Level No.	**1**	**2**	**3**	**4**	**5**	**6**	**7**	**8**	**9**	**10**	**11**	**12**	**13**	**14**	**15**
1		X	X	X			X	X	X		X		X	X	X
2	X		X		X	X		X		X	X	X		X	X
3	X	X		X			X	X	X		X		X	X	X
4	X		X		X	X	X		X	X	X	X	X		X
5		X		X		X	X	X	X	X		X	X	X	
6		X		X	X		X	X	X	X		X	X	X	
7	X		X	X	X	X			X	X	X	X	X		X
8	X	X	X		X	X				X	X	X		X	X
9	X		X	X	X	X	X			X	X	X	X		X
10		X		X	X	X	X	X	X			X	X	X	
11	X	X	X	X			X	X	X				X	X	X
12		X		X	X	X	X	X	X	X			X	X	
13	X		X	X	X	X	X		X	X	X	X			X
14	X	X	X		X	X		X		X	X	X			X
15	X	X	X	X			X	X	X		X		X	X	

Table 4.13: Optimized space coordinates of CH_2NH.

Atom	**Co-ordinates (Å)**		
	x	**y**	**z**
C	0.062372	0.778497	0.000000
H	–0.982293	1.102381	0.000000
H	0.926145	–1.015310	0.000000
N	0.062372	–0.523198	0.000000
H	–0.754690	–1.095667	0.000000

Table 4.14: The rotational and centrifugal distortional constants of CH_2NH in MHz. The columns 2 and 3 represent values calculated by using Gaussian.

Constant	**Experimental** [94]	**aug-cc-pVDZ**	**aug-cc-pVTZ**
$A \times 10^{-5}$	1.9621087629	2.085912975	2.115576292
$B \times 10^{-4}$	3.4641699423	3.41547219	3.45064373
$C \times 10^{-4}$	2.9351496787	2.93491023	2.96674771
$D_J \times 10^3$	56.00411	60.866127	62.932642
$D_{JK} \times 10^3$	598.6775	732.047923	741.932689
D_K	6.383483	5.839960126	6.093867395
$d_1 \times 10^3$	– 9.973179	– 9.531309	– 9.792946
$d_2 \times 10^3$	– 2.007905	– 1.773163	– 1.789099
$H_J \times 10^6$	0.01736	– 0.02763731158	– 0.03026010471
$H_{JK} \times 10^6$	2.6068	8.449668321	8.352378839
$H_{KJ} \times 10^6$	6.125	680.6931766	730.4186343
$H_K \times 10^6$	877.75	4.933638227	4.950073983
$h_1 \times 10^9$	33.067	21.18656635	21.85239675
$h_2 \times 10^9$	32.462	30.03815910	30.50159818
$h_3 \times 10^9$	9.091	6.960776290	7.059300501

Table 4.15: De-excitation Collisional rate coefficients for transitions between the lowest 15 levels of CH_2NH.

Transition	Collisional Rate Coefficients (cm^3s^{-1})				
	10K	**15K**	**20K**	**25K**	**30K**
$1_{01} \rightarrow 0_{00}$	7.15×10^{-11}	6.73×10^{-11}	6.38×10^{-11}	6.08×10^{-11}	5.83×10^{-11}
$2_{02} \rightarrow 0_{00}$	5.75×10^{-11}	5.20×10^{-11}	4.77×10^{-11}	4.45×10^{-11}	4.20×10^{-11}
$2_{02} \rightarrow 1_{01}$	1.33×10^{-10}	1.23×10^{-10}	1.15×10^{-10}	1.07×10^{-10}	1.01×10^{-10}
$1_{11} \rightarrow 0_{00}$	8.82×10^{-12}	7.31×10^{-12}	6.19×10^{-12}	5.34×10^{-12}	4.69×10^{-12}
$1_{11} \rightarrow 1_{01}$	2.07×10^{-11}	1.64×10^{-11}	1.34×10^{-11}	1.12×10^{-11}	9.54×10^{-12}
$1_{11} \rightarrow 2_{02}$	2.51×10^{-11}	2.02×10^{-11}	1.68×10^{-11}	1.43×10^{-11}	1.24×10^{-11}
$1_{10} \rightarrow 1_{01}$	2.11×10^{-11}	1.66×10^{-11}	1.36×10^{-11}	1.14×10^{-11}	9.82×10^{-12}
$1_{10} \rightarrow 2_{02}$	3.02×10^{-11}	2.35×10^{-11}	1.90×10^{-11}	1.58×10^{-11}	1.34×10^{-11}
$1_{10} \rightarrow 1_{11}$	9.70×10^{-11}	8.98×10^{-11}	8.50×10^{-11}	8.14×10^{-11}	7.86×10^{-11}
$2_{12} \rightarrow 1_{01}$	1.42×10^{-11}	1.14×10^{-11}	9.59×10^{-12}	8.28×10^{-12}	7.30×10^{-12}
$2_{12} \rightarrow 2_{02}$	1.58×10^{-11}	1.29×10^{-11}	1.07×10^{-11}	9.13×10^{-12}	7.90×10^{-12}
$2_{12} \rightarrow 1_{11}$	7.60×10^{-11}	7.03×10^{-11}	6.62×10^{-11}	6.30×10^{-11}	6.03×10^{-11}
$2_{12} \rightarrow 1_{10}$	1.00×10^{-10}	9.84×10^{-11}	9.56×10^{-11}	9.24×10^{-11}	8.93×10^{-11}
$2_{11} \rightarrow 0_{00}$	2.62×10^{-12}	2.15×10^{-12}	1.79×10^{-12}	1.52×10^{-12}	1.31×10^{-12}
$2_{11} \rightarrow 1_{01}$	9.84×10^{-12}	8.16×10^{-12}	6.86×10^{-12}	5.85×10^{-12}	5.05×10^{-12}
$2_{11} \rightarrow 2_{02}$	1.83×10^{-11}	1.53×10^{-11}	1.30×10^{-11}	1.13×10^{-11}	9.98×10^{-12}
$2_{11} \rightarrow 1_{11}$	5.99×10^{-11}	5.85×10^{-11}	5.82×10^{-11}	5.83×10^{-11}	5.87×10^{-11}
$2_{11} \rightarrow 1_{10}$	7.14×10^{-11}	6.77×10^{-11}	6.50×10^{-11}	6.28×10^{-11}	6.10×10^{-11}
$2_{11} \rightarrow 2_{12}$	6.45×10^{-11}	5.94×10^{-11}	5.51×10^{-11}	5.17×10^{-11}	4.90×10^{-11}
$3_{03} \rightarrow 0_{00}$	1.86×10^{-11}	1.71×10^{-11}	1.55×10^{-11}	1.41×10^{-11}	1.29×10^{-11}
$3_{03} \rightarrow 1_{01}$	9.29×10^{-11}	8.57×10^{-11}	7.98×10^{-11}	7.51×10^{-11}	7.12×10^{-11}
$3_{03} \rightarrow 2_{02}$	1.45×10^{-10}	1.38×10^{-10}	1.31×10^{-10}	1.23×10^{-10}	1.17×10^{-10}
$3_{03} \rightarrow 1_{11}$	8.46×10^{-12}	6.98×10^{-12}	5.87×10^{-12}	5.02×10^{-12}	4.37×10^{-12}
$3_{03} \rightarrow 1_{10}$	8.45×10^{-12}	7.36×10^{-12}	6.41×10^{-12}	5.63×10^{-12}	5.00×10^{-12}
$3_{03} \rightarrow 2_{12}$	1.27×10^{-11}	1.10×10^{-11}	9.57×10^{-12}	8.42×10^{-12}	7.50×10^{-12}
$3_{03} \rightarrow 2_{11}$	1.10×10^{-11}	9.83×10^{-12}	8.63×10^{-12}	7.60×10^{-12}	6.73×10^{-12}
$3_{13} \rightarrow 0_{00}$	3.62×10^{-12}	2.96×10^{-12}	2.50×10^{-12}	2.17×10^{-12}	1.93×10^{-12}
$3_{13} \rightarrow 1_{01}$	7.54×10^{-12}	6.20×10^{-12}	5.19×10^{-12}	4.44×10^{-12}	3.87×10^{-12}
$3_{13} \rightarrow 2_{02}$	1.43×10^{-11}	1.18×10^{-11}	9.98×10^{-12}	8.69×10^{-12}	7.72×10^{-12}

Transition	Collisional Rate Coefficients (cm^3s^{-1})				
	10K	15K	20K	25K	30K
$3_{13} \rightarrow 1_{11}$	5.19×10^{-11}	5.16×10^{-11}	5.09×10^{-11}	5.00×10^{-11}	4.90×10^{-11}
$3_{13} \rightarrow 1_{10}$	2.54×10^{-11}	2.37×10^{-11}	2.19×10^{-11}	2.02×10^{-11}	1.86×10^{-11}
$3_{13} \rightarrow 2_{12}$	9.67×10^{-11}	9.49×10^{-11}	9.24×10^{-11}	9.00×10^{-11}	8.78×10^{-11}
$3_{13} \rightarrow 2_{11}$	9.46×10^{-11}	9.09×10^{-11}	8.73×10^{-11}	8.38×10^{-11}	8.06×10^{-11}
$3_{13} \rightarrow 3_{03}$	1.45×10^{-11}	1.23×10^{-11}	1.06×10^{-11}	9.18×10^{-12}	8.09×10^{-12}
$3_{12} \rightarrow 1_{01}$	6.51×10^{-12}	5.43×10^{-12}	4.57×10^{-12}	3.91×10^{-12}	3.39×10^{-12}
$3_{12} \rightarrow 2_{02}$	9.18×10^{-12}	7.70×10^{-12}	6.52×10^{-12}	5.60×10^{-12}	4.88×10^{-12}
$3_{12} \rightarrow 1_{11}$	2.74×10^{-11}	2.54×10^{-11}	2.39×10^{-11}	2.27×10^{-11}	2.17×10^{-11}
$3_{12} \rightarrow 1_{10}$	4.01×10^{-11}	3.83×10^{-11}	3.72×10^{-11}	3.66×10^{-11}	3.61×10^{-11}
$3_{12} \rightarrow 2_{12}$	6.70×10^{-11}	6.30×10^{-11}	6.06×10^{-11}	5.92×10^{-11}	5.82×10^{-11}
$3_{12} \rightarrow 2_{11}$	8.15×10^{-11}	7.95×10^{-11}	7.69×10^{-11}	7.43×10^{-11}	7.18×10^{-11}
$3_{12} \rightarrow 3_{03}$	1.59×10^{-11}	1.37×10^{-11}	1.19×10^{-11}	1.05×10^{-11}	9.31×10^{-12}
$3_{12} \rightarrow 3_{13}$	5.69×10^{-11}	5.42×10^{-11}	5.12×10^{-11}	4.83×10^{-11}	4.57×10^{-11}
$4_{04} \rightarrow 0_{00}$	1.55×10^{-11}	1.47×10^{-11}	1.37×10^{-11}	1.28×10^{-11}	1.20×10^{-11}
$4_{04} \rightarrow 1_{01}$	4.22×10^{-11}	3.85×10^{-11}	3.51×10^{-11}	3.23×10^{-11}	2.99×10^{-11}
$4_{04} \rightarrow 2_{02}$	1.12×10^{-10}	1.04×10^{-10}	9.75×10^{-11}	9.19×10^{-11}	8.72×10^{-11}
$4_{04} \rightarrow 1_{11}$	4.87×10^{-12}	4.24×10^{-12}	3.72×10^{-12}	3.31×10^{-12}	2.98×10^{-12}
$4_{04} \rightarrow 1_{10}$	3.91×10^{-12}	3.35×10^{-12}	2.90×10^{-12}	2.54×10^{-12}	2.24×10^{-12}
$4_{04} \rightarrow 2_{12}$	6.80×10^{-12}	5.84×10^{-12}	5.08×10^{-12}	4.49×10^{-12}	4.01×10^{-12}
$4_{04} \rightarrow 2_{11}$	8.48×10^{-12}	7.50×10^{-12}	6.65×10^{-12}	5.95×10^{-12}	5.37×10^{-12}
$4_{04} \rightarrow 3_{03}$	1.27×10^{-10}	1.25×10^{-10}	1.20×10^{-10}	1.15×10^{-10}	1.11×10^{-10}
$4_{04} \rightarrow 3_{13}$	9.81×10^{-12}	8.58×10^{-12}	7.52×10^{-12}	6.66×10^{-12}	5.97×10^{-12}
$4_{04} \rightarrow 3_{12}$	9.84×10^{-12}	8.60×10^{-12}	7.51×10^{-12}	6.62×10^{-12}	5.89×10^{-12}
$4_{14} \rightarrow 1_{01}$	5.28×10^{-12}	4.53×10^{-12}	3.97×10^{-12}	3.55×10^{-12}	3.23×10^{-12}
$4_{14} \rightarrow 2_{02}$	6.79×10^{-12}	5.96×10^{-12}	5.24×10^{-12}	4.65×10^{-12}	4.18×10^{-12}
$4_{14} \rightarrow 1_{11}$	2.69×10^{-11}	2.55×10^{-11}	2.41×10^{-11}	2.28×10^{-11}	2.17×10^{-11}
$4_{14} \rightarrow 1_{10}$	3.06×10^{-11}	2.91×10^{-11}	2.78×10^{-11}	2.65×10^{-11}	2.55×10^{-11}
$4_{14} \rightarrow 2_{12}$	7.33×10^{-11}	7.18×10^{-11}	7.00×10^{-11}	6.82×10^{-11}	6.65×10^{-11}
$4_{14} \rightarrow 2_{11}$	3.96×10^{-11}	3.76×10^{-11}	3.53×10^{-11}	3.30×10^{-11}	3.10×10^{-11}
$4_{14} \rightarrow 3_{03}$	1.01×10^{-11}	8.68×10^{-12}	7.56×10^{-12}	6.70×10^{-12}	6.04×10^{-12}
$4_{14} \rightarrow 3_{13}$	8.95×10^{-11}	8.99×10^{-11}	8.88×10^{-11}	8.72×10^{-11}	8.56×10^{-11}

Transition	Collisional Rate Coefficients (cm^3s^{-1})				
	10K	15K	20K	25K	30K
$4_{14} \rightarrow 3_{12}$	8.63×10^{-11}	8.30×10^{-11}	7.97×10^{-11}	7.66×10^{-11}	7.37×10^{-11}
$4_{14} \rightarrow 4_{04}$	8.41×10^{-12}	7.53×10^{-12}	6.67×10^{-12}	5.95×10^{-12}	5.35×10^{-12}
$4_{13} \rightarrow 0_{00}$	8.03×10^{-13}	6.82×10^{-13}	5.86×10^{-13}	5.09×10^{-12}	4.46×10^{-13}
$4_{13} \rightarrow 1_{01}$	2.54×10^{-12}	2.20×10^{-12}	1.90×10^{-12}	1.65×10^{-12}	1.45×10^{-12}
$4_{13} \rightarrow 2_{02}$	5.27×10^{-12}	4.49×10^{-12}	3.88×10^{-12}	3.39×10^{-12}	3.01×10^{-12}
$4_{13} \rightarrow 1_{11}$	1.64×10^{-11}	1.56×10^{-11}	1.48×10^{-11}	1.41×10^{-11}	1.34×10^{-11}
$4_{13} \rightarrow 1_{10}$	1.84×10^{-11}	1.72×10^{-11}	1.60×10^{-11}	1.50×10^{-11}	1.41×10^{-11}
$4_{13} \rightarrow 2_{12}$	3.06×10^{-11}	2.94×10^{-11}	2.80×10^{-11}	2.66×10^{-11}	2.54×10^{-11}
$4_{13} \rightarrow 2_{11}$	4.99×10^{-11}	5.06×10^{-11}	5.10×10^{-11}	5.12×10^{-11}	5.12×10^{-11}
$4_{13} \rightarrow 3_{03}$	7.62×10^{-12}	6.40×10^{-12}	5.48×10^{-12}	4.77×10^{-12}	4.20×10^{-12}
$4_{13} \rightarrow 3_{13}$	6.45×10^{-11}	6.24×10^{-11}	6.05×10^{-11}	5.90×10^{-11}	5.76×10^{-11}
$4_{13} \rightarrow 3_{12}$	8.87×10^{-11}	8.87×10^{-11}	8.70×10^{-11}	8.47×10^{-11}	8.22×10^{-11}
$4_{13} \rightarrow 4_{04}$	1.15×10^{-11}	1.01×10^{-11}	8.97×10^{-12}	8.04×10^{-12}	7.29×10^{-12}
$4_{13} \rightarrow 4_{14}$	4.95×10^{-11}	4.82×10^{-11}	4.58×10^{-11}	4.33×10^{-11}	4.10×10^{-11}
$2_{21} \rightarrow 0_{00}$	2.25×10^{-12}	2.09×10^{-12}	1.92×10^{-12}	1.75×10^{-12}	1.60×10^{-12}
$2_{21} \rightarrow 1_{01}$	8.51×10^{-11}	8.62×10^{-11}	8.68×10^{-11}	8.68×10^{-11}	8.65×10^{-11}
$2_{21} \rightarrow 2_{02}$	3.42×10^{-11}	3.11×10^{-11}	2.87×10^{-11}	2.69×10^{-11}	2.54×10^{-11}
$2_{21} \rightarrow 1_{11}$	1.69×10^{-12}	1.44×10^{-12}	1.24×10^{-12}	1.09×10^{-12}	9.65×10^{-13}
$2_{21} \rightarrow 1_{10}$	3.55×10^{-12}	3.13×10^{-12}	2.82×10^{-12}	2.59×10^{-12}	2.41×10^{-12}
$2_{21} \rightarrow 2_{12}$	4.44×10^{-12}	3.98×10^{-12}	3.62×10^{-12}	3.34×10^{-12}	3.12×10^{-12}
$2_{21} \rightarrow 2_{11}$	3.91×10^{-12}	3.38×10^{-12}	2.96×10^{-12}	2.64×10^{-12}	2.38×10^{-12}
$2_{21} \rightarrow 3_{03}$	6.33×10^{-11}	5.87×10^{-11}	5.51×10^{-11}	5.23×10^{-11}	5.00×10^{-11}
$2_{21} \rightarrow 3_{13}$	5.32×10^{-12}	4.35×10^{-12}	3.69×10^{-12}	3.21×10^{-12}	2.84×10^{-12}
$2_{21} \rightarrow 3_{12}$	5.92×10^{-12}	5.04×10^{-12}	4.38×10^{-12}	3.88×10^{-12}	3.49×10^{-12}
$2_{21} \rightarrow 4_{04}$	4.56×10^{-11}	4.29×10^{-11}	4.01×10^{-11}	3.75×10^{-11}	3.54×10^{-11}
$2_{21} \rightarrow 4_{14}$	6.64×10^{-12}	5.86×10^{-12}	5.30×10^{-12}	4.87×10^{-12}	4.54×10^{-12}
$2_{21} \rightarrow 4_{13}$	5.33×10^{-12}	4.74×10^{-12}	4.22×10^{-12}	3.79×10^{-12}	3.44×10^{-12}
$2_{20} \rightarrow 0_{00}$	4.09×10^{-11}	4.16×10^{-11}	4.20×10^{-11}	4.21×10^{-11}	4.20×10^{-11}
$2_{20} \rightarrow 1_{01}$	1.97×10^{-11}	1.76×10^{-11}	1.60×10^{-11}	1.48×10^{-11}	1.38×10^{-11}
$2_{20} \rightarrow 2_{02}$	8.18×10^{-11}	8.08×10^{-11}	7.95×10^{-11}	7.80×10^{-11}	7.64×10^{-11}
$2_{20} \rightarrow 1_{11}$	3.06×10^{-12}	2.86×10^{-12}	2.67×10^{-12}	2.51×10^{-12}	2.38×10^{-12}

Transition	Collisional Rate Coefficients (cm^3s^{-1})				
	10K	**15K**	**20K**	**25K**	**30K**
$2_{20} \rightarrow 1_{10}$	1.89×10^{-12}	1.59×10^{-12}	1.37×10^{-12}	1.20×10^{-12}	1.06×10^{-12}
$2_{20} \rightarrow 2_{12}$	3.01×10^{-12}	2.63×10^{-12}	2.33×10^{-12}	2.10×10^{-12}	1.91×10^{-12}
$2_{20} \rightarrow 2_{11}$	4.44×10^{-12}	3.85×10^{-12}	3.41×10^{-12}	3.07×10^{-12}	2.80×10^{-12}
$2_{20} \rightarrow 3_{03}$	4.28×10^{-11}	3.88×10^{-11}	3.55×10^{-11}	3.28×10^{-11}	3.08×10^{-11}
$2_{20} \rightarrow 3_{13}$	6.08×10^{-12}	5.31×10^{-12}	4.76×10^{-12}	4.35×10^{-12}	4.04×10^{-12}
$2_{20} \rightarrow 3_{12}$	4.92×10^{-12}	4.24×10^{-12}	3.73×10^{-12}	3.34×10^{-12}	3.03×10^{-12}
$2_{20} \rightarrow 4_{04}$	5.34×10^{-11}	4.90×10^{-11}	4.51×10^{-11}	4.20×10^{-11}	3.93×10^{-11}
$2_{20} \rightarrow 4_{14}$	4.60×10^{-12}	4.12×10^{-12}	3.67×10^{-12}	3.29×10^{-12}	2.98×10^{-12}
$2_{20} \rightarrow 4_{13}$	5.20×10^{-12}	4.68×10^{-12}	4.19×10^{-12}	3.78×10^{-12}	3.44×10^{-12}
$2_{20} \rightarrow 2_{21}$	8.77×10^{-11}	9.15×10^{-11}	9.29×10^{-11}	9.33×10^{-11}	9.31×10^{-11}

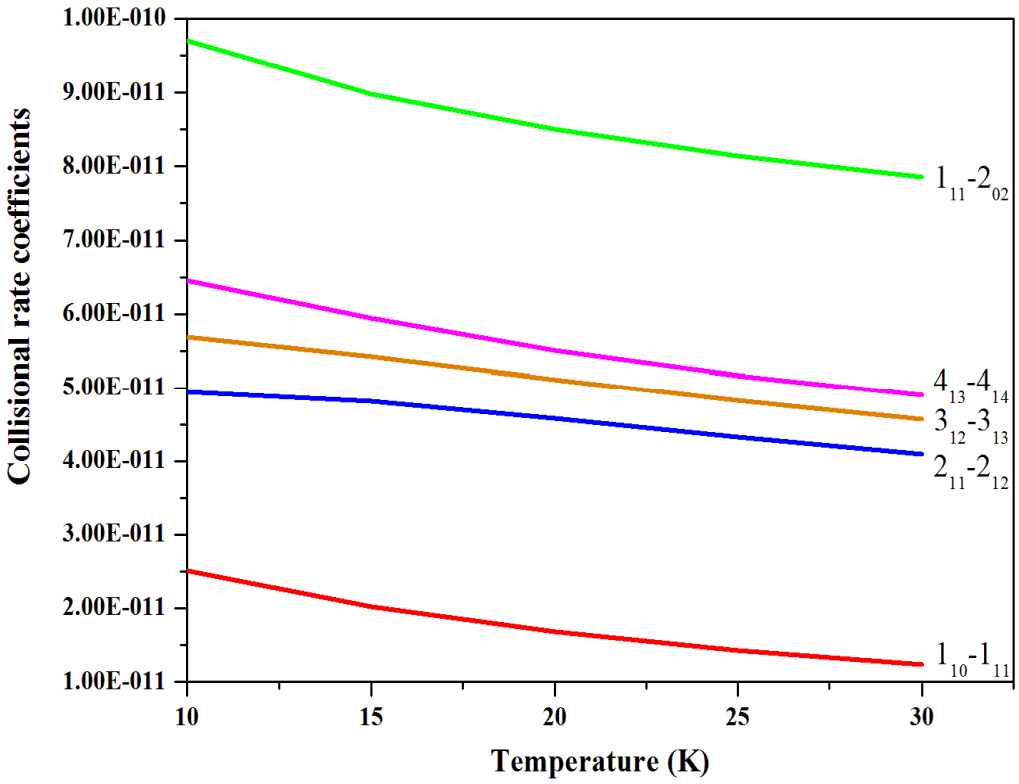

Figure 4.6: Variation of collisional rate coefficients with temperature for the transitions 1_{10}–1_{11}, 2_{11}–2_{12}, 3_{12}–3_{13}, 4_{13}–4_{14}, and 1_{11}–2_{02}.

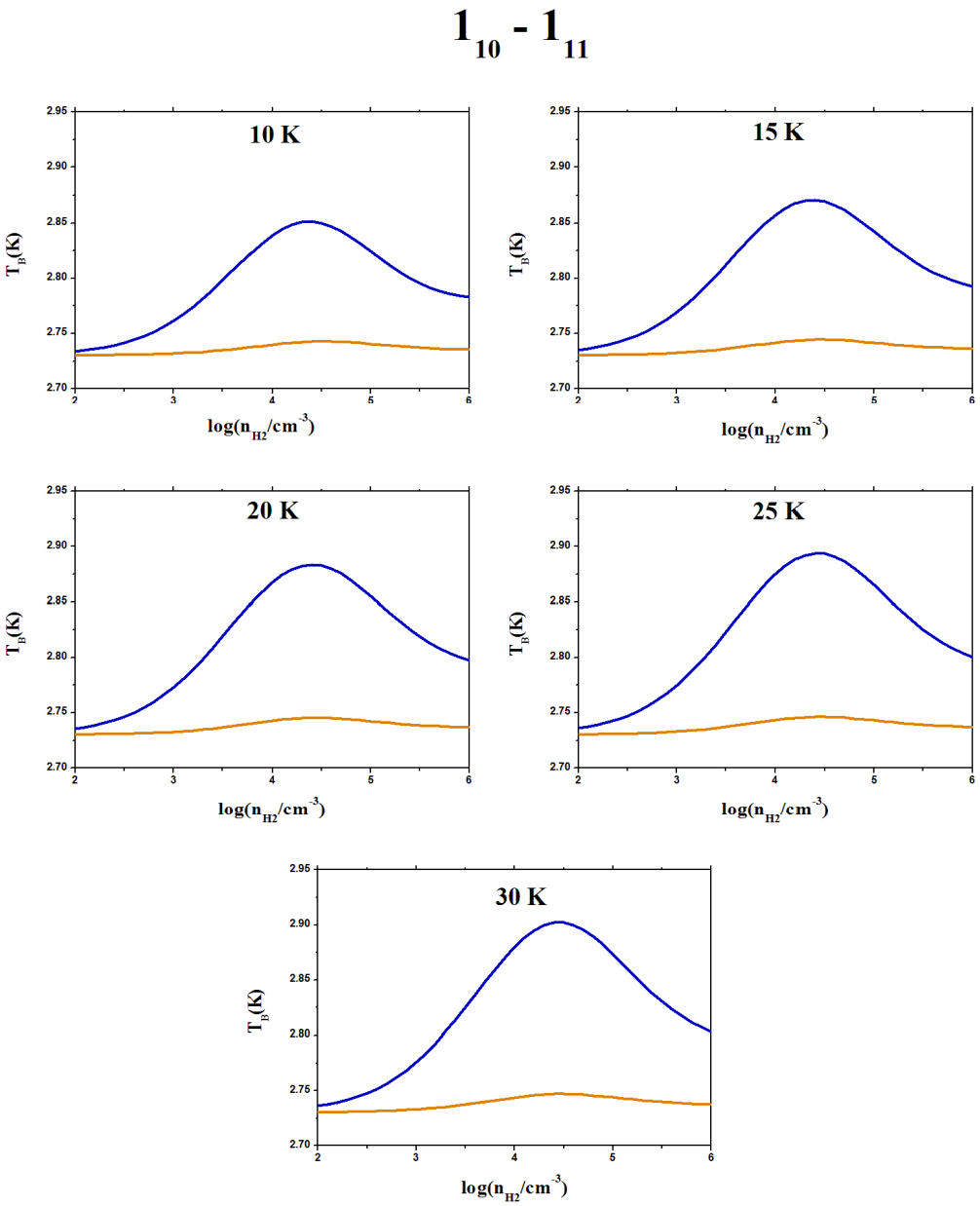

Figure 4.7: The variation of brightness temperature (T_B) with molecular hydrogen density (n_{H2}) for the transition 1_{10}–1_{11} at kinetic temperatures of 10K, 15K, 20K, 25K, and 30K. The blue line is for $\gamma = 10^{-5}$ $cm^{-3}(km/s)^{-1}$ pc and the orange line is for $\gamma = 10^{-6}$ $cm^{-3}(km/s)^{-1}$ pc.

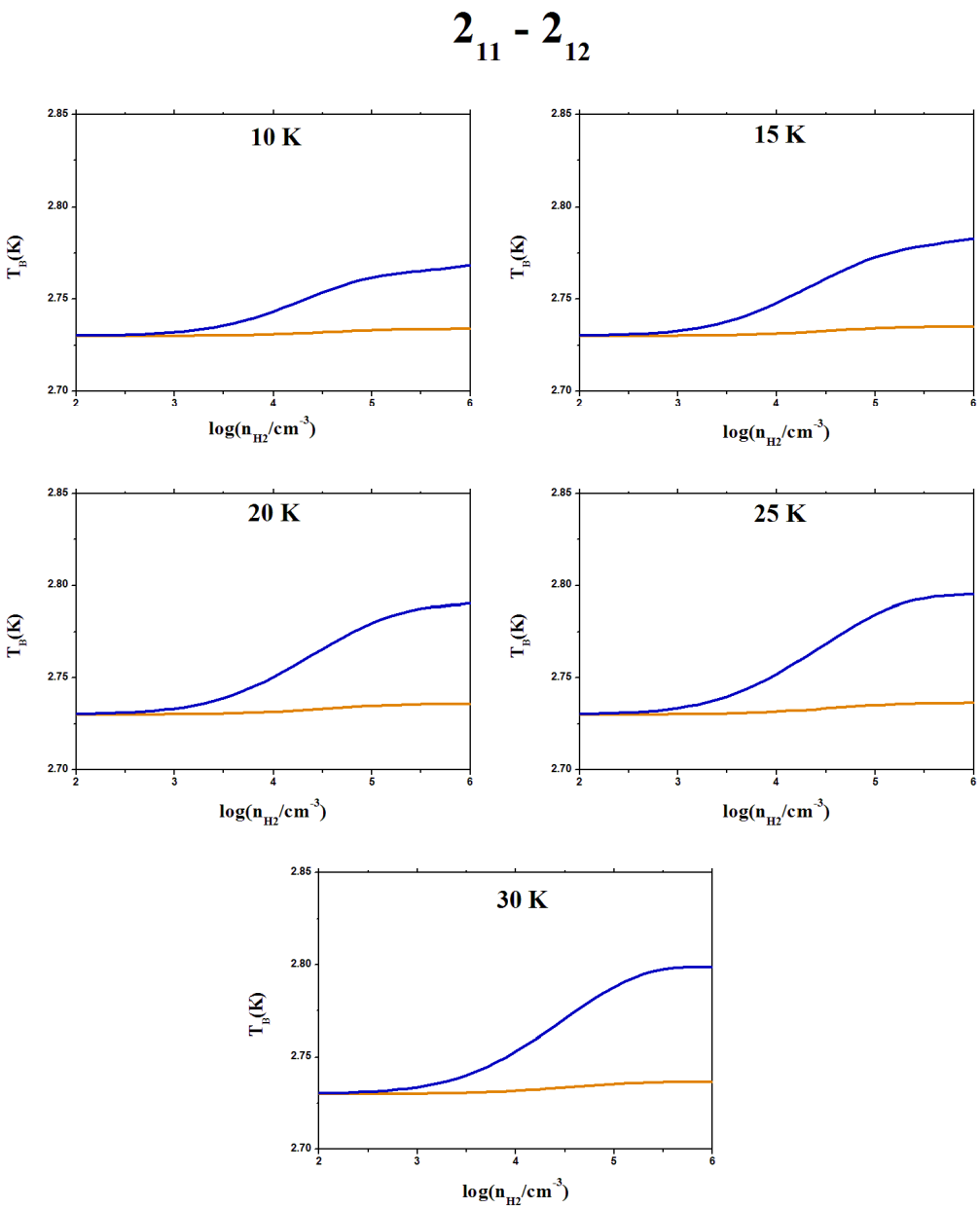

Figure 4.8: The variation of brightness temperature (T_B) with molecular hydrogen density (n_{H2}) for the transition 2_{11}–2_{12} at kinetic temperatures of 10K, 15K, 20K, 25K, and 30K. The blue line is for $\gamma = 10^{-5}$ cm^{-3}(km/s)$^{-1}$ pc and the orange line is for $\gamma = 10^{-6}$ cm^{-3}(km/s)$^{-1}$ pc.

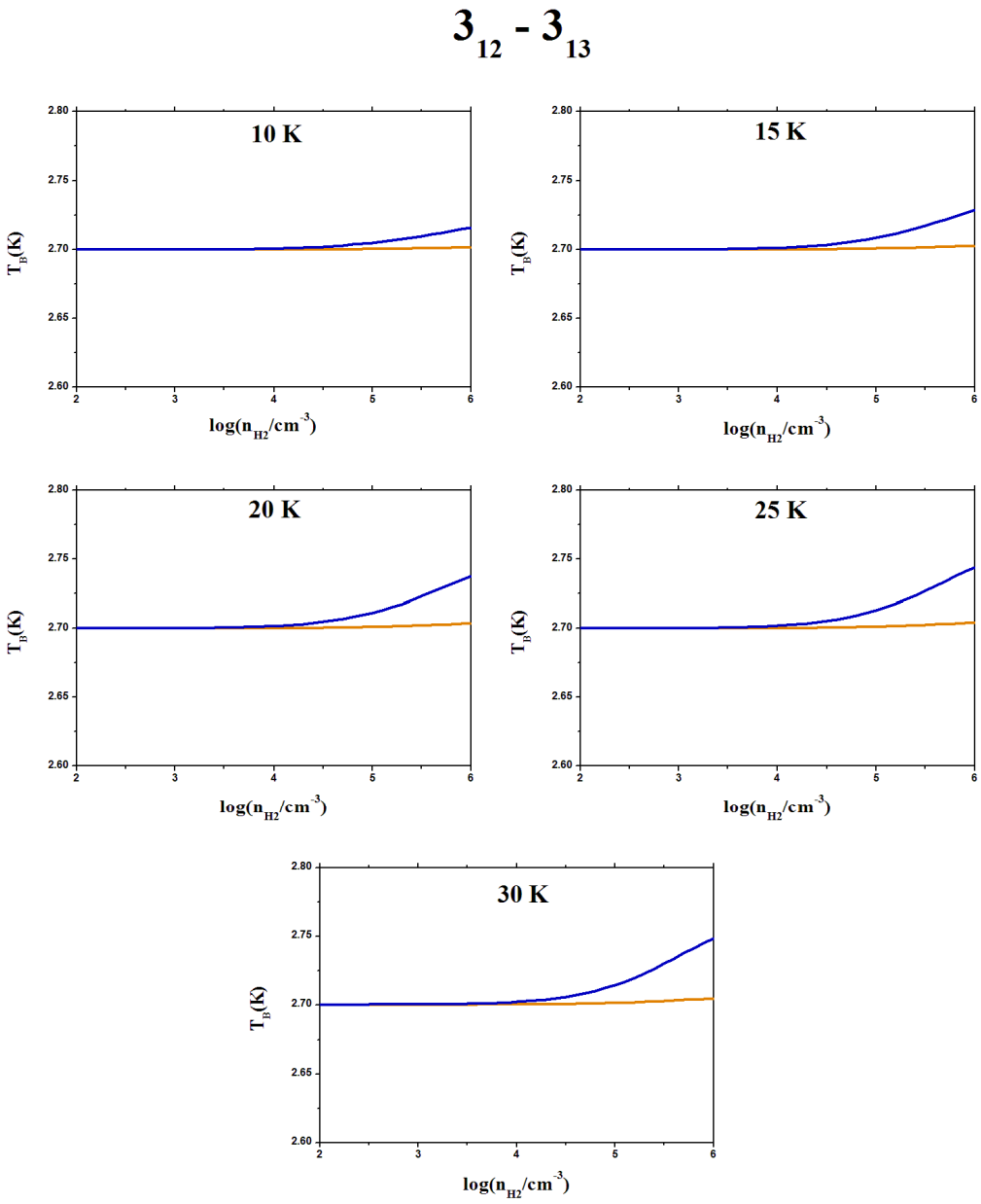

Figure 4.9: The variation of brightness temperature (T_B) with molecular hydrogen density (n_{H2}) for the transition 3_{12}–3_{13} at kinetic temperatures of 10K, 15K, 20K, 25K, and 30K. The blue line is for $\gamma = 10^{-5}$ $cm^{-3}(km/s)^{-1}$ pc and the orange line is for $\gamma = 10^{-6}$ $cm^{-3}(km/s)^{-1}$ pc.

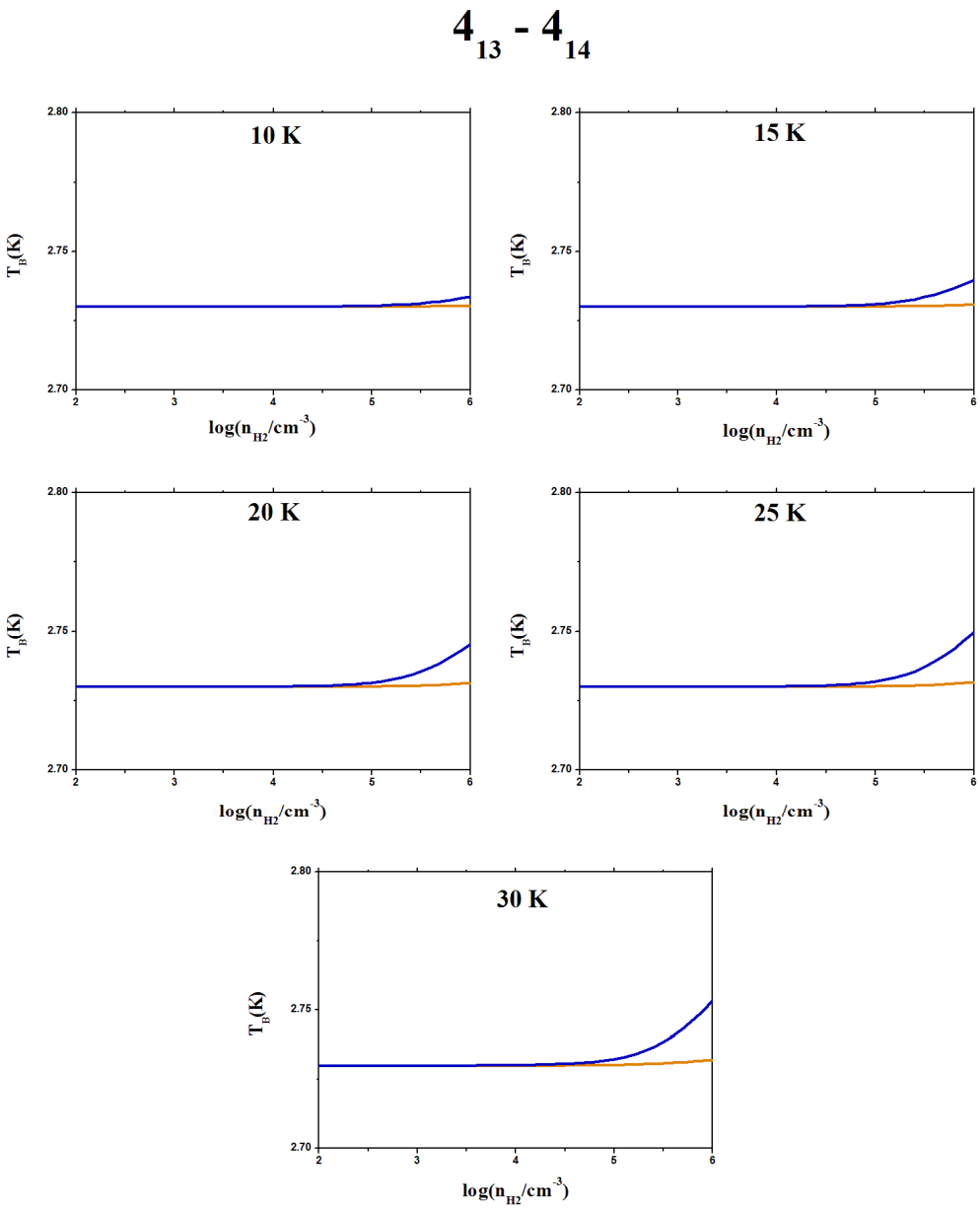

Figure 4.10: The variation of brightness temperature (T_B) with molecular hydrogen density (n_{H2}) for the transition 4_{13}–4_{14} at kinetic temperatures of 10K, 15K, 20K, 25K, and 30K. The blue line is for $\gamma = 10^{-5}$ $cm^{-3}(km/s)^{-1}$ pc and the orange line is for $\gamma = 10^{-6}$ $cm^{-3}(km/s)^{-1}$ pc.

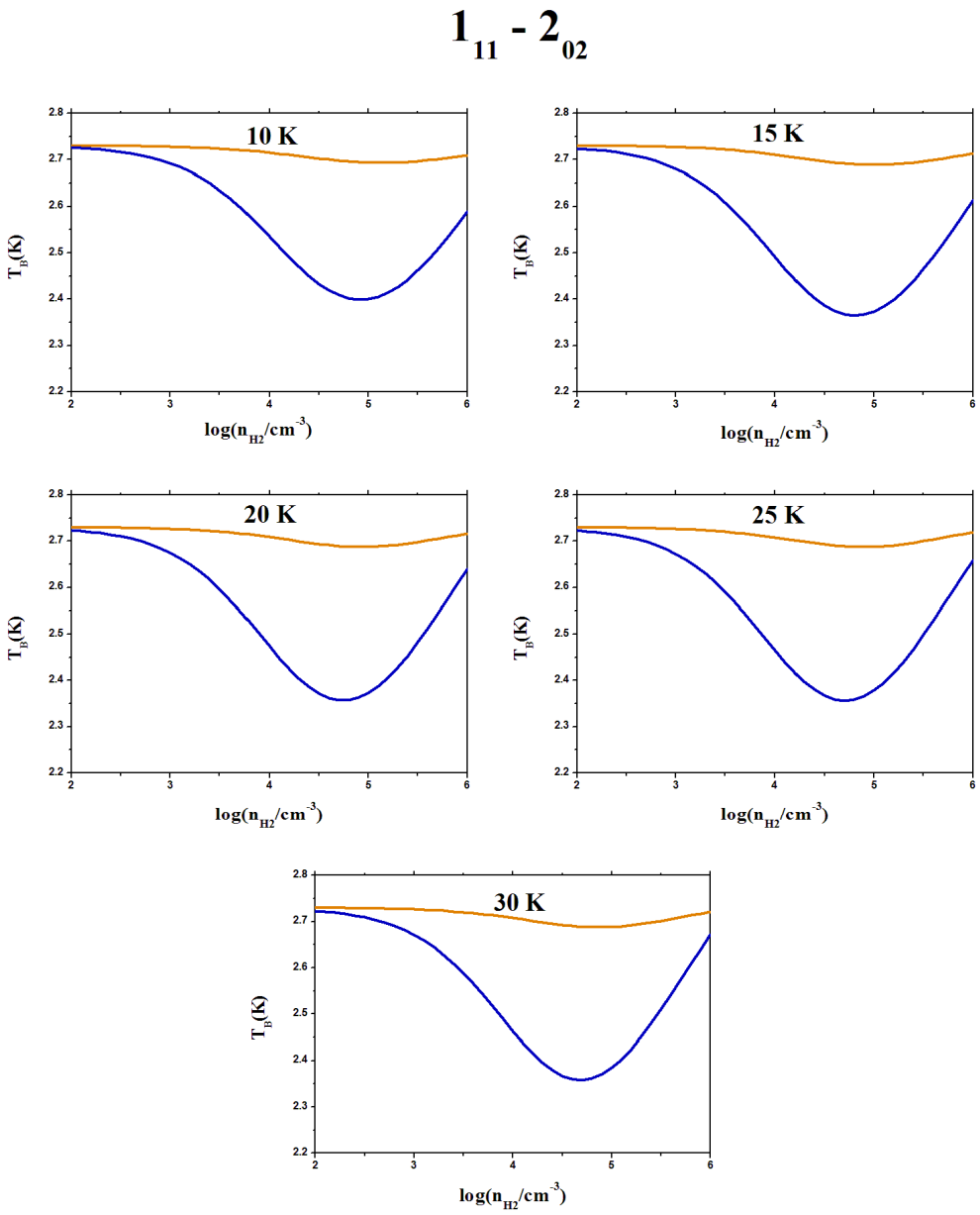

Figure 4.11: The variation of brightness temperature (T_B) with molecular hydrogen density (n_{H2}) for the transition 1_{11}–2_{02} at kinetic temperatures of 10K, 15K, 20K, 25K, and 30K. The blue line is for $\gamma = 10^{-5}$ $cm^{-3}(km/s)^{-1}$ pc and the orange line is for $\gamma = 10^{-6}$ $cm^{-3}(km/s)^{-1}$ pc.

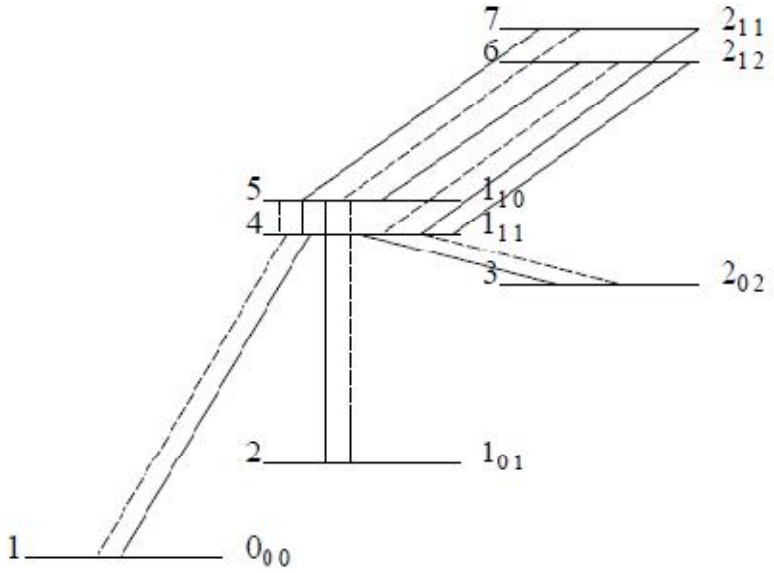

Figure 4.12: The possible transitions to and from the rotational energy levels 1_{11} and 1_{10}. The solid line shows radiative transitions while the dashed line shows collisional transitions.

CHAPTER 5: SUMMARY AND CONCLUSIONS

5.1 Summary

In this thesis entitled "The study of Methanimine in interstellar medium", we have studied about a prebiotic molecule methanimine in the interstellar medium. The methanimine molecule is an a and b type asymmetric top molecule having comparable magnitudes of a and b components of dipole moment. The transition rates between rotational energy levels are studied as vibrational and electronic transitions are not possible at low temperatures in the interstellar medium. The chapter-wise summary of the research work presented in the thesis is described below:

Chapter 1

The thesis is started with an introduction to the interstellar medium, its constituents, the conditions prevailing there, and the cosmic microwave background. The advantages of the radio window over the optical window are described in detail. Also, the types of virtual molecular laboratories in the interstellar medium and the molecules observed in the interstellar medium are given. The classification of molecules based on the moment of inertia and the theory of radiative and collisional transitions between rotational energy levels is provided. A relation between Einstein A-coefficients is derived to define the probability of radiative transitions. The theory of observed spectra of molecules along with the anomalous phenomenon is explained based on kinetic and excitation temperatures.

Chapter 2

An introduction to prebiotic molecules, their relevance to the origin of life, and the literature data of their search in the interstellar medium is presented. The attempts to discover the intelligent life outside the earth are described in detail. A brief introduction to methanimine and the mechanism of its formation in methanimine is given. The detail of observed transitions of methanimine in the interstellar medium (Cosmic laboratories) and the spectroscopic data of methanimine obtained in terrestrial laboratory studies is presented in tabular form.

Chapter 3

The objectives of the present study are given along with the methods used to achieve these objectives. The significance of all the computational tools used in our theoretical study is described. Also, the procedures to calculate Einstein A-coefficients, collisional rate coefficients, and solving the statistical equilibrium equations are described in detail.

Chapter 4

The results and the discussions of work done are divided into two sections and presented in a systematic manner. In section I, the calculated values of Einstein A-coefficients and line strengths are given. Those transitions are identified which are expected to be prominent under the conditions of cosmic objects based on two criteria namely, the upper energy level must be sufficiently populated and the radiative transition probability must be large. We have found more than 100 lines in addition to already observed lines, that may play an important role in the identification of methanimine in the interstellar medium. In section II, we have classified the energy levels according to the possibility of radiative and collisional transitions. The statistical equilibrium equations coupled with the equations of radiative transfer are solved. Further, the brightness temperature versus hydrogen molecular density is plotted for five selected transitions and two of them are found to show anomalous phenomena. The transition 1_{10}–1_{11} is found to show maser action while the transition 1_{11}–2_{02} shows anomalous absorption, both of which play a very significant role in the detection of methanimine in the interstellar medium.

5.2 Conclusions

The radiative transition probabilities (Einstein A-coefficients) for transitions between rotational energy levels of CH_2NH up to 141 cm^{-1} are calculated and more than 100 lines are obtained which can contribute to the identification of methanimine in the interstellar medium. A thorough study is done for the transitions $1_{10} - 1_{11}$, $2_{11} - 2_{12}$, $3_{12} - 3_{13}$, $4_{13} - 4_{14}$, and $1_{11} - 2_{02}$, by solving the statistical equilibrium equations coupled with the equations of radiative transfer by considering lowest 15 rotational

energy levels of CH_2NH. The MASER action in $1_{10}-1_{11}$ transition and anomalous absorption in $1_{11}-2_{02}$ transition are obtained with a maximum around the density of $10^{4.5}$ cm^{-3}, and both of them diminish on both sides of this density. Also, the transitions $2_{11} - 2_{12}$, $3_{12} - 3_{13}$, and $4_{13} - 4_{14}$ shows a weak emission feature. The brightness temperature of the $1_{10}-1_{11}$ transition is more as compared to other transitions, implying more probability of its detection. The population inversion in $1_{10} - 1_{11}$ transition is proved by an analytical technique using scaled values of collisional rate coefficients where we have found a little contribution of collisional transitions as compared to radiative transitions. The MASER action in transition $1_{10} - 1_{11}$ and anomalous absorption in transition $1_{11}-2_{02}$ makes them potential transitions in the detection of methanimine, along with other significant transitions that play an important role in the study of methanimine in interstellar medium.

5.3 Future Plans

(i). The collisional rate coefficients for CH_2NH colliding with H_2 will be calculated by considering a large number of rotational energy levels. Then the accuracy of results obtained after solving statistical equilibrium equations coupled with the equations of radiative transfer will increase. However, the computational calculation time will increase significantly in this case.

(ii). The identification of other prebiotic molecules will be pursued that will enhance our understanding of the universe and the search of life in the interstellar medium.

CHAPTER 6: BIBLIOGRAPHY

[1] A. N. Witt, T. McDonnell, and H. Palme, "The chemical composition of the interstellar medium," *Philos. Trans. R. Soc. A Math. Phys. Eng. Sci.* **359**, 1949–1959 (2001).

[2] L. H. Aller, "The chemical composition of the interstellar medium," *Ann. N. Y. Acad. Sci.* **194**, 45–55 (1972).

[3] B. T. Draine, "Interstellar dust grains," *Annu. Rev. Astron. Astrophys.* **41**, 241–289 (2003).

[4] R. Carbo and A. Ginebreda, "Interstellar chemistry," *J. Chem. Educ.* **62**, 832–836 (1985).

[5] L. Spitzer jr, "Review of publications: Physical processes in the interstellar medium," *J. R. Astron. Soc. Canada* **72**, 349–360 (1978).

[6] J. C. Higdon, "Density fluctuations in the interstellar medium: Evidence for anisotropic magnetogasdynamic turbulence. I. Model and astrophysical sites," *Astrophys. J.* **285**, 109–123 (1984).

[7] E. Herbst, "Chemistry in the interstellar medium," *Annu. Rev. Phys. Chem.* **46**, 27–54 (1995).

[8] J. Mathis, "Observations and theories of interstellar dust," *Reports Prog. Phys.* **56**, 605–652 (1993).

[9] J. Cordes, J. Weisberg, and V. Boriakoff, "Small-scale electron density turbulence in the interstellar medium," *Astrophys. J.* **288**, 221–247 (1985).

[10] D. Smith, "The ion chemistry of interstellar clouds," *Chem. Rev.* **92**, 1473–1485 (1992).

[11] G. Gamow, "The origin of elements and the separation of galaxies," *Phys. Rev.* **74**, 505–506 (1948).

[12] S. Weinrab, A. H. Barret, M. L. Meeks, and J. C. Henry, "Radio observations of OH in the interstellar medium," *Nature* **200**, 829–831 (1963).

[13] W. T. Huntress and G. F. Mitchell, "The synthesis of complex molecules in interstellar clouds," *Astrophys. J.* **231**, 456–467 (1979).

[14] S. Chandra, A. Kumar, B. K. Kumthekar, and M. K. Sharma, "Suggestion for the search of H_2CC in cool cosmic objects," *New Astron.* **16**, 152–156 (2011).

[15] S. Muller and et al., "An ALMA early science survey of molecular absorption lines toward PKS 1830-211 : Analysis of the absorption profiles," *Astron. Astrophys.* **566**, A112 (2014).

[16] S. Chandra, P. G. Musrif, R. M. Dharmkare, and M. Sharma, "Search for 1_{11}-1_{10} and 2_{11}-2_{12} transitions of H_2CCO, H_2CCC and H_2CCCC in cosmic objects," *New Astron.* **11**, 495–502 (2006).

[17] C. Chang, A. B. C. Patzer, W. H. Kegel, and S. Chandra, "Small Fe bearing ring molecules of possible astrophysical interest: Molecular properties and rotational spectra," *Astrophys. Space Sci.* **347**, 315–325 (2013).

[18] S. Muller and et al., "Molecules at z = 0.89: A 4-mm-rest-frame absorption-line survey toward PKS 1830-211," *Astron. Astrophys.* **535**, A103 (2011).

[19] P. Schilke, D. A. Neufeld, H. S. P. Muller, C. Comito, E. A. Bergin, D. C. Lis, M. Gerin, J. H. Black, M. Wolfire, et al., "Ubiquitous argonium (ArH^+) in the diffuse interstellar medium: A molecular tracer of almost purely atomic gas," *Astron. Astrophys.* **566**, 1–12 (2014).

[20] P. Schilke, S. Leurini, K. M. Menten, and J. Alcolea, "Interstellar SiN," *Astron. Astrophys.* **412**, L15–L18 (2003).

[21] M. Agundez, J. Cernicharo, M. Guelin, C. Kahane, E. Roueff, J. Kłos, F. J. Aoiz, F. Lique, N. Marcelino, et al., "Astronomical identification of CN^-, the smallest observed molecular anion," *Astron. Astrophys.* **517**, L2 (2010).

[22] C. A. Gottlieb, S. Brunken, M. C. McCarthy, and P. Thaddeus, "The rotational spectrum of CN^-," *J. Chem. Phys.* **126**, 191101–191104 (2007).

[23] S. Thorwirth, P. Schreier, T. Salomon, S. Schlemmer, and O. Asvany, "Pure rotational spectrum of CN^+," *Astrophys. J.* **882**, L6 (2019).

[24] V. Vinogradoff, F. Duvernay, G. Danger, P. Theulé, F. Borget, and T. Chiavassa, "Formaldehyde and methylamine reactivity in interstellar ice analogues as a source of molecular complexity at low temperature," *Astron. Astrophys.* **549**, A40 (2013).

[25] V. Vinogradoff, N. Fray, F. Duvernay, G. Briani, G. Danger, H. Cottin, P. Theulé, and T. Chiavassa, "Importance of thermal reactivity for hexamethylenetetramine formation from simulated interstellar ices," *Astron. Astrophys.* **551**, A128 (2013).

[26] R. V. Yelle, V. Vuitton, P. Lavvas, S. J. Klippenstein, M. A. Smith, S. M. Horst, and J. Cui, "Formation of NH_3 and CH_2NH in Titan's upper atmosphere," *Faraday Discuss.* **147**, 31–49 (2010).

[27] V. Vuitton, R. V. Yelle, and M. J. McEwan, "Ion chemistry and N-containing molecules in Titan's upper atmosphere," *Icarus* **191**, 722–742 (2007).

[28] V. Vuitton, R. V. Yelle, and V. G. Anicich, "The Nitrogen chemistry of Titan's upper atmosphere revealed," *Astrophys. J.* **647**, L175–L178 (2006).

[29] D. Skouteris, N. Balucani, N. Faginas-Lago, S. Falcinelli, and M. Rosi, "Dimerization of methanimine and its charged species in the atmosphere of Titan and interstellar/cometary ice analogs," *Astron. Astrophys.* **584**, 1–8 (2015).

[30] D. Mcelroy, C. Walsh, A. J. Markwick, M. A. Cordiner, K. Smith, and T. J. Millar, "The UMIST database for astrochemistry 2012," *Astron. Astrophys.* **550**, A36 (2013).

[31] M. K. Sharma, M. Sharma, and S. Chandra, "Suggestion for search of cyclopropenone (c-C_3H_2O) in a cosmic object," *Mol. Astrophys.* **6**, 1–8 (2017).

[32] M. L. Dubernet and A. Grosjean, "Collisional excitation rates of H_2O with H_2: I. Pure rotational excitation rates with para-H_2 at very low temperature," *Astron. Astrophys.* **390**, 793–800 (2002).

[33] T. R. Phillips, S. Maluendes, and S. Green, "Collisional excitation of H_2O by H_2 molecules," *Astrophys. J. Suppl. Ser.* **107**, 467–474 (1996).

[34] S. Green, S. Maluendes, and A. D. Mclean, "Improved collisional excitation rates for interstellar water," *Astrophys. J. Suppl. Ser.* **85**, 181–185 (1993).

[35] B. Yang, M. Nagao, W. Satomi, M. Kimura, and P. C. Stancil, "Rotational quenching of rotationally excited H_2O in collisions with He," *Astrophys. J.* **765**, 77 (2013).

[36] A. Palma and S. Green, "Collisional excitation of an asymmetric rotor, Silicon dicarbide," *Astrophys. J.* **316**, 830–835 (1987).

[37] A. Palma, S. Green, D. J. Defrees, and A. D. Mclean, "Collisional excitation of interstellar water," *Astrophys. J.* **68**, 287–318 (1988).

[38] R. Shapiro, "Prebiotic ribose synthesis: A critical analysis," *Orig. Life Evol. Biosph.* **18**, 71–85 (1988).

[39] G. F. Joyce, “RNA evolution and the origins of life,” *Nature* **338**, 217–224 (1989).

[40] A. Tielens, “The molecular universe,” *Rev. Mod. Phys.* **85**, 1021 (2013).

[41] M. Wolfire, D. Hollenbach, and C. F. Mckee, “The dark molecular gas,” *Astrophys. J.* **716**, 1191 (2010).

[42] J. Kwan, “The mass spectrum of interstellar clouds,” *Astrophys. J.* **229** (1979).

[43] E. Herbst and W. Klemperer, “The formation and depletion of molecules in dense interstellar clouds,” *Astrophys. J.* **185**, 505–534 (1973).

[44] W. D. Watson, “Interstellar molecule reactions,” *Rev. Mod. Phys.* **48**, 513 (1976).

[45] J. Attwater and P. Holliger, “A synthetic approach to abiogenesis,” *Nat. Methods* **11**, 495–498 (2014).

[46] S. I. Walker and P. C. W. Davies, “The algorithmic origins of life,” *J. R. Soc. Interface* **10**, 2012.0869 (2013).

[47] E. Grun and M. Landgraf, “Fast dust in the heliosphere,” *Space Sci. Rev.* **99**, 151–164 (2001).

[48] S. L. Miller, “A production of amino acids under possible primitive earth conditions,” *Science* **117**, 528–529 (1953).

[49] J. M. Greenberg, “Chemical evolution in space: A source of prebiotic molecules,” *Adv. Sp. Res.* **3**, 19–33 (1983).

[50] J. M. Greenberg, P. Weber, and W. Schutte, “Chemical and biological evolution in space,” *Adv. Sp. Res.* **4**, 41–49 (1984).

[51] V. R. Oberbeck, J. Marshall, and T. Shen, “Prebiotic chemistry in clouds,” *J. Mol. Evol.* **32**, 296–303 (1991).

[52] D. Silvestre and J. Fontanari, “Package models and the information crisis of prebiotic evolution,” *J. Theor. Biol.* **252**, 326–337 (2008).

[53] C. Ceccarelli, “Search for glycine in the solar type protostar IRAS 16293-2422,” *Astron. Astrophys.* **362**, 1122–1126 (2000).

[54] F. Combes, Nguyen-G-Rieu, and G. Wlodarczak, “Search for interstellar glycine,” *Astron. Astrophys.* **308**, 618–622 (1996).

[55] Y. Kuan, S. B. Charnley, H. Huang, W. Tseng, and Z. Kisiel, “Interstellar glycine,” *Astrophys. J.* **593**, 848–867 (2003).

[56] L. E. Snyder, F. J. Lovas, and et al., “A rigorous attempt to verify interstellar glycine,” *Astrophys. J.* **619**, 914–930 (2005).

[57] G. M. Munoz Caro, J. Comets, and et al., “Amino acids from ultraviolet irradiation of interstellar ice analogues,” *Nature* **416**, 403–406 (2002).

[58] M. P. Bernstein, J. P. Dworkin, S. A. Sandford, G. W. Cooper, and L. J. Allamandola, “Racemic amino acids from the ultraviolet photolysis of interstellar ice analogues,” *Nature* **416**, 401–403 (2002).

[59] Y. Takano, J. Takahashi, T. Kaneko, K. Marumo, and K. Kobayashi, “Asymmetric synthesis of amino acid precursors in interstellar complex organics by circularly polarized light,” *Earth Planet. Sci. Lett.* **254**, 106–114 (2007).

[60] P. Ehrenfreund, M. P. Bernstein, J. P. Dworkin, S. A. Sandford, and L. J. Allamandola, “The photostability of amino acids in space,” *Astrophys. J.* **550**, L95–L99 (2001).

[61] M. Lattelais, F. Pauzat, J. Pilmé, Y. Ellinger, and C. Ceccarelli, “About the detectability of glycine in the interstellar medium,” *Astron. Astrophys.* **532**, 1–7 (2011).

[62] Y. Takano, A. Ohashi, T. Kaneko, and K. Kobayashi, “Abiotic synthesis of high-molecular-weight organics from an inorganic gas mixture of carbon monoxide, ammonia, and water by 3 MeV proton irradiation,” *Appl. Phys. Lett.* **84**, 1410–1412 (2004).

[63] M. Allegrinia, J. W. C. Johns, and A. R. W. McKellar, “Laser stark spectroscopy of the ν4 fundamental band of CH_2NH at 6.1 μm,” *J. Chem. Phys.* **70**, 2829–2833 (1979).

[64] J. E. Elsila, J. P. Dworkin, M. P. Bernstein, M. P. Martin, and S. A. Sandford, “Mechanisms of amino acid formation in interstellar ice analogs,” *Astrophys. J.* **660**, 911–918 (2007).

[65] G. Danger, F. Borget, M. Chomat, F. Duvernay, P. Theule, J. C. Guillemin, L. Le Sergeant d’Hendecourt, and T. Chiavassa, “Experimental investigation of aminoacetonitrile formation through the Strecker synthesis in astrophysical-like conditions: reactivity of methanimine (CH_2NH), ammonia (NH_3), and hydrogen cyanide (HCN),” *Astron. Astrophys.* **535**, A47 (2011).

[66] A. Belloche, K. M. Menten, C. Comito, H. S. P. Muller, P. Schilke, J. Ott, S. Thorwirth, and C. Hieret, "Detection of amino acetonitrile in Sgr B2(N)," *Astron. Astrophys.* **482**, 179–196 (2008).

[67] P. Ehrenfreund and et al., "Astrophysical and astrochemical insights into the origin of life," *Reports Prog. Phys.* **65**, 1427–1487 (2002).

[68] V. Blagojevic, S. Petrie, and D. K. Bohme, "Gas-phase syntheses for interstellar carboxylic and amino acids," *Mon. Not. R. Astron. Soc.* **339**, L7–L11 (2003).

[69] R. D. Brown and et al., "Microwave spectrum and conformation of glycine," *J. Chem. Soc. Chem. Commun.* **13**, 547–548 (1978).

[70] B. E. Turner, R. Terzieva, and E. Herbst, "The physics and chemistry of small translucent molecular clouds. XII. more complex species explainable by gas-phase processes," *Astrophys. J.* **518**, 699–732 (1999).

[71] T. Suzuki, M. Ohishi, T. Hirota, M. Saito, L. Majumdar, and V. Wakelam, "Survey observations of a possible glycine precursor, Methanimine (CH_2NH)," *Astrophys. J.* **825**, 1–14 (2016).

[72] P. Theule, F. Borget, F. Mispelaer, G. Danger, F. Duvernay, J. C. Guillemin, and T. Chiavassa, " Hydrogenation of solid hydrogen cyanide HCN and methanimine CH_2NH at low temperature ," *Astron. Astrophys.* **534**, A64 (2011).

[73] D. E. Woon, "Pathways to glycine and other amino acids in ultraviolet-irradiated astrophysical ices determined via quantum chemical modeling," *Astrophys. J.* **571**, L177–L180 (2002).

[74] P. Redondo, F. Pauzat, and Y. Ellinger, "Theoretical survey of the $NH+CH_3$ potential energy surface in relation to Titan atmospheric chemistry," *Planet. Space Sci.* **54**, 181–187 (2006).

[75] L. E. Snyder, D. Buhl, B. Zuckerman, and P. Palmer, "Microwave detection of interstellar formaldehyde," *Phys. Rev. Lett.* **22**, 679–681 (1969).

[76] E. D. Tenenbaum, J. L. Dodd, S. N. Milam, N. J. Woolf, and L. M. Ziurys, "Comparative spectra of oxygen-rich versus carbon-rich circumstellar shells: VY canis majoris and IRC +10216 at 215-285 GHZ," *Astrophys. J. Lett.* **720**, 102–107 (2010).

[77] P. D. Godfrey, R. D. Brown, B. J. Robinson, and M. W. Sinclair, "Discovery of interstellar methanimine (formaldimine)," *Astrophys. Lett.* **13**, 119 (1973).

[78] M. Sinclair, N. Fourikis, J. Ribes, B. Robinson, R. Brown, and P. Godfrey, "Detection of interstellar thioformaldehyde," *Aust. J. Phys.* **26**, 85–91 (1973).

[79] B. E. Turner, "A molecular line survey of Sagittarius B2 and Orion -KL from 70 to 115 GHz. I. The observational data," *Astrophys. J. Suppl. Ser.* **70**, 539–622 (1989).

[80] E. C. Sutton, P. A. Jaminet, W. C. Danchi, and G. A. Blake, "Molecular line survey of Sagittarius B2(M) from 330 to 355 GHz and comparison with Sagittarius B2(N)," *Astrophys. J. Suppl. Ser.* **77**, 255–285 (1991).

[81] J. E. Dickens, W. M. Irvine, C. H. DeVries, and M. Ohishi, "Hydrogenation of interstellar molecules: A survey for methylenimine (CH_2NH)," *Astrophys. J.* **479**, 307–312 (1997).

[82] A. Nummelin, P. Bergman, A. Hjalmarson, P. Friberg, W. M. Irvine, T. J. Millar, M. Ohishi, and S. Saito, "A three-position spectral line survey of Sagittarius B2 between 218 and 263 GHz. I. The observational data," *Astrophys. J. Suppl. Ser.* **117**, 427–529 (1998).

[83] G. J. White, M. Araki, J. S. Greaves, M. Ohishi, and N. S. Higginbottom, "A spectral survey of the orion nebula from 455-507 GHz," *Astron. Astrophys.* **407**, 589–607 (2003).

[84] P. A. Jones, M. G. Burton, M. R. Cunningham, K. M. Menten, P. Schilke, A. Belloche, S. Leurini, J. Ott, and A. J. Walsh, "Spectral imaging of the Sagittarius B2 region in multiple 3-mm molecular lines with the Mopra telescope," *Mon. Not. R. Astron. Soc.* **386**, 117–137 (2008).

[85] P. A. Jones, M. G. Burton, N. F. H. Tothill, and M. R. Cunningham, "Spectral imaging of the Sagittarius B2 region in multiple 7-mm molecular lines," *Mon. Not. R. Astron. Soc.* **411**, 2293–2310 (2011).

[86] C. J. Salter, T. Ghosh, B. Catinella, M. Lebron, M. S. Lerner, R. Minchin, and E. Momjian, "The arecibo ARP 220 spectral census. I. Discovery of the pre-biotic molecule methanimine and new cm-wavelength transitions of other molecules," *Astron. J.* **136**, 389–399 (2008).

[87] S. L. Qin, Y. Wu, M. Huang, G. Zhao, D. Li, J. J. Wang, and S. Chen, "High-

resolution submillimeter multiline observations of G19.61 - 0.23: Small-scale chemistry," *Astrophys. J.* **711**, 399–416 (2010).

[88] D. T. Halfen, V. V. Ilyushin, and L. M. Ziurys, "Insights into surface hydrogenation in the interstellar medium: Observations of methanimine and methylamine in Sgr B2(N)," *Astrophys. J.* **767**, 1–11 (2013).

[89] D. R. Johnson and F. J. Lovas, "Microwave detection of the molecular transient methyleneimine (CH_2=NH)," *Chem. Phys. Lett.* **15**, 65–68 (1972).

[90] R. Pearson and F. J. Lovas, "Microwave spectrum and molecular structure of methylenimine (CH_2NH)," *J. Chem. Phys.* **66**, 4149–4156 (1977).

[91] L. Halonen and G. Duxbury, "The Fourier transform infrared spectrum of methyleneimine in the 10 μm region," *J. Chem. Phys.* **83**, 2078–2090 (1985).

[92] L. Dore, L. Bizzocchi, C. Degli Esposti, and J. Gauss, "The magnetic hyperfine structure in the rotational spectrum of H_2CNH," *J. Mol. Spectrosc.* **263**, 44–50 (2010).

[93] L. Dore, L. Bizzocchi, and C. Degli Esposti, "Accurate rotational rest-frequencies of CH_2NH at submillimetre wavelengths," *Astron. Astrophys.* **544**, A19 (2012).

[94] Y. Motoki, F. Isobe, H. Ozeki, and K. Kobayashi, "Terahertz spectroscopy of methanimine and its isotopologs," *Astron. Astrophys.* **566**, A28 (2014).

[95] R. W. Wilson, K. B. Jefferts, and A. A. Penzias, "Carbon monoxide in the orion nebula," *Astrophys. J.* **161**, L43–L44 (1970).

[96] J. H. Lacy, F. Baas, L. J. Allamandola, C. E. P. van de Bult, S. E. Persson, P. J. McGregor, C. J. Lonsdale, and T. R. Geballe, "4.6 micron absorption features due to solid phase CO and cyano group molecules toward compact infrared sources," *Astrophys. J.* **276**, 533–543 (1984).

[97] D. C. B. Whittet, A. J. Longmore, and A. D. McFadzean, "Solid CO in the taurus dark clouds," *MNRAS* **216**, 45–50 (1985).

[98] T. R. Geballe, "Absorption by solid and gaseous CO towards obscured infrared objects," *Astron. Astrophys.* **162**, 248–252 (1986).

[99] F. Combes, "Distribution of CO in the Milky Way," *Annu. Rev. Astron. Astrophys.* **29**, 195–237 (1991).

[100] A. Tielens and et al., "Interstellar solid CO-Polar and nonpolar interstellar

ices," *Astrophys. J.* **381**, 181–199 (1991).

[101] S. A. Sandford, L. J. Allamandola, A. G. G. M. Tielens, and G. J. Valero, "Laboratory studies of the infrared spectral propertries of CO in astrophysical ices," *Astrophys. J.* **329**, 498 (1988).

[102] T. M. Bania, "Carbon monoxide in the inner galaxy," *Astrophys. J.* **216**, 381–403 (1977).

[103] P. M. Solomon, N. Z. Scoville, A. A. Penzias, R. W. Wilson, and K. B. Jefferts, "Molecular clouds in the galactic center region: Carbon monoxide observations at 2.6 millimeters," *Astrophys. J.* **178**, 125–130 (1972).

[104] K. B. Jefferts, A. A. Penzias, and R. W. Wilson, "Observation of the CN radical in the Orion nebula and W51," *Astrophys. J.* **161**, L87–L89 (1970).

[105] P. Thaddeus and J. F. Clauser, "Cosmic microwave radiation at 2.63 mm from observations of interstellar CN," *Phys. Rev. Lett.* **16**, 819–822 (1966).

[106] C. Henkel, R. Mauersberger, and P. Schilke, "Molecules in external galaxies - The detection of CN, C_2H, and HNC, and the tentative detection of HC_3N," *Astron. Astrophys.* **201**, L23–L26 (1988).

[107] W. J. Wilson and A. H. Barret, "Characteristics of OH emission from infrared stars," *Astron. Astrophys.* **17**, 385–402 (1972).

[108] L. E. B. Johansson, W. M. Goss, and A. Winnberg, "A low latitude search for OH emission sources at 1612 MHz. I. Observational data," *Astron. Astrophys. Suppl. Ser.* **28**, 199–210 (1977).

[109] B. Baud, H. J. Habing, H. E. Matthews, and A. Winnberg, "A systematic search at 1612 MHz for OH maser sources I. Survey near the galactic centre," *Astron. Astrophys. Suppl. Ser.* **35**, 179–192 (1979).

[110] Y. Fukui and et al., "HCN emission in the Sagittarius A molecular cloud," *Publ. Astron. Soc. Japan* **29**, 643–667 (1977).

[111] L. E. Snyder and D. Buhl, "Observations of radio emission from interstellar hydrogen cyanide," *Astrophys. J.* **163**, L47–L52 (1971).

[112] L. D'Hendecourt and M. J. de Muizon, "The discovery of interstellar carbon dioxide," *Astron. Astrophys.* **223**, L5–L8 (1989).

[113] S. B. Charnley and M. J. Kaufman, "Carbon dioxide in star-forming regions," *Astrophys. J.* **529**, L111–L114 (2000).

[114] D. C. B. Whittet, P. A. Gerakines, and et al., "Detection of abundant CO_2 ice in the quiescent dark cloud medium toward Elias 16," *Astrophys. J.* **498**, L159–L163 (1998).

[115] D. C. B. Whittet and H. J. Walker, "On the occurrence of carbon dioxide in interstellar grain mantles," *Mon. Not. R. Astron. Soc.* **252**, 63–67 (1991).

[116] S. Ioppolo, I. Sangiorgio, G. A. Baratta, and M. E. Palumbo, "Solid CO_2 in low-mass young stellar objects," *Astron. Astrophys.* **554**, A34 (2013).

[117] E. T. Polehampton, K. M. Menten, S. Brünken, G. Winnewisser, and J.-P. Baluteau, "Far-infrared detection of methylene," *Astron. Astrophys.* **431**, 203–213 (2005).

[118] S. Chandra, "Einstein A-coefficeints for rotational transitions in CH_2," *Astrophys. Space Sci.* **98**, 269–273 (1984).

[119] J. M. Hollis, P. R. Jewell, and F. J. Lovas, "A search for methylene in the Orion nebula," *Astrophys. J.* **346**, 794–798 (1989).

[120] J. M. Hollis, P. R. Jewell, and F. J. Lovas, "Confirmation of interstellar methylene," *Astrophys. J.* **438**, 259–264 (1995).

[121] Y. C. Minh, W. M. Irvine, and L. M. Ziurys, "Observations of interstellar $HOCO^+$: Abundance enhancements toward the galactic center," *Astrophys. J.* **334**, 175–181 (1988).

[122] K. Hammami, F. Lique, N. Jaïdane, Z. Ben Lakhdar, A. Spielfiedel, and N. Feautrier, "Rotational excitation of $HOCO^+$ by helium at low temperature," *Astron. Astrophys.* **462**, 789–794 (2007).

[123] A. C. Cheung, D. M. Rank, C. H. Townes, D. D. Thornton, and W. J. Welch, "Detection of water in interstellar regions by its microwave radiation," *Nature* **221**, 626–628 (1969).

[124] J. A. Waak and C. H. Mayer, "The H_2O source in Sagittarius B2," *Astrophys. J.* **189**, 67–68 (1974).

[125] W. M. Goss, S. H. Knowles, M. Balister, R. A. Batchelor, and K. J. Wellington, "A survey of H_2O sources for wide-spectrum emission," *Mon. Not. R. Astron. Soc.* **174**, 541–553 (1976).

[126] P. D. Gensheimer, R. Mauersberger, and T. L. Wilson, "Water in galactic hot cores," *Astron. Astrophys.* **314**, 281–294 (1996).

[127] E. A. Bergin and E. F. van Dishoeck, “Water in star and planet forming regions,” *Philos. Trans. R. Soc. A Math. Phys. Eng. Sci.* **370**, 2778–2802 (2012).

[128] J. Cernicharo and J. Crovisier, “Water in space: The water world of ISO,” *Space Sci. Rev.* **119**, 29–69 (2005).

[129] A. C. Cheung, D. M. Rank, C. H. Townes, D. D. Thornton, and W. J. Welch, “Detection of NH_3 molecules in the interstellar medium by their microwave emission,” *Phys. Rev. Lett.* **21**, 1701–1705 (1968).

[130] M. Morris, B. Zuckerman, P. Palmer, and B. E. Turner, “Interstellar ammonia.,” *Astrophys. J.* **186**, 501–528 (1973).

[131] N. Kaifu, M. Morris, P. Palmer, and B. Zuckerman, “Distribution of NH_3 clouds in the galactic center region,” *Astrophys. J.* **201**, 98–101 (1975).

[132] R. Gusten, C. M. Walmsley, and T. Pauls, “Ammonia in the neighbourhood of galactic center,” *Astron. Astrophys.* **103**, 197–206 (1981).

[133] G. Winnewisser, E. Churchwell, and C. M. Walmsley, “Ammonia in absorption in the direction of Sagittarius B2,” *Astron. Astrophys.* **72**, 215–223 (1979).

[134] H. Feuchtgruber, F. P. Helmich, E. F. van Dishoeck, and C. M. Wright, “Detection of interstellar CH_3,” *Astrophys. J.* **535**, L111–L114 (2000).

[135] B. Bezard, H. Feuchtgruber, J. I. Moses, and T. Encrenaz, “Detection of methyl radicals (CH_3) on Saturn,” *Astron. Astrophys.* **334**, 41–44 (1998).

[136] R. F. Knacke, T. R. Geballe, K. S. Noll, and A. T. Tokunaga, “Search for interstellar methane,” *Astrophys. J.* **298**, L67–L69 (1985).

[137] G. F. Mitchell, “Methane in dense interstellar clouds,” *Astron. Astrophys.* **55**, 303–304 (1977).

[138] D. N. B. Hall and S. T. Ridgway, “Circumstellar methane in the infrared spectrum of IRC+10216,” *Nature* **273**, 281–282 (1978).

[139] L. E. Snyder, D. Buhl, B. Zuckerman, and P. Palmer, “Microwave detection of interstellar formaldehyde,” *Phys. Rev. Lett.* **22**, 679–681 (1969).

[140] S. Chandra, P. Musrif, and S. Shinde, “Anomalous absorption in H_2CO molecule,” *Bull. Astron. Soc. India* **34**, 11 (2006).

[141] F. F. Gardner and J. B. Whiteoak, “Interstellar formaldehyde absorption near

the galactic center," *Astrophys. Lett.* **5**, 161–166 (1970).

[142] R. Gusten and D. Downes, "Formaldehyde in the galactic center region - Interpretation," *Astron. Astrophys.* **87**, 6–19 (1980).

[143] J. Beiging, D. Downes, T. L. Wilson, A. H. M. Martin, and R. Gusten, "Formaldehhyde in the galactic center region," *Astron. Astrophys. Suppl. Ser.* **42**, 163–176 (1980).

[144] N. Z. Scoville and P. G. Wannier, "Molecular cloud structure from 2-cm formaldehyde and 2.6-mm carbon monoxide lines," *Astron. Astrophys.* **76**, 140–149 (1979).

[145] T. Pauls, K. J. Johnston, and T. L. Wilson, "Formaldehyde absorption toward Sagittarius A," *Astrophys. J.* **461**, 223–230 (1996).

[146] J. B. Whiteoak, D. H. Rogstad, and I. A. Lockhart, "Aperture synthesis of formaldehyde absorption in Sgr A," *Astron. Astrophys.* **36**, 245–251 (1974).

[147] B. Zuckerman, D. Buhl, P. Palmer, and L. E. Snyder, "Observations of interstellar formaldehyde," *Astrophys. J.* **160**, 485–506 (1970).

[148] E. B. Fomalont and L. Weliachew, "Interferometric observations of formaldehyde absorption in front of strong galactic sources," *Astrophys. J.* **181**, 781–794 (1973).

[149] R. J. A. Grim, F. Baas, T. R. Geballe, J. M. Greenberg, and W. Schutte, "Detection of solid methanol toward W33A," *Astron. Astrophys.* **243**, 473–477 (1991).

[150] W. A. Schutte, A. G. G. M. Tielens, and S. A. Sandford, "10 micron spectra of protostarts and the solid methanol abundance," *Astrophys. J.* **382**, 523–529 (1991).

[151] J. A. Ball, C. A. Gottlieb, A. E. Lilley, and H. E. Radford, "Detection of methyl alcohol in Sagittarius," *Astrophys. J.* **162**, L203–L210 (1970).

[152] A. H. Barrett, P. R. Schwartz, and J. W. Waters, "Detection of methyl alcohol in Orion at a wavelength of 1 centimeter," *Astrophys. J.* **168**, L101–L106 (1971).

[153] M. Cato, T. Cato, P. Landgren, and A. Sume, "Search for interstellar formic acid at 1638.806 MHz in radio sources," *Astrophys. J.* **160**, L131–L132 (1970).

[154] B. Zuckerman, J. A. Ball, and C. A. Gottlieb, "Microwave detection of

interstellar formic acid," *Astrophys. J.* **163**, L41–L45 (1971).

[155] G. Winnewisser and E. Churchwell, "Detection of formic acid in Sagittarius B2 by its 2_{11}-2_{12} transition," *Astrophys. J.* **200**, L33–L36 (1975).

[156] C. A. Gottlieb, P. Palmer, L. J. Rickard, and B. Zuckerman, "Studies of interstellar formamide," *Astrophys. J.* **182**, 699–710 (1973).

[157] P. Palmer, C. A. Gottlieb, L. J. Rickard, and B. Zuckerman, "Detection of the 1_{11}-1_{10} transition of interstellar formamide," *Bull. Astron. Soc.* **3**, 499–499 (1971).

[158] R. H. Rubin, J. Swenson, G. W., R. C. Benson, H. L. Tigelaar, and W. H. Flygare, "Microwave detection of interstellar formamide," *Astrophys. J.* **169**, L39–L44 (1971).

[159] F. J. Lovas, J. M. Hollis, A. J. Remijan, and P. R. Jewell, "Detection of ketenimine (CH_2CNH) in Sagittarius B2(N) hot cores," *Astrophys. J.* **645**, L137–L140 (2006).

[160] K. K. Singh, Shivani, P. Tandan, and A. Misra, "A quantum chemical study on the formation of ethanimine (CH_3CHNH) in the interstellar ice," *Astrophys. Space Sci.* **363**, 213 (2018).

[161] D. Quan, E. Herbst, J. F. Corby, A. Durr, and G. Hassel, "Chemical simulations of prebiotic molecules: interstellar ethanimine isomers," *Astrophys. J.* **824**, 129 (2016).

[162] R. A. Loomis, D. P. Zaleski, and et al., "The detection of interstellar ethanimine (CH_3CHNH) from observations taken during the GBT Primos survey," *Astrophys. J.* **765**, L9 (2013).

[163] F. Vazart, C. Latouche, D. Skouteris, N. Balucani, and V. Barone, "Cyanomethanimine isomers in cold interstellar clouds: insights from electronic structure and kinetic calculations," *Astrophys. J.* **810**, 111 (2015).

[164] D. P. Zaleski, N. A. Seifert, and et al., "Detection of E-cyanomethanimine toward Sagittarius B2 (N) in the Green Bank Telescope Primos survey," *Astrophys. J.* **765**, L10 (2013).

[165] Shivani, A. Misra, and P. Tandon, "Formation of E-cyanomethamine in a nitrile rich environment," *Res. Astron. Astrophys.* **17**, 1–10 (2017).

[166] N. Kaifu and et al., "Detection of interstellar methylamine," *Astrophys. J.* **191**,

L135–L137 (1974).

[167] N. Kaifu, K. Takagi, and T. Kojima, "Excitation of interstellar methylamine," *Astrophys. J.* **198**, L85–L88 (1975).

[168] E. G. Bogelund, B. A. McGuire, M. R. Hogerheijde, E. F. van Dishoeck, and N. F. W. Ligterink, "Methylamine and other simple N-bearing species in the hot cores NGC 6334I MM1–3," *Astron. Astrophys.* **624**, A82 (2019).

[169] N. F. W. Ligterink, E. D. Tenenbaum, and E. F. Van Dishoeck, "Search for methylamine in high mass hot cores," *Astron. Astrophys.* **576**, 1–11 (2015).

[170] M. K. Sharma, M. Sharma, A. K. Sharma, and S. Chandra, "Search of amino group in the universe: 2-Aminopyridine," *Serbian Astron. J.* **2015**, 81–86 (2015).

[171] F. J. Lovas, R. J. McMahon, J. Grabow, M. Schnell, J. Mack, L. T. Scott, and R. L. Kuczkowski, "Interstellar chemistry: A strategy for detecting polycyclic aromatic hydrocarbons in space," *J. Am. Chem. Soc.* **127**, 4345–4349 (2005).

[172] L. J. Allamandola, A. Tielens, and J. R. Barker, "Interstellar polycyclic aromatic hydrocarbons: the infrared emission bands, the excitation/emission mechanism, and the astrophysical implications," *Astrophys. J. Suppl. Ser.* **71**, 733–775 (2000).

[173] M. J. Frisch, G. W. Trucks, H. B. Schlegel, and et al., "Gaussian," *Gaussian Inc., Wallingford CT* (2003).

[174] T. H. Dunning, "Gaussian basis sets for use in correlated molecular calculations. I. The atoms boron through neon and hydrogen," *J. Chem. Phys.* **90**, 1007–1023 (1989).

[175] G. Knizia, T. B. Adler, and H. J. Werner, "Simplified CCSD(T)-F12 methods: Theory and benchmarks," *J. Chem. Phys.* **130**, 054104 (2009).

[176] J. M. Hutson and S. Green, "MOLSCAT: Molecular Scattering," *Astrophysics Source Code Libr.* (2012).

[177] S. Chandra and A. Sahu, "Einstein A-coefficients for rotational transitions in the v3 vibrationally excited state of SiC_2," *Astron. Astrophys.* **272**, 700–704 (1993).

[178] S. Chandra and Rashmi, "Einstein A -coefficients for rotational transitions in the ground vibrational state of $^{28}SiC_2$, $^{29}SiC_2$ and $^{30}SiC_2$," *Astron. Astrophys.*

Suppl. Ser. **131**, 137–139 (1998).

[179] S. Chandra, "Einstein A-coefficients for rotational transitions in the ground vibrational state of Si_2C molecule," *Indian J. Phys.* **76B**, 649–655 (2002).

[180] S. Chandra, W. H. Kegel, and D. A. Varshalovich, "Einstein A-values for purely rotational transitions in the HDO molecule," *Astron. Astrophys. Suppl. Ser.* **58**, 687–691 (1984).

[181] S. Chandra, D. A. Varshalovich, and W. H. Kegel, "Einstein A-values for rotational transitions in the H_2O molecule," *Astron. Astrophys. Suppl. Ser.* **55**, 51–53 (1984).

[182] S. Chandra and W. H. Kegel, "Collisional rates for asymmetrical top molecules," *Astron. Astrophys. Suppl. Ser.* **142**, 113–118 (2000).

[183] G. Piehler, W. H. Kegel, and T. Tsuji, "Optical pumping of circumstellar SiO masers," *Astron. Astrophys.* **245**, 580–586 (1991).

[184] Z. Kisiel, "Assignment and analysis of complex rotational spectra," *Spectrosc. from Space, Kluwer Acad. Publ. Dordr.*, 91–106 (2001).

[185] M. K. Sharma, M. Sharma, U. P. Verma, and S. Chandra, "Collisional excitation of thioformaldehyde and of silylidene," *Adv. Sp. Res.* **55**, 434–439 (2015).

[186] S. Chandra, Sakshi, M. K. Sharma, and N. Kumar, "Methanimine in interstellar medium: line intensities," *Indian J. Phys.* **90**, 733–739 (2016).

[187] C. Lee, W. Yang, and R. G. Parr, "Development of the Colic-Salvetti correlation-energy into a functional of the electron density," *Phys. Rev. B* **37**, 785–789 (1988).

[188] A. D. Becke, "Density-functional thermochemistry. III. The role of exact exchange," *J. Chem. Phys.* **98**, 5648–5652 (1993).

[189] A. Faure, F. Lique, and A. J. Remijan, "Collisional excitation and weak maser action of interstellar methanimine," *J. Phys. Chem. Lett.* **9**, 3199–3204 (2018).

[190] M. K. Sharma, M. Sharma, and S. Chandra, "Temperature dependence of collisional rate coefficients for rotational transitions: a-type asymmetric top molecules," *New Astron.* **52**, 48–54 (2017).

[191] F. Dumouchel, A. Faure, and F. Lique, "The rotational excitation of HCN and HNC by He: Temperature dependence of the collisional rate coefficients,"

Mon. Not. R. Astron. Soc. **406**, 2488–2492 (2010).

[192] S. Chandra, A. Kumar, and M. K. Sharma, "Anomalous absorption in thioformaldehyde," *New Astron*. **15**, 318–323 (2010).

LIST OF PUBLICATIONS

A. Publications in Journals

1. Methanimine in interstellar medium: line intensities

S. Chandra, Sakshi, M.K. Sharma and N. Kumar

Indian Journal of Physics, (Springer) Vol. **90**, No. 7, 2016, 733-739

DOI: 10.1007/s12648-015-0813-6.

B. Publications in Conference Proceedings

1. Anomalous absorption in 2_{02}-1_{11} transition of methanimine

N. Kumar, S.Chandra, N.Kant, M.K. Sharma and M. Sharma

Journal of Physics: Conference Series (IOP Science) Vol. **1531**, 2020, 012020

DOI: 10.1088/1742-6596/1531/1/012020.

C. Papers Accepted in Journals

1. Transition 1_{10}-1_{11} of methanimine in interstellar medium

M.K. Sharma, M.Sharma, N. Kumar and S. Chandra

Paper **in-press (accepted)** in "Indian Journal of Physics" (Springer)

Date of submission: Jan 24, 2019

Date of acceptance: Jun 19, 2020.

D. Paper Presentations in Conferences/Seminars

1. National conference on "Recent Trends in Experimental and Theoretical Physics-2017" held at Sri Sai University, Palampur (HP) from Nov. 23 to Nov. 24, 2017.

2. National seminar on "Solar and Sustainable Energy Applications of Material Science and Physico-chemical innovations" held at DAV College, Abohar, on Mar 19, 2019.

3. International conference on "Recent Advances in Fundamental and Applied Sciences (RAFAS-2019) held at Lovely Professional University, Phagwara, from Nov. 5 to Nov. 6, 2019.